

**Application of the Multiple Quantum NMR
Spectroscopy for Investigation of the
Dipole-Dipole Couplings in Amorphous Polymers**

Dissertation

zur Erlangung des akademischen Grades

Dr. rerum naturalium (Dr. rer. nat.)

vorgelegt der

Mathematisch-Naturwissenschaftlich-Technischen Fakultät

der Martin-Luther-Universität Halle-Wittenberg

von Herrn Dipl. Phys.

Juraj Pivarč

geb. am: 4.10.1971 in Bratislava, Slovak Republic

Gutachter:

1. Prof. Dr. H. Schneider
2. Prof. Dr. D. Freude
3. Prof. Dr. D. E. Demco

Halle(Saale), den 4.7.2000

Contents

Summary	iii
Zusammenfassung	vii
Introduction	1
1 Theoretical bases	5
1.1 Types of interactions in NMR	6
1.2 Equilibrium density operator	11
1.3 Average Hamiltonian theory	12
1.4 Dipolar interaction and irreducible tensors	14
1.5 One pulse experiment	16
1.6 Magic Angle Spinning	17
1.7 Two-dimensional NMR spectroscopy	22
2 Multiple Quantum NMR	25
2.1 Basics definitions	26
2.2 Three pulse Experiment	28
2.3 General scheme of MQ experiment	31
2.3.1 Excitation and Reconversion	32
2.4 Static MQ experiment	33
2.4.1 Time reversal pulse sequences	34
2.4.1.1 Determining toggling-frame states for four pulse sequence	38
2.4.1.2 Eight pulse sequence	41
2.4.1.3 Thirty-two pulse sequence	42
2.4.2 Separation of MQ coherences	43
2.4.3 TPPI MQ experiment	45
2.4.4 Spin counting MQ experiment	47
2.5 MAS MQ experiment	48
2.5.1 Recoupling pulse sequences	50

2.5.1.1	DRAMA	51
2.5.1.2	BABA	54
2.5.1.3	C7	57
2.5.2	Two-dimensional MQ experiment	59
2.5.3	Spin counting MQ experiment	61
3	Measuring of Homonuclear Dipole-Dipole couplings	64
3.1	Single Quantum MAS experiment	65
3.2	DQ sideband pattern under MAS	68
3.2.1	DRAMA/BABA	70
3.2.2	C7/POST C7	75
3.3	DQ spectroscopy under MAS	78
3.3.1	DQ build-up curves	81
3.3.2	Residual dipolar couplings in natural rubber.	83
3.4	Spin counting under MAS	89
3.5	MQ coherences for static solids	91
3.5.1	DQ build-up curves of polybutadiene melt	93
3.5.2	Spin counting in polybutadiene rubber	97
4	Realization of MQ Experiment	100
4.1	Spectrometer	100
4.1.1	Requirements for MAS	100
4.2	Hypercomplex versus TPPI acquisition	101
4.3	Double quantum filtering	104
4.4	MQ phase cycling techniques	105
	Conclusions	108
	Appendix	111
A.	Irreducible tensors	111
B.	Wigner rotation matrices	113
C.	Intensity of the DQ coherence for two spins- $\frac{1}{2}$ coupled via dipolar coupling	114
	References	118
	Acknowledgements	123
	Curriculum vitae	125

Summary

One of the main interest in polymer science is to obtain information about the structure of the sample correlated with spatial distribution of the neighbouring nuclei. For determining distances between atoms and the orientation of their connecting vectors, measurement of the direct spin-spin interaction (dipolar coupling) can be used.

Nuclear magnetic resonance (NMR) has been used in this work to measure dipolar couplings in amorphous polymers. For this purpose multiple quantum (MQ) coherences excited by proper multiple r.f. pulse sequences are used. In this work MQ NMR methods based on protons ^1H have been chosen to accomplish it. Because the spin quantum number of ^1H is $1/2$, energy level system has to be formed with a certain number of spins to permit occurrence of MQ transitions. The efficiency of their excitation is the larger the stronger the coupling between the spins is. Thus, estimation and comparison of the intensities of the excited coherences can give information about the relative strength of the coupling. The main aim of this work was to compare high resolution MQ and double quantum (DQ) NMR techniques under fast *magic angle spinning* (MAS) with low resolution static MQ techniques with respect to elastomers and to determine the residual couplings in natural rubber.

In MQ spectroscopy which usually deals with a lot of r.f. pulses precise timing between them is one of the most important requirements. Usually NMR spectrometers can not provide ideal pulses with the rectangular shape as well as phase switching delays between them are of importance. The theoretical calculations presented in this work show that the influence of finite switching times between r.f. pulses to the zero-order average Hamiltonian for BABA r.f. pulse sequence is small if the delays between these pulses are smaller than $0.5 \mu\text{s}$, which is nowadays in commercial spectrometers good fulfilled. Care has to be taken for proper design of the multiple-pulse sequences especially under fast MAS. The timing of the pulses has to be symmetric with respect to the rotor period. In addition

new phase cycling techniques to remove r.f. field inhomogeneities for MQ experiment as well as improvements of already existing techniques to select DQ coherence are presented. Detailed description of performing MQ experiments for static solids as well as for high resolution MAS is made in this work. Comparing of standard TPPI techniques with 'hypercomplex' methods in connection to DQ spectroscopy are detailed discussed which was up to now not reported. It is shown that 'hypercomplex' acquisition may be preferred for C7 based r.f. pulse sequences but on the other hand for BABA and DRAMA r.f. pulse sequences TPPI acquisition is preferred.

In systems where chemical shift anisotropy interactions can be neglected with comparison to the dipolar coupling strength ω_D , simple MAS methods are suitable for measuring dipolar couplings ([Got95]). The important information about it is comprised in the sideband intensities. Comparing intensities of the spinning sidebands the ratio between dipolar coupling and rotational frequency can be calculated if the spin- $\frac{1}{2}$ pair approximation is valid. Already existing theoretical approaches for calculating this ratio are extended for moderate spinning speeds where spinning angular frequency is much more close to the dipolar coupling strength ($\omega_r \simeq \omega_D$).

The r.f. pulse sequences POST C7, C7, BABA and DRAMA used in high resolution MQ MAS experiments were applied for elastomers. Their advantages and disadvantages are discussed. With the help of them residual dipolar couplings in Natural Rubber (NR) systems were measured. C7 ([Lee95]) as well as its modified version POST C7 ([Hoh98]) were found to be the most effective for elastomers. They provide unique selectivity of the dipolar couplings between protons in the same as well as between protons belonging to the different functional groups.

New low resolutions static DQ experiments were successfully applied on polymers. As a test sample polybutadiene melt was chosen. It was shown that static DQ experiments can be sometimes preferred besides higher resolution MAS experiments. They does not require high spinning speeds, therefore higher filling factors are possible. This has a consequence in improving signal to noise ratios. MAS, on the other hand, is limited to the size of the rotor which is necessarily small enough to obtain high spinning speeds.

A thirty-two r.f. pulse sequence was used to excite higher order coherences in high crosslinked polybutadiene rubber (PBR) under static conditions. Up to the 6-th order of coherence was clearly visible which was not up to now not realized on elastomers.

MQ as well as DQ spectroscopy are well established in modern NMR. They are not

restricted to use only for ^1H systems. They can be extended also to other spin- $\frac{1}{2}$ nuclei. Recently published experiment based on C7 r.f. pulse sequence shows that modified C7 ([Hon99]) can be used to achieve even higher selectivity in INADEQUATE experiment. This with connection to DQ techniques presented in this work might be used to measure connectivities between functional groups which were not distinguished to measure with classical DQ spectroscopy.

Zusammenfassung

Ein wichtiges Teilgebiet der Polymerforschung befasst sich mit der Untersuchung der molekularen Struktur und Beweglichkeit. Für die Bestimmung von Atomabständen sowie von Orientierungen bestimmter Molekülsegmente kann die dipolare Kopplung zwischen den Kernspins als Sonde dienen.

In der hier vorgestellten Arbeit wurde die kernmagnetische Resonanz (NMR) zur Messung dipolarer Kopplungen in amorphen Polymeren eingesetzt. Zu diesem Zwecke wurden mittels geeigneter Impulsgruppen Multiquanten (MQ) - Kohärenzen im Protonenspinsystem angeregt. Da die Spinquantenzahl der Protonen $\frac{1}{2}$ beträgt, ist eine bestimmte Anzahl von gekoppelten Spins notwendig, damit ein komplexes Energieniveauschema vorliegt, in dem Multiquanten-Übergänge stattfinden können. Die Effizienz von deren Anregung ist um so größer, je stärker die Kopplung der Spins ist, so dass die Bestimmung und der Vergleich der Intensitäten der angeregten Kohärenzen Aussagen über die relative Stärke von Kopplungen und über die Größe von Clustern gekoppelter Spins gestattet. Das Ziel dieser Arbeit ist dabei zum einen der Vergleich von hochauflösenden MQ- und DQ- Verfahren unter MAS mit statischen MQ-Techniken hinsichtlich der Anwendung auf Elastomere, zum anderen die Bestimmung von dipolaren Rest-Kopplungen in Naturkautschuk.

Die MQ-Spektroskopie, die normalerweise eine Vielzahl von Impulsen verwendet, erfordert eine genaue Einhaltung der vorgesehenen Impulslängen und der Abstände. Reale Impulse weichen jedoch mehr oder weniger von der idealen Rechteckform ab. Hinzu kommt, dass das Schalten der Phasen eine zusätzliche Verzögerung erzeugen kann. Theoretische Berechnungen in dieser Arbeit zeigen, dass der Einfluss von endlichen Schaltzeiten zwischen den HF-Impulsen einer BABA-Impulsfolge auf den gemittelten Hamilton-Operator sehr klein ist, wenn die Impulsabstände kleiner als 0,5 s sind. Diese Bedingung kann mit den heutigen Spektrometern meist erfüllt werden. Es sollte aber darauf geachtet werden, dass die unter schnellem MAS verwendeten Impulsfolgen symmetrisch

bezüglich einer Rotationsperiode aufgebaut sind. Darüberhinaus werden neue Phasenzyklen vorgestellt, mit deren Hilfe der Einfluss der Inhomogenitäten der HF-Impulse auf die MQ-Experimente reduziert und gleichzeitig die Doppelquanten-Selektion verbessert werden kann. Detailliert wird die Ausführung von MQ-Experimenten beschrieben, die sowohl statisch als auch unter MAS-Bedingungen ausgeführt wurden. Die Selektion der DQ-Kohärenzen entweder mit Standard-TPPI (Time-Proportional Phase Incrementation)-Verfahren oder durch Erzeugung hyperkomplexer Datensätze wird detailliert beschrieben. Beide Möglichkeiten wurden erstmalig miteinander verglichen. Dabei zeigte sich, dass die hyperkomplexe Datenaufnahme bei auf C7 basierenden Impulsfolgen bevorzugt werden sollte, während bei BABA- und DRAMA-Impulsfolgen die TPPI-Methode günstiger ist.

In Stoffsystemen, bei denen die Anisotropie der chemischen Verschiebung gegenüber der dipolaren Kopplung vernachlässigbar ist, sind einfache MAS-Experimente ausreichend um diese Kopplungen zu bestimmen ([Got95]). Die Information hierüber ist in den Seitenbandintensitäten enthalten. Aus deren gegenseitigem Verhältnis kann man unter der Voraussetzung der Zwei-Spin-Näherung den Quotienten von dipolarer Kopplung und Rotationsfrequenz bestimmen. Bereits hierfür existierende theoretische Ansätze wurden erweitert, um sie für den Fall, dass Rotationsfrequenz und dipolare Kopplung nahe beieinander liegen ($\omega_r \simeq \omega_D$), anwenden zu können.

Die Impulsfolgen C7, POST C7, BABA und DRAMA wurden als hochauflösende MQ-Experimente auf Elastomere angewandt. Die Vor- und Nachteile der einzelnen Verfahren werden hier diskutiert. Mit deren Hilfe wurden dipolare Rest-Kopplungen in Naturkautschuk bestimmt. Dabei erwiesen sich C7 ([Lee95]) und deren modifizierte Variante POST-C7 ([Hoh98]) bezüglich der Selektivität der Kopplungen sowohl zwischen den Protonen der gleichen Atomgruppe als auch zwischen denen verschiedener Gruppen als die geeignetsten Methoden.

Neuere statische DQ-Experimente wurden erfolgreich auf Polymere angewandt. Als Testsubstanz ist dabei eine Polybutadien-Schmelze verwendet worden. Es zeigte sich, dass die statischen Experimente in manchen Fällen den MAS-Verfahren überleben sind trotz des höheren Auflösungsvermögens der zuletztgenannten. Die statischen Verfahren ermöglichen größere Substanzmengen, wodurch sich ein günstigeres Signal-Rausch-Verhältnis ergibt. MAS-Proben sind demgegenüber auf die Größe der Rotoren-Innenräume beschränkt, die umso kleiner sein werden, je höher die angestrebte Rotationsfrequenz ist.

Mit einer Impulsfolge, die aus Zyklen zu je 32 Impulsen besteht, konnten unter

statischen Bedingungen auch Kohärenzen höherer Ordnung in vernetztem Polybutadien-Kautschuk (PBR) angeregt werden. Dabei gelang es, auch die 6. Ordnung noch klar sichtbar zu machen, was bisher in Elastomeren nicht bekannt war.

MQ- und speziell DQ-Experimente können auch auf andere Spin- $\frac{1}{2}$ -Kerne angewandt werden. Jüngst veröffentlichte Experimente auf der Basis von C7 ([Hon99]) zeigen, dass man in Verbindung mit INADEQUATE eine höhere Selektivität erreichen kann. Dies könnte eine Möglichkeit sein, um die Konnektivitäten zwischen solchen Gruppen zu bestimmen, deren Resonanzen mit den bisherigen DQ-Verfahren nicht voneinander getrennt werden konnten.

Introduction

The aim of this work is to develop and to implement the methods for determining the local structure and dynamics of amorphous solids like e.g. polymers or glasses. Due to the missing periodicity in these systems X-ray and neutron scattering give not enough sufficient results with comparison to the crystalline samples. Therefore, nuclear magnetic resonance (NMR) has been chosen in this work to study the structure and dynamics. The main advantage of NMR spectroscopy is its unique selectivity. It allows to monitor selectively different nuclei with characteristic Larmor frequency ω_0 . The fine structure of the NMR spectrum for spin- $\frac{1}{2}$ nuclei is mainly determined by two interactions, the chemical shift interaction describing the shielding of the nuclear spin from the external field by the electron clouds and by the direct spin-spin interaction. Both interactions can be used to get an information about the chemical structure and the space distribution of the neighbouring nuclei. Measuring of the direct spin-spin interaction the distances between nuclear spins and the orientation of their connecting vectors can be determined.

In solids the direct spin-spin interaction for protons is formed by interactions between a lot of strongly coupled spins, which leads to very broad spectral lines. Therefore, information about the chemical shift interaction is usually suppressed and can not be resolved. Various techniques have been used in past to compensate to the certain order the effects of dipolar couplings for increasing the spectral resolution ([Ern87, Rhi73]). They can be in principle divided into three categories: static multiple-pulse techniques, simple magic angle spinning (MAS), and combination of multiple-pulses and MAS. All three methods can be used to get the higher resolution spectra, where dipolar couplings corresponding to the different chemical shifts can be assigned.

To get detailed information about the structure and dynamics of amorphous polymers multiple quantum (MQ) spectroscopy will be used. Multiple quantum NMR is nowadays well established for determining dipolar couplings. MQ coherences used for this purpose

are coherent transitions between states, which differs in magnetic quantum number p about more than one unit. The excitation of this coherences in spin- $1/2$ systems is possible only when the coupling between spins exists ([Pin88]) and under the usage of special r.f. pulse sequences designed for this purpose. MQ coherences does not induce directly the signal to the detecting coil in NMR instruments hence, indirect detection scheme is required. Thus, MQ NMR experiment requires an experiment with two-dimensional structure ([Ern87]).

In recent years a substantial effort has been recorded in combination of MAS and multiple-pulse techniques for exciting MQ coherences. With increasing rotational frequencies resolution and sensitivity have been improved and it was possible to achieve high resolution spectra also for abundant nuclei like e.g. protons ^1H . This so-called fast MAS effectively averages out dipolar couplings, which was a disadvantage, so it was necessary to reintroduce them by designing appropriate multiple-pulse sequences ([Gee94, Fei96a, Lee95, Hoh98]). In the case of amorphous polymers well above the glass temperature high resolution MQ spectra can be used to obtain new information about the local structure and dynamics. This is a prerequisite for improving the material.

In this work we concentrate to develop and demonstrate NMR measuring methods for detecting MQ and double (DQ) coherences for spin- $1/2$ systems coupled via dipolar coupling. This was done with designing special multiple-pulse sequences which are applicable in modern NMR instruments. Besides this methodical developments we compared static as well as MAS multiple quantum techniques with connection to polymer melts and elastomers well above the glass temperature.

MQ spectroscopy was used to determine dipolar connectivities between spin- $1/2$ nuclei for protons and carbons in organic solids ([Spi97, Got95, Gra98b, Som95]) and for ^{31}P in crystalline or glassy phosphates ([Fei98, Gee97]). Elastomers represent a technologically important class of materials. They have been investigated by various techniques ([Add93]) including also MQ spectroscopy ([Gra98a, Sch99]). From the view point of NMR, crosslinked elastomers exhibit both liquid-like and solid-like features. At temperatures well above the glass temperature, the time scales of molecular motions are liquid-like. However, the presence of topological constraints and permanent crosslinks prevents the chain motion from being isotropic. Thus, anisotropic spin interactions, such as direct spin-spin interaction are not fully averaged out and give rise to solid like NMR properties. This allows us to use high resolution proton MQ spectroscopy to measure residual dipolar interactions under the conditions of fast MAS.

The aim of this work is to compare high resolution MQ and DQ NMR techniques under fast MAS with low resolution static MQ techniques with connection to elastomers. Various multiple-pulse sequences have to be compared which are useful to study the structure and dynamics in polymer melts and crosslinked elastomers.

The chapters are organized as follows:

In chapter 1 the theoretical bases of NMR are elucidated. We concentrated to the homonuclear dipolar interaction which is extensively used in this work. Irreducible tensors representation of dipolar coupling Hamiltonian can be found in section 1.4. Simple magic angle spinning (MAS) experiment is theoretically described in section 1.6. Basics of two-dimensional NMR which is necessary for MQ experiment can be found in section 1.7.

Chapter 2 deals with detailed theoretical analysis of MQ experiment for static solids (section 2.4) and for high resolution MQ techniques under MAS (section 2.5). The basics of average Hamiltonian theory (section 1.3) are extensively used for characterizing multiple-pulse sequences exciting even order coherences in sections 2.4.1 and 2.5.1. Influence of finite switching delays between r.f. pulses on the zero order average Hamiltonian are derived and discussed for BABA r.f. pulse sequence in section 2.5.1.2.

In chapter 3 MQ as well as double quantum coherences have been used to measure mainly residual dipolar couplings in elastomers. In sections 3.2 and 3.3 DQ build-up curves are used for measuring residual dipolar couplings in polybutadiene melt and in natural rubber. Effectiveness of high resolution r.f. pulse sequences like C7, POST C7, BABA and DRAMA are compared with connection to elastomers. Section 3.4 deals with NMR experiment used for determining sizes of the dipolar clusters of coupled spins in solids under fast MAS. In section 3.5 new DQ and multiple quantum experiments for static solids are presented. Comparison with high resolution MAS techniques is also made. High order coherences in high crosslinked polybutadiene rubber are measured in section 3.5.2.

In chapter 4 practical hints for NMR spectroscopists to realize MQ experiments are discussed. Comparison of hypercomplex and TPPI acquisition with connection to DQ spectroscopy can be found in section 4.2. DQ filtering and phase cycling techniques are explained in sections 4.3 and 4.4, respectively.

Chapter 1

Theoretical bases

Just after the discovery of nuclear magnetic resonance (NMR) in 1945 in bulk matter [Blo46, Pur46] this phenomenon has become of interest for many structural elucidation techniques. NMR can measure a magnetic moment produced by spin charged atoms embedded to the strong magnetic field. It took 25 years from continuous wave (CW) low resolution detection techniques till development of pulse Fourier spectroscopy, which enables an expansion of modern high-resolution NMR techniques. The response to a δ -function pulse according to the superposition principle, which is valid in linear systems, is a linear superposition of the responses of all frequency components called FID (*free induction decay*) and the transfer function, called spectrum, can be obtained from the FID by a Fourier transformation. The Fourier transformation became a routine for characterization of a spectrum in modern NMR instruments. Further improvements were made with discovery of a new dimension, where frequency response spectrum $S(\omega)$ became a spectrum of two variables $S(\omega_1, \omega_2)$. The two-dimensional (2D) spectroscopy [Ern87] was able to distinguish between two independent precession periods, i.e. evolution and detection period. The evolution during preceding period is monitored indirectly through the phase and amplitude of the magnetization at the beginning of the detection period. This scheme has many crucial advantages, for example, to observe multiple quantum coherence indirectly.

In this chapter the theoretical bases of NMR will be presented in a very short overview. We will focus our interest to the solid state NMR with connection to the spin- $\frac{1}{2}$ systems. Magic angle spinning experiment for dipolar coupled spin- $\frac{1}{2}$ pair will be also presented. We will conclude this chapter with the bases of 2D spectroscopy. Deep theoretical descriptions

of NMR can be found in monographs like e.g. Abragam ([Abr61]) and Ernst et al. ([Ern87]). The methods of solid state NMR spectroscopy are fully or partially described in monographs from Mehring ([Meh83]) and Slichter ([Sli92]). The possible applications on polymers are discussed in monograph from Schmidt-Rohr/Spiess ([SR94]). In this monograph, for convenience, we will assume all Hamiltonians as the operators correspond to E/\hbar , where energy eigenvalues are measured in angular frequency units.

1.1 Types of interactions in NMR

The dynamics of N coupled spins is not possible to describe in terms of the motion of classical magnetization vectors, but it is necessary to treat quantum mechanical formalism. The most convenient description of quantum mechanical system dynamics can be made with the help of density operator $\hat{\rho}$. We will recall some of its basic properties

$$\hat{\rho} = \hat{\rho}^\dagger, \quad \text{Tr} \{ \hat{\rho} \} = 1, \quad \hat{\rho}^2 = \hat{\rho}. \quad (1.1)$$

For the time-dependent Schrödinger equation [Ern87, Sli92], one can derive the equation of motion for the density operator $\hat{\rho}$ under Hamiltonian \hat{H}

$$\frac{d}{dt} \hat{\rho}(t) = -i[\hat{H}(t), \hat{\rho}(t)], \quad (1.2)$$

called Liouville-von Neumann equation or simply density operator equation. Its formal solution may be written

$$\hat{\rho}(t) = \hat{U}(t) \hat{\rho}(0) \hat{U}^\dagger(t), \quad (1.3)$$

with the time evolution unity operator (propagator)

$$\hat{U}(t) = \hat{T} e^{-i \int_0^t \hat{H}(t') dt'}, \quad (1.4)$$

where the Dyson time-ordering operator \hat{T} defines a prescription for evaluating the exponential functions in cases where the Hamiltonians at different times do not commute, $[\hat{H}(t'), \hat{H}(t'')] \neq 0$. For the time independent Hamiltonians $\hat{H}(t) = \hat{H}$ equation (1.4) can be rewritten in the form

$$\hat{U}(t) = e^{-i\hat{H}t}, \quad (1.5)$$

where time-ordering operator \hat{T} has no more importance. The expectation value of an arbitrary observable operator \hat{A} in the Schrödinger representation can be found

$$\langle \hat{A} \rangle = \text{Tr} \{ \hat{A} \cdot \hat{\rho}(t) \} \quad (1.6)$$

by evaluating the trace of the product of the observable operator and density operator.

In most of the cases the complete Hamiltonian \hat{H} of the molecular system is enormously complex, and to derive the exact solutions of equation of motion (1.2) is very complicated. This is a good reason to describe magnetic resonance experiments by a spin Hamiltonian \hat{H}_S . It acts only on the spin variables and is obtained by averaging the full Hamiltonian over the lattice coordinates,

$$\hat{H}_S = \text{Tr}_f \left\{ \hat{H} \right\}. \quad (1.7)$$

The nuclear spin Hamiltonian contains only nuclear spin operators and some phenomenological constants [Ern87]. In solid state NMR we are going to distinguish nuclear spin interactions between external fields and internal fields, and the nuclear spin Hamiltonian \hat{H}_S can be written

$$\hat{H}_S = \hat{H}_{ext} + \hat{H}_{int}, \quad (1.8)$$

where

$$\hat{H}_{ext} = \hat{H}_Z + \hat{H}_{RF} \quad \text{and} \quad \hat{H}_{int} = \hat{H}_{CS} + \hat{H}_D + \hat{H}_J + \hat{H}_Q, \quad (1.9)$$

where \hat{H}_Z , \hat{H}_{RF} , \hat{H}_{CS} , \hat{H}_D , \hat{H}_J , and \hat{H}_Q are **Zeeman**, **radio-frequency field**, **chemical shift**, **direct spin-spin**, **indirect spin-spin**, and **quadrupole** interactions, respectively.

If we assume a strong external magnetic field \vec{B}_0 ($B_0 \gg 1$ T) thus the **Zeeman** interaction \hat{H}_Z has the dominant contribution to the spin Hamiltonian \hat{H}_S :

$$\hat{H}_Z = -\vec{M} \cdot \vec{B}_0, \quad (1.10)$$

where \vec{M} is the macroscopic magnetization of the nuclear spins I^i . All other terms (except \hat{H}_Q) can be written as perturbations. If we assume the orientation of the external magnetic field to the z-direction $\vec{B}_0 = B_0 \vec{e}_z$ of a laboratory system, equation (1.10) may be expressed as

$$\hat{H}_Z = - \sum_i \gamma_i B_0 \hat{I}_z^i = \sum_i \omega_{0,i} \hat{I}_z^i, \quad (1.11)$$

where the Larmor frequency $\omega_{0,i}$ of spin i is defined through the magnetogyric ratio γ_i and the strength of the external magnetic field

$$\omega_{0,i} = -\gamma_i B_0. \quad (1.12)$$

All measurements in this work were done under the external magnetic field $B_0 = 9.4$ T which corresponds to the Larmor frequency for protons 1H : $\omega_{0,{}^1H}/2\pi = 400$ MHz and for carbons ${}^{13}C$: $\omega_{0,{}^{13}C}/2\pi = 100$ MHz.

Radio-frequency (r.f.) field interaction $\hat{\mathbf{H}}_{RF}$ has the same form as the Zeeman interaction

$$\hat{\mathbf{H}}_{RF}(t) = - \sum_i \gamma_i \vec{\mathbf{I}}^i \cdot \vec{\mathbf{B}}_1(t). \quad (1.13)$$

The applied r.f. field $\vec{\mathbf{B}}_1$ oscillate with the frequency ω_1 and is normally linearly polarized with the phase φ

$$\vec{\mathbf{B}}_1(t) = 2 B_1 \cos(\omega_1 t) [\vec{\mathbf{e}}_x \cos \varphi + \vec{\mathbf{e}}_y \sin \varphi]. \quad (1.14)$$

In this conditions equation (1.13) can be written in the form:

$$\hat{\mathbf{H}}_{RF}(t) = - 2 B_1 \cos(\omega_1 t) \sum_i \gamma_i \left\{ \hat{\mathbf{I}}_x^i \cos \varphi + \hat{\mathbf{I}}_y^i \sin \varphi \right\}. \quad (1.15)$$

To solve the density operator equation (1.2), it is advisable to make the r.f. field Hamiltonian time independent by the transformation in to the *rotating frame*. In general a Hamiltonian $\hat{\mathbf{H}}(t) = \hat{\mathbf{H}}_Z + \hat{\mathbf{H}}_1(t)$ can be transformed to the $\hat{\mathbf{H}}_Z$ -interaction representation by the transformation [SR94]

$$\hat{\mathbf{H}}^r = e^{i\hat{\mathbf{H}}_Z t} \hat{\mathbf{H}}(t) e^{-i\hat{\mathbf{H}}_Z t} = \hat{\mathbf{H}}_Z + e^{i\hat{\mathbf{H}}_Z t} \hat{\mathbf{H}}_1(t) e^{-i\hat{\mathbf{H}}_Z t}. \quad (1.16)$$

The transformation of the r.f. field Hamiltonian to the *rotating frame* as follows from the equation (1.16) can be written as

$$\hat{\mathbf{H}}_{RF}^r = e^{i\hat{\mathbf{H}}_Z t} \hat{\mathbf{H}}_{RF}(t) e^{-i\hat{\mathbf{H}}_Z t}. \quad (1.17)$$

After assumption $\hat{\mathbf{H}}_Z = \sum_i \omega_{0,i} \hat{\mathbf{I}}_z^i$ (see equation (1.11)) and the basics trigonometric relations, equation (1.17) may be expressed as

$$\hat{\mathbf{H}}_{RF}^r = - 2 B_1 \cos(\omega_1 t) \sum_i \gamma_i \left\{ \hat{\mathbf{I}}_x^i \cos(\omega_{0,i} t - \varphi) - \hat{\mathbf{I}}_y^i \sin(\omega_{0,i} t - \varphi) \right\}. \quad (1.18)$$

Further mergence of the trigonometric functions in the equation (1.18) will lead to the equation which contains two sets of coefficients $\omega_1 + \omega_{0,i}$, $\omega_1 - \omega_{0,i}$ as an arguments in the *cos*, *sin* functions, respectively. Choosing $\omega_1 \simeq \omega_{0,i}$, the oscillations at frequencies $\omega_1 + \omega_{0,i} \simeq 2\omega_{0,i}$ can be neglected since the nuclear magnetization is influenced appreciably only by fields rotating with the angular frequency close to the nuclear Larmor frequency $\omega_{0,i}$. It can be written that

$$\hat{\mathbf{H}}_{RF}^r = -B_1 \sum_i \gamma_i \left\{ \hat{\mathbf{I}}_x^i \cos(\Omega_i t + \varphi) + \hat{\mathbf{I}}_y^i \sin(\Omega_i t + \varphi) \right\}, \quad (1.19)$$

where $\Omega_i = \omega_1 - \omega_{0,i}$ is the offset with respect to the carrier frequency ω_1 . If the spins are in resonance ($\Omega_i \simeq 0$) the r.f. field Hamiltonian became explicitly time independent and it may be written in the form of

$$\hat{\mathbf{H}}_{RF}^r = -B_1 \sum_i \gamma_i \left\{ \hat{\mathbf{I}}_x^i \cos(\varphi) + \hat{\mathbf{I}}_y^i \sin(\varphi) \right\}. \quad (1.20)$$

The **chemical shift** Hamiltonian $\hat{\mathbf{H}}_{CS}$ describes the shielding of the nuclear spin from the external $\vec{\mathbf{B}}_0$ field by the electron clouds. Due to the strong $\vec{\mathbf{B}}_0$ field the orbital angular momentum of the electron cloud is partially aligned in the external field direction which generate local field $\vec{\mathbf{B}}_S$ scaled with the $\vec{\mathbf{B}}_0$ field, $\vec{\mathbf{B}}_S = \tilde{\boldsymbol{\sigma}} \vec{\mathbf{B}}_0$. Under such conditions the Hamiltonian of the chemical shift leads ([Meh83], p.11 and Appendix A):

$$\hat{\mathbf{H}}_{CS} = \sum_i \gamma_i \vec{\mathbf{I}}^i \cdot \tilde{\boldsymbol{\sigma}}^{i,LF} \cdot \vec{\mathbf{B}}_0 = - \sum_i \omega_{0,i} \left\{ \hat{\mathbf{I}}_x^i \sigma_{xz}^{i,LF} + \hat{\mathbf{I}}_y^i \sigma_{yz}^{i,LF} + \hat{\mathbf{I}}_z^i \sigma_{zz}^{i,LF} \right\}. \quad (1.21)$$

The $\vec{\mathbf{B}}_0$ field was chosen to the z-direction (0,0, B_0). The $\tilde{\boldsymbol{\sigma}}^{i,LF}$ represent the chemical-shift (CS) tensor in the laboratory-frame representation with elements $\tilde{\boldsymbol{\sigma}}_{\alpha\beta}^{i,LF}$ ($\alpha, \beta = x, y, z$). In the case of high external fields ($B_0 \gg 1$ T), local fields felt by ^1H , ^2H , ^{13}C , ^{15}H , ^{19}F , ^{29}Si , or ^{31}P nuclei are smaller compared with B_0 field and CS Hamiltonian (equation (1.21)) can be simplified assuming first-order perturbation theory so

$$\hat{\mathbf{H}}_{CS} = - \sum_i \omega_{0,i} \hat{\mathbf{I}}_z^i \sigma_{zz}^{i,LF}. \quad (1.22)$$

The asymmetric components $\frac{1}{2}(\tilde{\boldsymbol{\sigma}} - \tilde{\boldsymbol{\sigma}}^T)$ of the CS tensor $\tilde{\boldsymbol{\sigma}}$ contribute to the resonance frequency shift only in the second order and can be usually neglected ([Meh83], Appendix C). The symmetric part of the CS tensor $\frac{1}{2}(\tilde{\boldsymbol{\sigma}} + \tilde{\boldsymbol{\sigma}}^T)$ is characterized most conveniently in the coordinate system in which it is diagonal. This is the 'principal axes system' (PAS). For polar coordinate system where φ and ϑ are the polar coordinates of $\vec{\mathbf{B}}_0$ in PAS, equation (1.22) with the CS tensor $\tilde{\boldsymbol{\sigma}}$ and its eigenvalues σ_{xx}^{PAS} , σ_{yy}^{PAS} , and σ_{zz}^{PAS} , may be for a single spin written [SR94] as

$$\hat{\mathbf{H}}_{CS} = \left\{ -\omega_0 \sigma_{iso} + \frac{1}{2} \delta (3 \cos^2 \vartheta - 1 - \eta \sin^2 \vartheta \cos 2\varphi) \right\} \hat{\mathbf{I}}_z, \quad (1.23)$$

where

$$\begin{aligned} \sigma_{iso} &= \frac{1}{3} \{ \sigma_{xx}^{\text{PAS}} + \sigma_{yy}^{\text{PAS}} + \sigma_{zz}^{\text{PAS}} \} \\ \delta &= -\omega_0 (\sigma_{zz}^{\text{PAS}} - \sigma_{iso}) \\ \eta &= \frac{\sigma_{yy}^{\text{PAS}} - \sigma_{xx}^{\text{PAS}}}{\sigma_{zz}^{\text{PAS}} - \sigma_{iso}} \end{aligned} \quad (1.24)$$

are the isotropic chemical shift parameter, the anisotropy parameter and the asymmetry parameter, respectively. The first part of the equation (1.23) corresponds to an isotropic frequency and the second part to an anisotropic frequency. To make the CS interaction independent on the magnetic field B_0 it is useful to measure it in dimensionless units independent to each nucleus ($\omega_{0,i} \cdot 10^{-6}$). The scale is called ppm-scale. The typical values for protons ^1H lays between 0 and 10 ppm.

The **direct spin-spin** interaction among spin i and j can be described by **dipolar** Hamiltonian \hat{H}_D according to the Correspondence Principle

$$\hat{H}_D = - \sum_{i < j} \frac{\mu_0 \hbar}{4\pi} \gamma_i \gamma_j \frac{3 \left(\vec{\hat{I}}^i \cdot \vec{e}_r^{ij} \right) \left(\vec{\hat{I}}^j \cdot \vec{e}_r^{ij} \right) - \vec{\hat{I}}^i \cdot \vec{\hat{I}}^j}{|\vec{r}_{ij}|^3} \quad (1.25)$$

$$= \sum_{i < j} \vec{\hat{I}}^i \cdot \tilde{\mathbf{D}}^{ij} \cdot \vec{\hat{I}}^j, \quad (1.26)$$

where \vec{r}_{ij} determines the vector from nucleus i to nucleus j with its basis vector $\vec{e}_r^{ij} = \vec{r}_{ij} / |\vec{r}_{ij}|$. $\tilde{\mathbf{D}}^{ij}$ represents the dipolar coupling tensor in the appropriate base defined through \vec{e}_r^{ij} vector. The dipolar-coupling constant is measured in the angular frequency units and is defined as

$$d_{ij} = \frac{\mu_0 \hbar}{4\pi} \frac{\gamma_i \gamma_j}{r_{ij}^3}. \quad (1.27)$$

For example, we calculate that for $^1\text{H} - ^1\text{H}$ spin pair in a CH_2 group ($\gamma_{^1\text{H}} = 2.675 \times 10^8 \text{ T}^{-1}\text{s}^{-1}$) with a distance of 1.8 Å (0.18 nm), the coupling strength is $d_{^1\text{H}-^1\text{H}} = 105.4 \text{ kHz} \times (2.675)^2 / (1.8)^3 = 2\pi \times 20.6 \text{ kHz}$. In the case of high static field (similar like for the CS interaction) only those components of the Hamiltonian contribute to the spectrum in the first order approximation which are time independent and the Hamiltonian defined by equation (1.25) can be truncated. For homonuclear dipolar interactions between spins I^i the truncated Hamiltonian can be written [Meh83] as

$$\hat{H}_D^{II} = - \sum_{i < j} d_{ij}^{II} \frac{1}{2} (3 \cos^2 \vartheta_{ij} - 1) \left(3 \hat{I}_z^i \hat{I}_z^j - \vec{\hat{I}}^i \cdot \vec{\hat{I}}^j \right). \quad (1.28)$$

Angle ϑ_{ij} is the angle between the magnetic field B_0 and the vector \vec{e}_r^{ij} connecting spin I^i and I^j (Index $\{II\}$ on the dipolar-coupling constant d_{ij} represent the equivalence of nuclei: $\gamma_i = \gamma_j = \gamma_I$). The truncated Hamiltonian of heteronuclear dipolar couplings is given by (I^i and S^i spins)

$$\hat{H}_D^{IS} = - \sum_{i,j} d_{ij}^{IS} \frac{1}{2} (3 \cos^2 \vartheta_{ij} - 1) 2 \hat{I}_z^i \hat{S}_z^j. \quad (1.29)$$

The **indirect spin-spin** coupling (J -coupling), which result from electron-nuclear interactions have the form

$$\hat{H}_J = - \sum_{i < j} \vec{\hat{I}}^i \cdot \tilde{\mathbf{J}}^{ij} \cdot \vec{\hat{I}}^j, \quad (1.30)$$

where $\tilde{\mathbf{J}}^{ij}$ is the indirect spin-spin coupling tensor. On contrary to the direct coupling between spins (dipolar coupling) the J -coupling provide an information about the connectivities of the electron clouds surrounding nuclei to the neighboured nuclear spins I^i . Usually it is very weak ($\approx 100\text{Hz}$) and in the solid-state NMR it can be neglected. In liquids, in the case of high static external field B_0 only the scalar component of the J -coupling tensor ($J_{ij} = \frac{1}{3}\text{Tr}\{\tilde{\mathbf{J}}\}$) contribute to the spectrum and the time independent part of the Hamiltonian 'secular part' reads:

$$\hat{H}_J = - \sum_{i < j} J_{ij} \hat{I}_z^i \hat{I}_z^j. \quad (1.31)$$

Nuclei with $I^i \geq 1$ generates electric field gradients with the nuclear **quadrupole** moment Q^i and their interaction with other nuclei can be described by the Hamiltonian

$$\hat{H}_Q = \sum_i \frac{eQ^i}{2I^i(2I^i - 1)\hbar} \vec{\hat{I}}^i \cdot \tilde{\mathbf{V}}^i \cdot \vec{\hat{I}}^i, \quad (1.32)$$

where $\tilde{\mathbf{V}}^i$ is the electric field gradient tensor at the site of nucleus i and e is the elementary charge. After averaging ($B_0 \gg 1 \text{ T}$) the secular part of the **quadrupolar** Hamiltonian can be written in the form [SR94] of

$$\hat{H}_Q = \sum_i \frac{eQ^i}{2I^i(2I^i - 1)\hbar} V_{zz}^{i,LF} \frac{1}{2} \left(3 \hat{I}_z^i \hat{I}_z^i - \vec{\hat{I}}^i \cdot \vec{\hat{I}}^i \right). \quad (1.33)$$

Typical values for quadrupolar coupling are in the range 200 kHz–2 GHz (Br, I, As, ...). In this work the quadrupolar coupling has no importance because we were concentrated to the nuclei with spin $I = \frac{1}{2}$ and in such cases it vanishes.

1.2 Equilibrium density operator

The density operator represents a valid synthesis of quantum mechanics with statistical mechanics. In thermal equilibrium at a temperature T and with Hamiltonian \hat{H} of the system, the density operator of the spin system is analogous to the classical Boltzmann distribution (we will reintroduce for a moment \hbar into Hamiltonian \hat{H} in order to obtain unitless ratio $\hbar\gamma B_0/k_B T$)

$$\hat{\rho}_{eq} = \frac{e^{-\hbar \hat{H}/k_B T}}{Z} \quad \text{with} \quad Z = \text{Tr} \left\{ e^{-\hbar \hat{H}/k_B T} \right\}, \quad (1.34)$$

where k_B is the Boltzmann constant. The dominant contribution to the spin Hamiltonian \hat{H} has the Zeeman interaction (equation (1.11)) for a B_0 fields stronger than 1 Tesla and for individual spins can be written

$$\hat{\rho}_{eq}^i = \frac{e^{-\frac{\hbar\omega_{0,i}}{k_B T} \hat{I}_z^i}}{Z^i}. \quad (1.35)$$

At temperatures above 1 K in the fields currently available $|\hbar\omega_0| \gg k_B T$, exponential function in equation (1.35) can be expanded so that the quadratic and all higher terms vanish compared to the linear term

$$e^{-\frac{\hbar\omega_{0,i}}{k_B T} \hat{I}_z^i} \simeq \hat{\mathbf{1}}^i - \frac{\hbar\omega_{0,i}}{k_B T} \hat{I}_z^i. \quad (1.36)$$

The denominator of equation (1.35) corresponds to all possible states of the system $2I^i + 1$ and for N equivalent spins equilibrium density operator takes a form

$$\hat{\rho}_{eq} \simeq \frac{N}{(2I + 1)^N} \left(\hat{\mathbf{1}} - \frac{\hbar\omega_0}{k_B T} \hat{I}_z \right). \quad (1.37)$$

The unity operator $\hat{\mathbf{1}}$ commutes with all operators and is irrelevant in most cases. According to equation (1.37) it can be defined the initial density operator of the system so

$$\hat{\rho}(0) \stackrel{\text{def}}{=} c \hat{I}_z, \quad (1.38)$$

where $c = -\hbar\omega_0/k_B T$.

1.3 Average Hamiltonian theory

In NMR the spin interaction Hamiltonian is usually time-dependent and it is much more convenient to describe an experiment by the average Hamiltonian ([Hae76]) which represent the 'average' motion of the spin system. Most of the multiple quantum experiments can be described by an average Hamiltonian theory and this is the goal of this work.

In general the Hamiltonian in the rotating frame is split into two parts (equation (1.8))

$$\hat{H} = \hat{H}_{ext}(t) + \hat{H}_{int}, \quad (1.39)$$

where \hat{H}_{ext} and \hat{H}_{int} are defined by the equation (1.9). To find the solution for the density operator equation (equation (1.2)) one has to derive the time evolution propagator

$$\hat{U}(t) = \hat{T} e^{-i \int_0^t dt' (\hat{H}_{ext}(t') + \hat{H}_{int})}. \quad (1.40)$$

\hat{T} is the Dyson time-ordering operator (see also equation (1.4)) defined through the following relations

$$\hat{T} \left\{ \hat{H}(t_1) \hat{H}(t_2) \right\} = \begin{cases} \hat{H}(t_1) \hat{H}(t_2) & \text{for } t_1 > t_2 \\ \hat{H}(t_2) \hat{H}(t_1) & \text{for } t_1 < t_2. \end{cases} \quad (1.41)$$

Now we attempt to separate the effects of explicitly time-independent Hamiltonian \hat{H}_{int} and time-dependent Hamiltonian $\hat{H}_{ext}(t)$ and to divide the propagator from the equation (1.40) into two products

$$\hat{U}(t) = \hat{U}_1(t) \hat{U}_{int}(t) \quad (1.42)$$

with

$$\hat{U}_1(t) = \hat{T} e^{-i \int_0^t \hat{H}_{ext}(t') dt'} \quad (1.43)$$

and

$$\hat{U}_{int}(t) = \hat{T} e^{-i \int_0^t \hat{\tilde{H}}(t') dt'}, \quad (1.44)$$

where $\hat{U}_1(t)$ depends only on the perturbation $\hat{H}_{ext}(t)$. $\hat{\tilde{H}}(t)$ in equation (1.44) is the Hamiltonian in the time-dependent interaction representation with respect to $\hat{H}_{ext}(t)$, often called the *toggling frame*. To assume \hat{H} Hermitian it follows $\hat{U}^+(t) = \hat{U}^{-1}(t)$ and the initially time-dependent toggling frame Hamiltonian can be written

$$\hat{\tilde{H}}(t) = \hat{U}_1^{-1}(t) \hat{H}_{int} \hat{U}_1(t). \quad (1.45)$$

We can further assume, that the external field may be periodic with a period τ_c i.e.

$$\hat{H}_{ext}(t + n \tau_c) = \hat{H}_{ext}(t); \quad n = 0, 1, 2, \dots \quad (1.46)$$

which is for our cases good fulfilled (see chapter 2). From equation (1.46) follows

$$\hat{U}_1(n \tau_c) = \hat{U}_1^n(\tau_c) \quad (1.47)$$

and it also leads to a periodicity of toggling frame Hamiltonian with

$$\hat{\tilde{H}}(t) = \hat{\tilde{H}}(t + n \tau_c) \quad (1.48)$$

and

$$\hat{U}_{int}(n \tau_c) = \hat{U}_{int}^n(\tau_c). \quad (1.49)$$

If in addition the external field is cyclic in the sense

$$\hat{U}_1(\tau_c) = \hat{\mathbf{1}}, \quad (1.50)$$

the general propagator $\hat{U}(\tau_c)$ (equation (1.42)) is described by the one cycle propagator $\hat{U}_{int}(\tau_c)$ i.e.

$$\hat{U}(\tau_c) = \hat{U}_{int}(\tau_c) \quad \text{and} \quad \hat{U}(n\tau_c) = \hat{U}_{int}^n(\tau_c). \quad (1.51)$$

Our goal is to express equation (1.44) in the sense

$$\hat{U}_{int}(\tau_c) = e^{-i\hat{H}\tau_c}, \quad (1.52)$$

where \hat{H} is an average Hamiltonian and it can be divided into contributions from different orders

$$\hat{H} = \hat{H}^{(0)} + \hat{H}^{(1)} + \hat{H}^{(2)} + \dots \quad (1.53)$$

Using Magnus expansion [Ern87] which forms the basis of average Hamiltonian theory it can be written

$$\hat{H}^{(0)} = \frac{1}{\tau_c} \int_0^{\tau_c} dt \hat{H}(t) \quad (1.54)$$

$$\hat{H}^{(1)} = \frac{-i}{2\tau_c} \int_0^{\tau_c} dt_2 \int_0^{t_2} dt_1 [\hat{H}(t_2), \hat{H}(t_1)] \quad (1.55)$$

$$\begin{aligned} \hat{H}^{(2)} = & -\frac{1}{6\tau_c} \int_0^{\tau_c} dt_3 \int_0^{t_3} dt_2 \int_0^{t_2} dt_1 \left\{ [\hat{H}(t_3), [\hat{H}(t_2), \hat{H}(t_1)]] \right. \\ & \left. + [\hat{H}(t_1), [\hat{H}(t_2), \hat{H}(t_3)]] \right\}. \quad (1.56) \end{aligned}$$

In most cases multiple-pulse sequences are designed to remove higher terms $\hat{H}^{(1)}, \dots$ from average Hamiltonian and only zero-order $\hat{H}^{(0)}$ term survive. Zero-order term has a particularly simple form. It is just the time average of the toggling frame Hamiltonian $\hat{H}(t)$ and it has the most importance for the multiple-pulse sequences which we will investigate in this work.

1.4 Dipolar interaction and irreducible tensors

In this section we would like to represent dipolar Hamiltonian introduced at the page 10 in another form i.e. with the help of irreducible spherical tensors. This representation of spin Hamiltonian is much more convenient in the case of magic-angle-spinning experiment described in the section 1.6.

The spin interaction Hamiltonian may be expressed in the terms of irreducible spherical tensors as [Meh83, Spi78, SR94]

$$\hat{H} = \sum_{k=0}^2 \sum_{q=-k}^{+k} (-1)^q A_{k,q} \hat{T}_{k,-q}, \quad (1.57)$$

where $A_{k,q}$ contains all lattice and $\hat{T}_{k,q}$ all spin variables. Due to the fact that the spin interactions in NMR are expressed by second rank tensors the summation in equation (1.57) goes only until $k = 2$. In the high field case ($B_0 \gg 1$ T) all terms with $q \neq 0$ are neglected in the first order approximation and only secular terms ($q = 0$) remains. In addition antisymmetric part with $k = 1$ of spin interactions does not contribute to the spectrum in the first order and can also be neglected ([Meh83] p.41). Under these conditions equation (1.57) is reduced to

$$\hat{H}^{(0)} = A_{0,0} \hat{T}_{0,0} + A_{2,0} \hat{T}_{2,0}. \quad (1.58)$$

In the case of dipolar coupling due to the symmetry of dipolar coupling tensor \tilde{D} $A_{0,0} = 0$ ($A_{0,0} = -\frac{1}{\sqrt{3}} \text{Tr}\{D_{ij}\}$) and equation (1.58) for homonuclear coupling may be expressed in the form¹

$$\hat{H}_D = - \sum_{i < j} d_{ij}^{II} R_{2,0}^{ij} \hat{T}_{2,0}^{ij} \quad (1.59)$$

with

$$R_{2,0}^{ij} = \sqrt{\frac{3}{2}} (3 \cos^2 \vartheta_{ij} - 1) \quad (1.60)$$

$$\hat{T}_{2,0}^{ij} = \frac{1}{\sqrt{6}} (3 \hat{I}_z^i \hat{I}_z^j - \vec{I}^i \cdot \vec{I}^j). \quad (1.61)$$

$R_{2,0}^{ij}$ contains only pure geometrical variables and d_{ij}^{II} is the dipolar-coupling constant defined by equation (1.27). With the help of spherical harmonics $Y_{2,q}$, geometrical parameter $R_{2,q}$ can be defined in more general way

$$R_{2,q} = \sqrt{\frac{24\pi}{5}} Y_{2,q}. \quad (1.62)$$

Definitions of $Y_{k,q}$ can be found in [SR94] p.451.

¹We will not use the mark (0) for secular dipolar Hamiltonian to prevent interchange it with zero order average Hamiltonian using in Magnus expansion series (see equation (1.54))

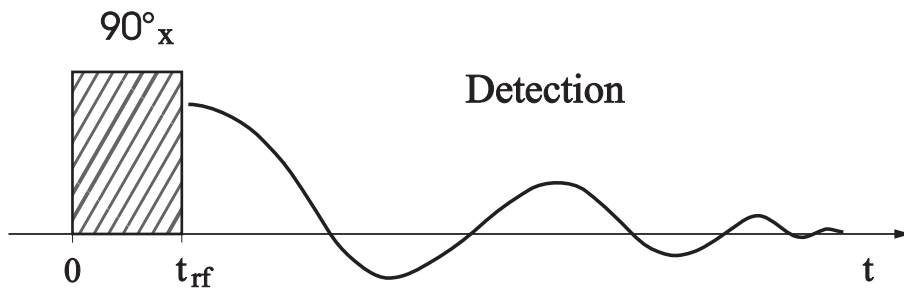


Figure 1.1: Schematic picture of one pulse experiment. The r.f. pulse is oriented in x -direction and rotates the magnetization in rotating frame about 90° ($\frac{\pi}{2}$).

1.5 One pulse experiment

The most simplest experiment in NMR is an one pulse experiment, schematically showed in Figure 1.1. The interactions between spins can be detected in the detection period just after the excitation of the system with the r.f. pulse in detection period. To describe an experiment we will assume an ensemble of equivalent spins $I^i = \frac{1}{2}$ where the initial state of the system is defined through the initial density operator (equation (1.38)). The effect of r.f. pulse in the rotating frame is described by the equation (1.20) and using equations (1.3–1.5) the density operator just after the r.f. pulse applied in the x -direction has the form

$$\hat{\rho}(t_{\text{rf}}) = e^{i\gamma B_1 t_{\text{rf}} \hat{\mathbf{I}}_x} c \hat{\mathbf{I}}_z e^{-i\gamma B_1 t_{\text{rf}} \hat{\mathbf{I}}_x}. \quad (1.63)$$

If the strength B_1 and the duration t_{rf} of the r.f. pulse matches the condition

$$\gamma B_1 t_{\text{rf}} = \frac{\pi}{2}, \quad (1.64)$$

the pulse rotate the magnetization about 90° (left handed sense rotation around x -axis using the definitions in equation (1.20) and (1.11)) equation (1.63) may be rewritten

$$\hat{\rho}(t_{\text{rf}}) = \hat{\rho}(0^+) = c \hat{\mathbf{I}}_y. \quad (1.65)$$

The state prepared by the initial pulse now decays due to the Zeeman interaction and an internal spin interaction according to the Liouville-von Neumann equation

$$\frac{d}{dt} \hat{\rho}(t) = -i[\hat{\mathbf{H}}_Z + \hat{\mathbf{H}}_{\text{int}}, \hat{\rho}(t)] \quad (1.66)$$

and the NMR decay signal can be obtained in the α ($\alpha = x, y$) direction of the rotating frame as

$$S_\alpha(t) = \frac{\text{Tr} \left\{ \hat{\mathbf{I}}_\alpha \hat{\rho}(t) \right\}}{\text{Tr} \left\{ \hat{\mathbf{I}}_z \hat{\rho}(0) \right\}}. \quad (1.67)$$

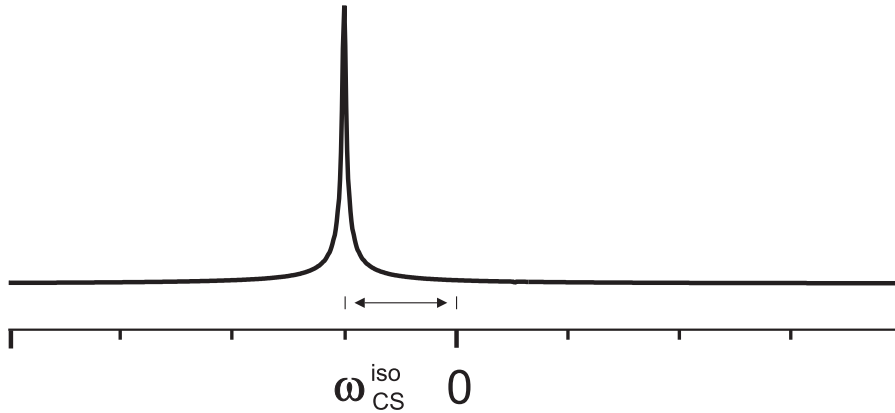


Figure 1.2: *The shift of frequency due to isotropic chemical shift interaction.*

Let us assume only isotropic chemical shift interaction ($\omega_{CS}^{iso} = \omega_0 \sigma_{iso}$) from internal Hamiltonian \hat{H}_{int} . The density operator for a single spin after the x -pulse at $t > t_{rf}$ can be found

$$\begin{aligned} \hat{\rho}(t) &= e^{i\omega_{CS}^{iso}t \hat{I}_z} \hat{\rho}(0^+) e^{-i\omega_{CS}^{iso}t \hat{I}_z} \\ &= c \left[\hat{I}_y \cos(\omega_{CS}^{iso}t) + \hat{I}_x \sin(\omega_{CS}^{iso}t) \right]. \end{aligned} \quad (1.68)$$

To evaluate the NMR signal from equation (1.68), which corresponds to the magnetization, with the help of equation (1.67) we will get

$$S_y(t) = \cos(\omega_{CS}^{iso}t) \quad (1.69)$$

and

$$S_x(t) = \sin(\omega_{CS}^{iso}t) \quad (1.70)$$

for a signal detected in the y, x -direction, respectively. Due to the strong magnetic field B_0 applied to the system, NMR signal relax with the typical relaxation time T_2 and is called FID (*free induction decay*). In modern NMR spectrometers the acquisition of both signals (equation (1.69) and (1.70)) at the same time often called *quadrature detection* is possible. After digitalization and complex fourier transformation of the data we will get a spectrum shown in Figure 1.2.

1.6 Magic Angle Spinning

One of the experimental technique to improve the resolution of NMR spectra is *magic-angle-spinning* (MAS). The sample rotates about an axis which is tilted by an angle ϑ_m

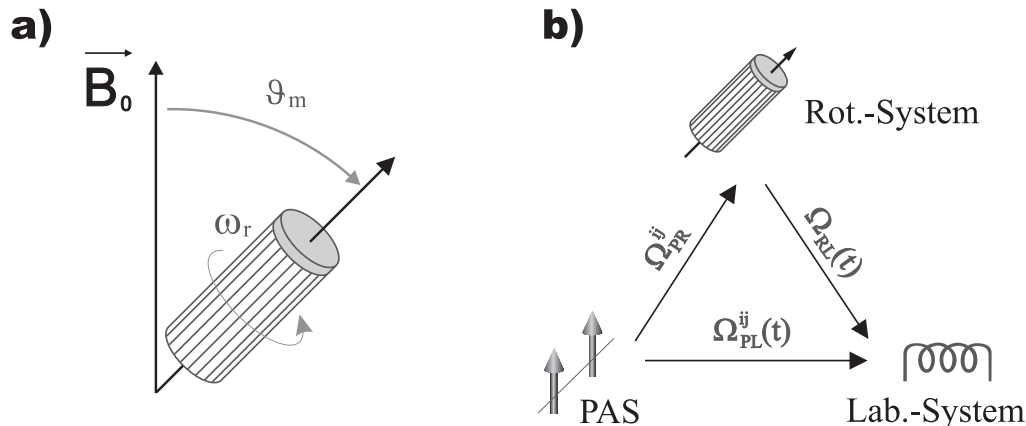


Figure 1.3: a) Schematic description of MAS where rotor axis is tilted from the \vec{B}_0 field by the angle $\vartheta_m = 54.7^\circ$. b) Relative orientation of PAS and LabS under sample rotation described by the angle $\Omega_{PL}^{ij}(t)$, which is built up by two successive rotational transformations with angles Ω_{PR}^{ij} and $\Omega_{RL}(t)$.

(called 'magic angle') with respect to the magnetic field \vec{B}_0 (see Figure 1.3a). It was noted independently by Andrew ([And58]) and Lowe ([Low58]) that in such a case dipolar interactions and chemical shift anisotropy are averaged out from the spectrum and usually only narrow isotropic lines remains. If the spinning rate ω_r of the sample is much larger than the anisotropic spin interaction the spinning sidebands² are well separated from the isotropic lines and became vanishingly small with increasing ω_r . We are going to consider only dipolar spin interactions in this section because this is of main interest in this work.

To derive dipolar Hamiltonian under MAS lets start with a little bit different representation of geometrical part of the Hamiltonian used in equations (1.59) and (1.60)

$$R_{2,0}^{ij} = \sqrt{6} \mathcal{D}_{0,0}^{(2)}(\Omega_{PL}^{ij}), \quad (1.71)$$

where the Wigner rotation matrices $\mathcal{D}_{k,q}^{(2)}$ can be found in Appendix B. The Euler angle $\Omega_{PL}^{ij} = (\varphi_{PL}^{ij}, \vartheta_{PL}^{ij}, \psi_{PL}^{ij})$ specify the relative orientation of two coordinate systems i.e. Principle axis system (PAS) and Laboratory system (LabS). If the sample rotate about an axis tilted by an angle ϑ_{RL} from the main field \vec{B}_0 director the geometrical part $R_{2,0}^{ij}$ became time dependent $R_{2,0}^{ij}(t)$. It is convenient to describe it by two successive rotations (see Figure 1.3b) and by the time dependent rotation matrix $\mathcal{D}_{0,0}^{(2)}(t)$. According to

²Additional lines in the spectrum originating from the sample rotation, separated from the isotropic line exactly at the rotor frequency intervals.

equation (B.2) it can be written as

$$\mathcal{D}_{0,0}^{(2)}(\Omega_{PL}^{ij}(t)) = \sum_{q=-2}^2 \mathcal{D}_{0,q}^{(2)}(\Omega_{PR}^{ij}) \mathcal{D}_{q,0}^{(2)}(\Omega_{RL}(t)), \quad (1.72)$$

where Ω_{PR}^{ij} corresponds to the relative orientation of PAS and *Rotor system* and $\Omega_{RL}(t)$ describe the rotation of the rotor seen from the *Laboratory system* through the Wigner matrices (see equation (B.1))

$$\mathcal{D}_{q,0}^{(2)}(\Omega_{RL}(t)) = e^{-iq\varphi_{RL}(t)} d_{q,0}^{(2)}(\vartheta_{RL}). \quad (1.73)$$

Factors $d_{q,0}^{(2)}$ are defined in Table B.1. Due to the fix angle ϑ_{RL} in *Rotor system* the time dependence in equation (1.73) is introduced through an angle $\varphi_{RL}(t) = \varphi_0 + \omega_r t$ with the starting point φ_0 . Combining equations (1.71–1.73) we will get

$$R_{2,0}^{ij}(t) = \sum_{q=-2}^2 \sqrt{6} \mathcal{D}_{0,q}^{(2)}(\Omega_{PR}^{ij}) e^{-iq\varphi_0} d_{q,0}^{(2)}(\vartheta_{RL}) e^{-iq\omega_r t}, \quad (1.74)$$

where $R_{2,0}^{ij}(t)$ describes the time dependence of dipolar Hamiltonian:

$$\hat{\mathbf{H}}_D(t) = - \sum_{i<j} d_{ij}^{II} R_{2,0}^{ij}(t) \hat{\mathbf{T}}_{2,0}^{ij}. \quad (1.75)$$

It is immediately evident from equation (1.74) that rotational sidebands appear at multiples of the frequency ω_r and $2\omega_r$ away from the central isotropic lines (see Figure 1.4). Before proofing this aspect further, let us go back to the rapid spinning case. If ω_r is very large ($\omega_r \gg \|\hat{\mathbf{H}}_D\|$) or stroboscopic observation at time intervals $\tau = n 2\pi/\omega_r$ is performed, only the time independent part (with $q = 0$) of $R_{2,0}^{ij}(t)$ in equation (1.74) survives, i.e.

$$\bar{R}_{2,0}^{ij} = d_{0,0}^{(2)}(\vartheta_{RL}) R_{2,0}(\Omega_{PR}^{ij}). \quad (1.76)$$

In this case, the time independent dipolar Hamiltonian

$$\hat{\mathbf{H}}_D = -\frac{1}{2} (3 \cos^2 \vartheta_{RL} - 1) \sum_{i<j} d_{ij}^{II} R_{2,0}(\Omega_{PR}^{ij}) \hat{\mathbf{T}}_{2,0}^{ij} \quad (1.77)$$

governs the spectrum. It is evident from equation (1.77) that for the angle $\vartheta_{RL} := \vartheta_m = \arccos(\sqrt{\frac{1}{3}}) \doteq 54.7^\circ$ called '*magic angle*' the dipolar coupling Hamiltonian vanish and only isotropic part of the secular Hamiltonian remain ([Meh83]).

In the case of moderate spinning speed $\omega_r \simeq \|\hat{\mathbf{H}}_D\|$ dipolar coupling influence the spectrum and the spinning sidebands become visible. Analytical description of this situation is for the behaviour of the spin system with many spins usually very complicated due

to the complexity of the dipolar Hamiltonian in equation (1.75). Therefore it will be made only for two dipolar coupled spins- $\frac{1}{2}$. After applying 90° -pulse in the x -direction of the rotating frame the initial state of the system for I^i and I^j spins is according to equation (1.65) given by

$$\hat{\rho}(0^+) = c \left(\hat{\mathbf{I}}_y^i + \hat{\mathbf{I}}_y^j \right). \quad (1.78)$$

The time evolution of the density matrix is described by the Liouville-von Neumann equation (1.2) with its formal solution in equation (1.3). The Dyson time-ordering operator in equation (1.4) has for two spin system no importance and the Liouville-von Neumann equation can be formally solved (see also Table A.1 and equation (A.4)):

$$\begin{aligned} \hat{\rho}(t) &= e^{-i \int_0^t \hat{\mathbf{H}}_D(t') dt'} \hat{\rho}(0^+) e^{i \int_0^t \hat{\mathbf{H}}_D(t') dt'} \\ &= c e^{i \int_0^t dt' d_{ij}^{II} R_{2,0}^{ij}(t') \hat{\mathbf{T}}_{2,0}^{ij}} \left(\hat{\mathbf{I}}_y^i + \hat{\mathbf{I}}_y^j \right) e^{-i \int_0^t dt' d_{ij}^{II} R_{2,0}^{ij}(t') \hat{\mathbf{T}}_{2,0}^{ij}} \\ &= c \left(\hat{\mathbf{I}}_y^i + \hat{\mathbf{I}}_y^j \right) \cos \left[\int_0^t \omega_D^{ij}(t') dt' \right] - 2c \left(\hat{\mathbf{T}}_{2,1}^{ij} - \hat{\mathbf{T}}_{2,-1}^{ij} \right) \sin \left[\int_0^t \omega_D^{ij}(t') dt' \right] \end{aligned} \quad (1.79)$$

with

$$\omega_D^{ij}(t) = \sqrt{\frac{3}{8}} d_{ij}^{II} R_{2,0}^{ij}(t). \quad (1.80)$$

The products with $\hat{\mathbf{T}}_{2,\pm 1}^{ij}$ have no influence on the signal detected in $\alpha = x, y$ direction of the rotating frame because their trace vanish

$$\mathbf{Tr} \left\{ \hat{\mathbf{I}}_\alpha^i \hat{\mathbf{T}}_{2,\pm 1}^{ij} \right\} = \mathbf{Tr} \left\{ \hat{\mathbf{I}}_\alpha^j \hat{\mathbf{T}}_{2,\pm 1}^{ij} \right\} = 0 \quad (1.81)$$

and can be neglected. According to equation (1.67) the NMR decay signal in the y -direction of the rotating frame can be obtained through the trace:

$$S_y^{MAS}(t) = \frac{\mathbf{Tr} \left\{ \left(\hat{\mathbf{I}}_y^i + \hat{\mathbf{I}}_y^j \right) \hat{\rho}(t) \right\}}{\mathbf{Tr} \left\{ \left(\hat{\mathbf{I}}_z^i + \hat{\mathbf{I}}_z^j \right) \hat{\rho}(0) \right\}} = \cos \left[\int_0^t \omega_D^{ij}(t') dt' \right]. \quad (1.82)$$

To calculate the integral of the $\omega_D^{ij}(t)$ function defined by equation (1.80) it is convenient to neglect initial starting point of the rotor $\varphi_0 = 0$ (see equation (1.74)). Also coefficient $d_{q,0}(\vartheta_m)$ with $q = 0$ under MAS conditions vanish and equation (1.82) can be solved [Got95]

$$\begin{aligned} S_y^{MAS}(t) &= \left\langle \cos \left\{ \frac{3}{2} \frac{d_{ij}^{II}}{\omega_r} \left[\sqrt{2} \sin(2\vartheta^{ij}) \sin\left(\frac{1}{2}\omega_r t\right) \cos(\psi^{ij} + \frac{1}{2}\omega_r t) \right. \right. \right. \\ &\quad \left. \left. \left. - \frac{1}{2} \sin^2(\vartheta^{ij}) \sin(\omega_r t) \cos(2\psi^{ij} + \omega_r t) \right] \right\} \right\rangle, \end{aligned} \quad (1.83)$$

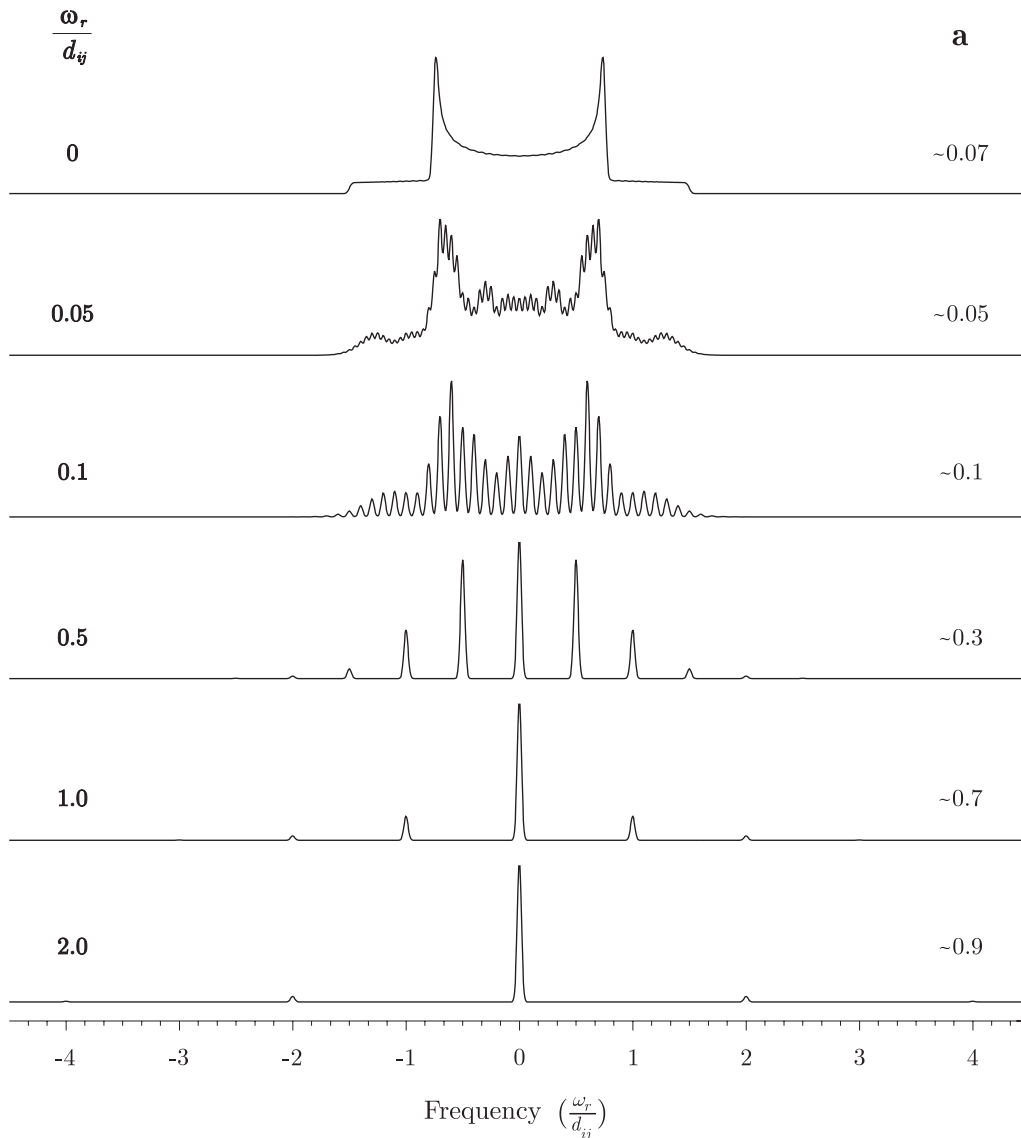


Figure 1.4: Simulated spinning sideband pattern of single MAS experiment for different ratios between rotational frequency ω_r and dipole-dipole coupling d_{ij}^{II} ($\frac{\omega_r}{d_{ij}}$). Parameter **a** represents the amplitude of the highest point in each spectrum. Theoretical signal intensity (see equation (1.83)) is multiplied with Gaussian decay function to simulate more or less experimental FID.

where $\langle \dots \rangle$ means the powder averaging over the orientation of the dipolar coupled spin pairs. Analysing equation (1.83) it can be directly seen that for times $t = k \cdot \tau_r$ ($k \in \mathbf{N}$) the argument of the *cos* function vanish because $\sin(\frac{1}{2}\omega_r t) = 0$ as well as $\sin(\omega_r t) = 0$ so the signal becomes maximal for this time points. In addition intensity of the signal strongly depends on the orientation of the PAS to the rotor system. If PAS is oriented along the rotor axes i.e. $\vartheta_{ij} = 0$ signal will be constant and no rotor modulation can be

seen. For another orientation of the PAS system rotor modulation of the signal will be already preset. The Fourier transformation of equation (1.83) directly leads to the NMR spectrum with the sideband pattern. Simulated results³ for powder sample are shown in Figure 1.4 for different ratios between rotational frequency ω_r and dipolar coupling d_{ij}^{II} . Static spectrum of dipolar coupled spin- $1/2$ pair ($\frac{\omega_r}{d_{ij}^{II}} = 0$ in the figure) is clearly split to the sideband pattern spectra with increasing spinning speed. At higher rotational frequencies ($\omega_r > 0.5 d_{ij}^{II}$) central line already dominate the spectrum. Further increasing of ω_r leads to decreasing spinning sidebands as well as to increasing intensity of the central line as it is indicated in Figure 1.4. Experimental results from MAS experiment can be found in section 3.1.

1.7 Two-dimensional NMR spectroscopy

Up to now only one-dimensional (1D) spectroscopy has been considered where signal intensity is plotted only along one frequency axis. One r.f. pulse has been used to disturb the spin system from its equilibrium. Just after that the system has been evolved under the influence of local interactions as FID (*free induction decay*), $S(t_2)$, during time t_2 . Fourier transformation of $S(t_2)$ converts the time-domain signal into a frequency domain spectrum $S(\omega_2)$. In most of the cases in liquids as well as in solids the spectrum of desired sample is so complicated that lines of different nuclear species overlap and wished information can not be obtained. To overcome this difficulty a second time period, t_1 , between preparation and detection periods can be included. During this period, called evolution period, nuclear motions may be different than during t_2 which can eventually influence the signal $S(t_2)$.

An intuitive scheme of two-dimensional (2D) experiment is shown in Figure 1.5. It consist of four periods in general: preparation, evolution, mixing and detection. Mixing period is not each time necessary ([Ern87, Rah86, Fre97]). The preparation period may be formed by a series of r.f. pulses to convert the system to the desired state. It can also consist of a delay long enough to allow the nuclei to reach equilibrium. During evolution time t_1 the system propagates under the influence of some internal Hamiltonians (see section 1.1). To manipulate the spin system after the evolution period the mixing period

³Home made computer program has been used for performing integrations over angles ϑ, ψ in equation (1.83).

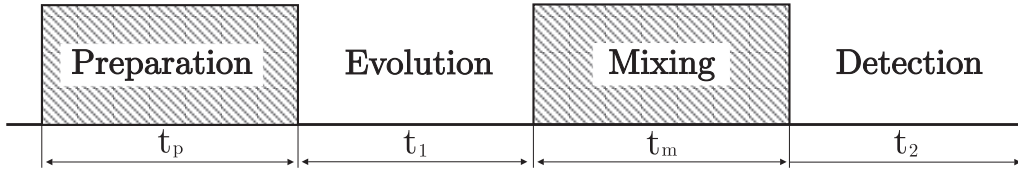


Figure 1.5: *Symbolic scheme for two-dimensional experiment.*

can be included (see e.g. [SR94]). In the last period a signal is detected for each increment of t_1 separately, thus a 2D free induction decay signal $S(t_1, t_2)$ is obtained. Double Fourier transformation of $S(t_1, t_2)$ will lead to the two-dimensional spectrum $S(\omega_1, \omega_2)$.

So far the relaxation of the time-domain signal has not been considered. Including it into FID artificial broadening of the spectrum lines is introduced. Fourier transformation (FT) of such a damping signal leads to the spectrum which can be written in terms of absorptive (A) and dispersive (D) components ([SR94]):

$$S(t_2) \xrightarrow{\text{FT}} S(\omega_2) = A(\omega_2) + i D(\omega_2) \quad (1.84)$$

In most of the cases only absorptive part $A(\omega_2)$ is interesting. It is positive definite and its integral does not vanish. Dispersive lineshape $D(\omega_2)$ exhibits antisymmetry and always consists of positive and negative intensities which superimposes in a complicated way. Thus, due to the antisymmetry, the integral over the dispersive lineshape vanishes. In addition dispersive signal has broader wings than the absorption component, resulting in a worse resolution.

In 2D spectroscopy it is often necessary to have purely absorptive spectrum $A(\omega_1)A(\omega_2)$, in short A_1A_2 , in order to have optimum resolution and no spectral distortions. However, two successive Fourier transformations, over t_2 (FT_2) and t_1 (FT_1), from the 2D time-domain signal $S(t_1, t_2)$ give the spectrum

$$S(t_1, t_2) \xrightarrow{\text{FT}_1(\text{FT}_2)} S(\omega_1, \omega_2) = (A_1A_2 - D_1D_2) + i(D_1A_2 - A_1D_2) \quad (1.85)$$

which contains a mixture of absorptive and dispersive parts. To obtain pure absorptive spectrum the data processing has to be modified (see [SR94] chapter 4, or [Ern87] chapter 6). It is often required to obtain real (cosine), S_c , and imaginary (sine), S_s , part of the time-domain signal according to t_1 . This can be written shortly ([SR94])

$$\begin{aligned} S_c(t_1, t_2) &= \cos(\tilde{\omega}_1 t_1) e^{i\tilde{\omega}_2 t_2} \\ S_s(t_1, t_2) &= i \sin(\tilde{\omega}_1 t_1) e^{i\tilde{\omega}_2 t_2}, \end{aligned}$$

where $\tilde{\omega}_1$ and $\tilde{\omega}_2$ represent schematically all components present. Performing separately for both S_c and S_s Fourier transformation and setting dispersive part to zero, $D_2 = 0$, the real part of the spectrum corresponds to

$$\text{Re}[S_{c,s}(\omega_1, \omega_2)] = \frac{1}{2} (A(\omega_1 - \tilde{\omega}_1) \pm A(\omega_1 + \tilde{\omega}_1)) A_2. \quad (1.86)$$

Adding both $S_c(\omega_1, \omega_2)$ and $S_s(\omega_1, \omega_2)$ full absorption spectrum is obtained $A_1 A_2$. This technique is usually encountered in modern NMR instruments. It requires measuring of both $S_c(t_1, t_2)$ and $S_s(t_1, t_2)$ which together represent a *hypercomplex* dataset ([Ern87]). On the other hand an equivalent absorption spectrum can be obtained by TPPI (*time-proportional phase incrementation*) method of the sampling of the data. This method will be extensively used in this work. More details about TPPI used in the connection to a multiple quantum spectroscopy can be found in sections 2.4.3, 2.5.2 and 4.2.

2D spectroscopy covers a huge part of NMR. It can be intuitively divided in three categories: separation experiments, correlation experiments and exchange experiments. Basis overview of these experiments can be found in the excellent monographs [SR94] and [Ern87]. Besides this experimental techniques 2D spectroscopy enables also to study coherent transitions which do not contribute to the magnetization and can not be detected directly. This multiple quantum transitions/coherences can be detected indirectly during time t_1 with the help of 2D Fourier spectroscopy as will be seen in next chapters.

Chapter 2

Multiple Quantum NMR

In the following sections, we want to elucidate the meaning of multiple quantum (MQ) coherence in the special case of dipolar coupled spin- $\frac{1}{2}$ systems, and to illustrate how the experiment is accomplished to produce and detect such a phenomenon. We will focus our interest to the excitation and detection of MQ and double quantum (DQ) coherence on the proton (^1H) systems under static and MAS experimental conditions, respectively.

The first experimental evidence of MQ phenomenon was made by the CW NMR spectroscopy in the end of 1950s. But until the mid 1970s the time domain MQ spectra of this kind were not investigated, because the theoretical and experimental methods of average Hamiltonian theory were not sufficiently developed. The literature overview of most of the important methods and applications of this phenomenon through 1980 can be found in [Bod81]. A highly detailed analysis of the major theoretical concepts and experimental techniques up to the middle of 1982 was made in [Wei83]. The first solid state MQ experiments were done in the group of A. Pines ([Mun87, Wei83]) in the middle of 1980s. They have used the samples (like Benzene partially oriented in nematic liquid crystal) where no other NMR methods were necessary to improve the spectral resolution, because the dipole-dipole coupling between spins was much reduced due to the high mobility of the system. In this chapter it will be also shown how MQ methods can be combined with the MAS experiment to get the high resolution spectra in solids.

2.1 Basics definitions

The definition of the coherence is based on the expansion of the time-dependent wave function $|\Psi(t)\rangle$ of the system in terms of stationary basis function $|i\rangle$:

$$|\Psi(t)\rangle = \sum_{i=1}^n c_i(t)|i\rangle \quad (2.1)$$

with time dependent coefficients $c_i(t)$ and n as the dimension of the Hilbert space. A coherence between states $|r\rangle$ and $|s\rangle$ exist when the ensemble average of the product of coefficients

$$\rho_{rs}(t) = \overline{c_r(t) c_s^*(t)} \quad (2.2)$$

does not vanish ([Sli92]). The elements $\rho_{rs}(t)$ defined by equation (2.2) forms the density matrix. It has to be noted that a coherent state is not an eigenstate of the Hamiltonian operator and it is time dependent. The coherent state should not be exchange with the statistical ensemble where the spins can be always found in the eigenstates $|r\rangle$ and $|s\rangle$. In the high field NMR the Zeeman interaction cause the splitting of the energy levels according to the field direction and the difference between magnetic quantum numbers

$$\Delta m_{rs} = m_r - m_s \quad (2.3)$$

defines the order of coherence. In general, a matrix element ρ_{rs} represents p -quantum coherence ($p = m_r - m_s$).

One special case of the coherence is a single quantum (SQ) coherence ($\Delta m_{rs} = \pm 1$), which corresponds to an observable transverse magnetization. It can be excited e.g. by the one 90° -pulse like was shown in the section 1.5. Such a coherence corresponds to the NMR signal, which is induced in the detection coil and can be directly observed. It can be schematically represented by the transitions between two energy levels $|\uparrow\rangle$ and $|\downarrow\rangle$ for one isolated spin $I = \frac{1}{2}$, where \uparrow reflects the "spin-up" state and \downarrow the "spin-down" state of the spin.

Let us consider a spin pair, where are four Zeeman energy levels corresponding to the four possible states, which can be noted $|\uparrow\uparrow\rangle$, $|\downarrow\downarrow\rangle$, $|\uparrow\downarrow\rangle$ and $|\downarrow\uparrow\rangle$. In the case of homonuclear spins (i.e. $\gamma_1 = \gamma_2$), the energy levels corresponding to $|\uparrow\downarrow\rangle$ and $|\downarrow\uparrow\rangle$ are degenerated and three Zeeman levels remain that are equally spaced (see Figure 2.1a). Thus, one single NMR line would result in the spectrum from the 'allowed'¹ ($p = \pm 1$)

¹Directly detected in the magnetization with the r.f. coil.

SQ transitions. This would be the result only if no coupling between them is taken into account. If now the dipolar coupling between is present, the resulting energy levels are slightly shifted due to the Hamiltonian \hat{H}_D (see equation (1.28)). This shift is such, that the two allowed SQ transitions now have different frequencies (see Figure 2.1b). Hence, a splitting of the line by $2\omega_D$ results (see Figure 2.1b) which depends on the dipolar coupling strength. Coherence between the states $|\uparrow\uparrow\rangle$ and $|\downarrow\downarrow\rangle$ (see Figure 2.1), so-called double quantum (DQ) coherence, and between $|\uparrow\downarrow\rangle$ and $|\downarrow\uparrow\rangle$, so-called zero-quantum (ZQ) coherence, is 'forbidden', that is, it cannot be detected directly. When extending this consideration from the two-spin system to a multiple-spin system, we find a wealthy of such p -quantum ($p \neq \pm 1$) 'forbidden' coherence. We are calling it multiple quantum (MQ) coherence. In liquids it is caused by indirect spin-spin coupling (J -coupling) and in solids by direct dipolar coupling (Quadrupolar coupling is not considered). J -coupling is in solids usually very small with comparison to the direct dipolar coupling, so it will be not considered latter in this work.

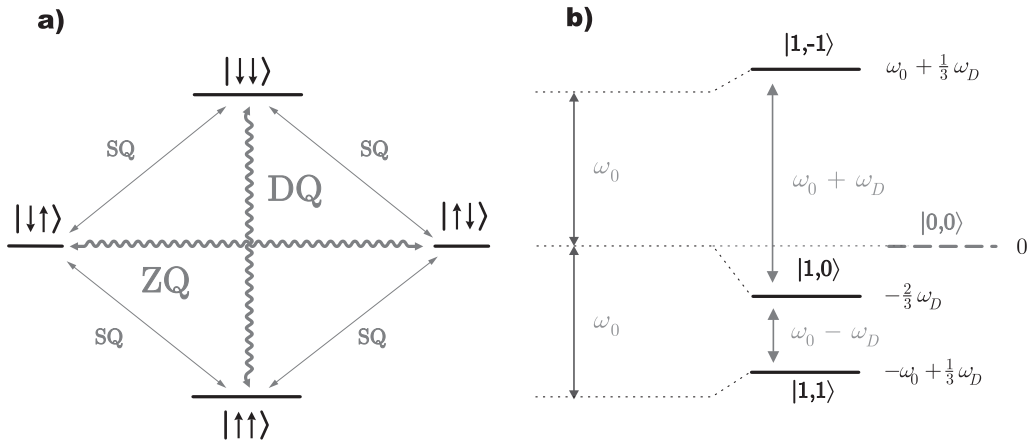


Figure 2.1: Energy levels of a two-spin system with equivalent spins. a) Zeeman energy levels for the states $|\uparrow\uparrow\rangle$, $|\downarrow\downarrow\rangle$, $|\uparrow\downarrow\rangle$ and $|\downarrow\uparrow\rangle$. The allowed single quantum (SQ) transitions and 'forbidden' zero-quantum (ZQ) and double quantum (DQ) transitions are indicated. b) Energy level diagram of the spin pair including the effect of the dipolar coupling. The eigenstates of the Hamiltonian are now superpositions of the states $|\uparrow\uparrow\rangle$, $|\downarrow\downarrow\rangle$, $|\uparrow\downarrow\rangle$, $|\downarrow\uparrow\rangle$, so-called triplet (symmetric) and singlet (antisymmetric) states. The energy levels of the triplet states $|1,1\rangle = |\uparrow\uparrow\rangle$, $|1,-1\rangle = |\downarrow\downarrow\rangle$ and $|1,0\rangle = \frac{1}{\sqrt{2}}(|\uparrow\downarrow\rangle + |\downarrow\uparrow\rangle)$ are shifted compared to the Zeeman levels as indicated. Transitions between antisymmetric $|0,0\rangle = \frac{1}{\sqrt{2}}(|\uparrow\downarrow\rangle - |\downarrow\uparrow\rangle)$ and symmetric states (triplet states) are not allowed. As indicated only SQ transitions are directly observable, so that the lines appear at the positions $\pm\omega_D = \frac{3}{2}d_{12}^I(3\cos^2\vartheta - 1)$ in the spectrum. d_{12}^I is the dipolar-coupling constant for two homonuclear spins (see the page 10).

2.2 Three pulse Experiment

A simple three pulse sequence [Aue76] was historically the first example of nonselective pulsed MQ excitation. It is capable to create coherences of orders zero through N in a system of N coupled spins- $1/2$. To understand the working of this basic experiment, we will once again consider a pair of dipolar coupled spin- $1/2$ nuclei. For convenience we will define initial state of the two spin system I^i and I^j through overall spin operator $\hat{\mathbf{I}}_z$:

$$\hat{\mathbf{I}}_z = \hat{\mathbf{I}}_z^i + \hat{\mathbf{I}}_z^j. \quad (2.4)$$

After the first $\frac{\pi}{2}$ -pulse applied in the x -direction of the rotating frame the density matrix is found as a transverse magnetization (see section 1.5):

$$\hat{\rho}(0^+) = c \left(\hat{\mathbf{I}}_y^i + \hat{\mathbf{I}}_y^j \right) = c \hat{\mathbf{I}}_y. \quad (2.5)$$

Just after the pulse the system evolves under the influence of dipolar Hamiltonian and for two coupled spins the Liouville-von Neumann equation (1.2) can be formally solved (see e.g. equation (1.79)):

$$\hat{\rho}(\tau^-) = c \hat{\mathbf{I}}_y \cos \left[\omega_D^{ij} \tau \right] - 2c \left(\hat{\mathbf{T}}_{2,1}^{ij} - \hat{\mathbf{T}}_{2,-1}^{ij} \right) \sin \left[\omega_D^{ij} \tau \right] \quad (2.6)$$

$$\omega_D^{ij} = \sqrt{\frac{3}{8}} d_{ij}^{II} R_{2,0}^{ij}.$$

To excite DQ coherence the second pulse has to be applied. The best time τ for introducing that pulse is, when the second coefficient in equation (2.6) has the maximal value. This is the point when $\cos \left[\omega_D^{ij} \tau \right]$ (the first term) is zero. The schematic evolution of the $\hat{\mathbf{I}}_y$ spin operator is shown in Figure 2.2. The result of the second pulse consist of two components²:

$$\hat{\rho}(\tau^+) = e^{i\frac{\pi}{2}\hat{\mathbf{I}}_x} \hat{\rho}(\tau^-) e^{-i\frac{\pi}{2}\hat{\mathbf{I}}_x} = -c \hat{\mathbf{I}}_z \cos \left[\omega_D^{ij} \tau \right] - i 2c \left(\hat{\mathbf{T}}_{2,2}^{ij} - \hat{\mathbf{T}}_{2,-2}^{ij} \right) \sin \left[\omega_D^{ij} \tau \right]. \quad (2.7)$$

²Marks $\tau^{-/+}$ means before/after the r.f. pulse.

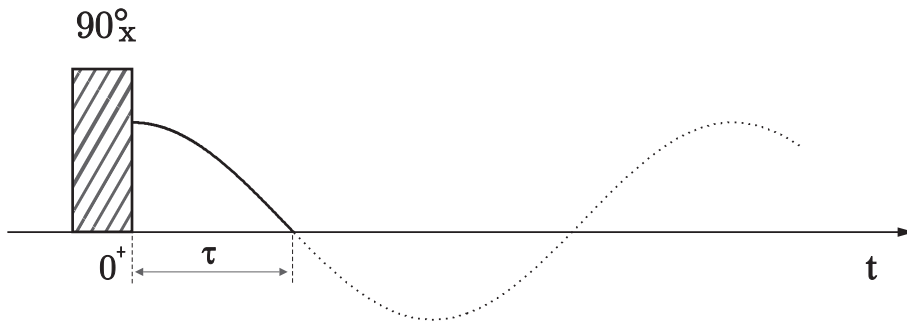


Figure 2.2: Optimal time τ for the second pulse in the three pulse experiment.

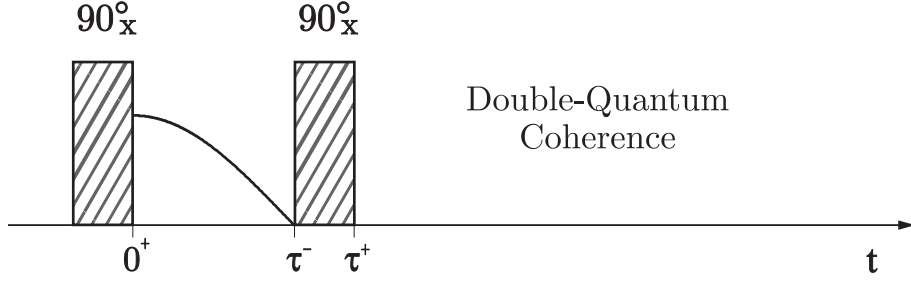


Figure 2.3: Excitation of double quantum coherence.

The first one represents to the longitudinal magnetization \hat{I}_z and the second one describes the DQ coherence $\hat{T}_{2,\pm 2}$. According to the definition of $\hat{T}_{2,\pm 2}$ (see Appendix A) DQ coherence can be formally illustrated as the change of the orientation of the two spins at the same time (Figure 2.1):

$$\hat{T}_{2,2}^{ij} - \hat{T}_{2,-2}^{ij} = \frac{1}{2} \left(\hat{I}_+^i \hat{I}_+^j - \hat{I}_-^i \hat{I}_-^j \right). \quad (2.8)$$

If the second pulse is applied at time $\tau = 1/\omega_D^{ij}$ (Figure 2.3) the first term in equation (2.7) vanishes and the DQ coherence will become maximal:

$$\hat{\rho}(\tau^+) = -i c \left(\hat{I}_+^i \hat{I}_+^j - \hat{I}_-^i \hat{I}_-^j \right). \quad (2.9)$$

It is necessary to note that the coherence described by this equation is not visible in the magnetization because the expectation value vanishes ($\alpha = x, y$):

$$\text{Tr} \left\{ \hat{I}_\alpha^i \hat{T}_{2,\pm 2}^{ij} \right\} = \text{Tr} \left\{ \hat{I}_\alpha^j \hat{T}_{2,\pm 2}^{ij} \right\} = 0. \quad (2.10)$$

To detect it the third last pulse called detection pulse has to be added after time t_1 .

If we again assume the dipolar coupled spin pair, after the second pulse the DQ coherence does not evolve because the Hamiltonian operator \hat{H}_D of the two dipolar coupled spin pair commute with the operator $\hat{T}_{2,\pm 2}^{ij}$:

$$[\hat{T}_{2,0}^{ij}, \hat{T}_{2,\pm 2}^{ij}] = 0. \quad (2.11)$$

In this case the density matrix at time t_1 is given like

$$\hat{\rho}(\tau + t_1^-) = -c e^{-i\hat{H}_D t_1} \hat{I}_z e^{i\hat{H}_D t_1} \cos \left[\omega_D^{ij} \tau \right] - i 2c \left(\hat{T}_{2,2}^{ij} - \hat{T}_{2,-2}^{ij} \right) \sin \left[\omega_D^{ij} \tau \right]. \quad (2.12)$$

The first term also does not evolve under the dipolar Hamiltonian but it appears as detectable magnetization. But by means of the cycling of the phases of the pulses it can

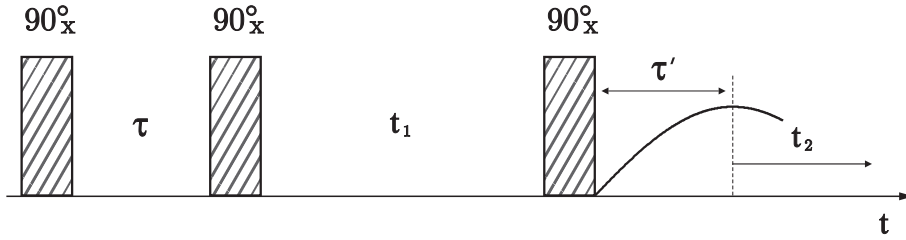


Figure 2.4: The complete three pulse sequence used for excitation and detection of DQ coherence in the coupled two spin system. The optimal time τ is connected to the coupling strength ω_D^{ij} and the same is valid for time τ' , $\tau' = \tau$.

be filtered out and we will not assume it in the next calculations. The second term in equation (2.12) describes DQ coherence which does not evolve during time t_1 (only when in resonance excitation is assumed, more details see section 2.4.2). The third $\frac{\pi}{2}$ -pulse converts it to the SQ coherence and under the above spoken condition for excitation time $\tau = 1/\omega_D^{ij}$ the density matrix can be written as

$$\hat{\rho}(\tau + t_1^+) = e^{i\frac{\pi}{2}\hat{I}_x} \hat{\rho}(\tau + t_1^-) e^{-i\frac{\pi}{2}\hat{I}_x} = 2c \left(\hat{T}_{2,1}^{ij} - \hat{T}_{2,-1}^{ij} \right). \quad (2.13)$$

The terms $\hat{T}_{2,\pm 1}^{ij}$ are still not visible in the magnetization but under the evolution due to dipolar coupling they can be detected and then

$$\hat{\rho}(\tau + t_1 + \tau') = 2c \left(\hat{T}_{2,1}^{ij} - \hat{T}_{2,-1}^{ij} \right) \cos \left[\omega_D^{ij} \tau' \right] + c \hat{I}_y \sin \left[\omega_D^{ij} \tau' \right]. \quad (2.14)$$

The second term in equation (2.14) represents the measurable magnetization induced in the detecting coil. It can be seen that the signal is maximal only when $\tau' = \tau$ (see Figure 2.4). To detect the DQ time-evolution it is not necessary to acquire whole spectrum but only one point at time $t_2 = 0$ (see Figure 2.4) is enough. The signal at this point is then given by

$$\hat{\rho}(\tau, \tau', t_1, t_2 = 0) = c \left(\hat{I}_y^i + \hat{I}_y^j \right) \sin \left[\omega_D^{ij} \tau \right] \sin \left[\omega_D^{ij} \tau' \right]. \quad (2.15)$$

Under the optimal conditions for times τ and τ' the whole magnetization in the case of two spins interaction is transferred to the DQ coherence and at the end it is completely reconverted back. The signal is for the isolated spin-pair independent to evolution time t_1 . An interesting information is not the modulation of the signal but the amplitude. It carries an information about the amount of the magnetization transferred to the DQ coherence at defined time τ . If a system consists of more strongly coupled spin pairs their intensities in the spectrum carry the relative information about their strength. If in addition one of

the coupling strength is known the others can be calculated from their intensities. This method will be more extensively used in this work.

If we assume now also chemical shift interactions, some additional terms have to be added to the above calculations. More detailed description can be found in [Sli92] or [Mun87]. It can be seen from their calculations that introducing chemical shifts and resonant offsets the simple three pulse sequence (Figure 2.4) generates also SQ transverse magnetization terms and other unwanted terms which can not be filtered out by the phase cycling of the pulses. The problem can be overcome by inserting of a π -pulse midway into the excitation period between the first and the second $\frac{\pi}{2}$ -pulse. The resulting sequence will after that look like

$$\overbrace{\left(\frac{\pi}{2}\right)_x \cdots \frac{\tau}{2} \cdots (\pi)_x \cdots \frac{\tau}{2} \cdots \left(\frac{\pi}{2}\right)_x}^{\text{Excitation}} \underbrace{\cdots \cdots t_1 \cdots \cdots}_{\text{Evolution}} \overbrace{\left(\frac{\pi}{2}\right)_{x,y} \cdots \tau'}^{\text{Reconversion}} \underbrace{\cdots \cdots t_2 \cdots \cdots}_{\text{Detection}} .$$

It can be seen that in such a sequence chemical shift and resonant offset terms have influence to DQ coherence only during evolution time t_1 . The DQ coherence operator will oscillate during time t_1 at the frequency defined by a sum of chemical shift frequencies for two spins.

To study the time evolution of the multiple quantum (MQ) coherence the two-dimensional experiment has to be accomplished where time t_1 is increased step by step. At the certain point t_1 the time evolution of MQ coherence will be interrupted and transferred by the reconversion pulse to the transverse magnetization. Only the first point of the time signal at $t_2 = 0$ is necessary to acquire to get the overall information. More detailed description can be found in the next sections.

2.3 General scheme of MQ experiment

Any experimental attempt to monitor the dynamic evolution of the spin system in which there exists a condition of multiple quantum (MQ) coherence must inevitably be used upon the detection of single quantum (SQ) transverse magnetization. However, complex the structure of a multilevel system may be, these relatively few magnetic dipole modes still remain the only coherences directly observable with conventional radio-frequency (r.f.) technology. Operating within this constraint, MQ experiments typically employ a method of indirect detection using two-dimensional spectroscopy (see section 1.7) and then to record their response to either naturally occurring or externally manipulated local fields.

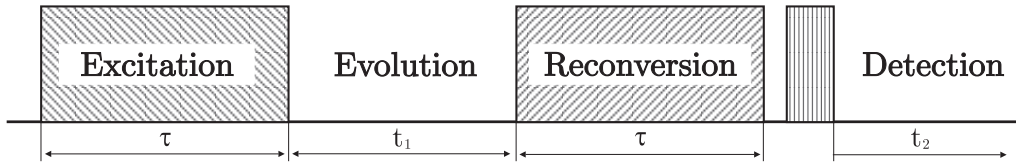


Figure 2.5: General form of a two-dimensional MQ experiment.

The basics scheme for detecting MQ coherence is illustrated in Figure 2.5. The first part called *excitation* period is designed to excite MQ coherence by the proper design of the high frequency pulses. Selection of the correct pulse sequence is strongly dependent on the system which we want to study. The basic sequence was shown in the section 2.2. In the second part *evolution* period, MQ coherence evolves during time t_1 under the influence of local fields of the system and the strong static external field \vec{B}_0 . Because MQ coherences can not be observed directly they have to be transferred to the SQ modes in the *reconversion* period. After this step they are still laying parallel to the \vec{B}_0 field and they can not be seen in the magnetization. To make them visible a last detection pulse has to be added to the sequence after which they can be acquired during time t_2 in the *detection* period by the conventional spectrometer. Only one condition has to be fulfilled for a reconversion operator \hat{U}_{rec} . It has to be equal to the time reversal excitation propagator \hat{U}_{exc}^+ ([Mun87]).

2.3.1 Excitation and Reconversion

In this part we will discuss the basic properties of the reconversion period and how it can be constructed from the excitation period. We will see that it depends on the order of coherence p excited by the excitation Hamiltonian. Two Hamiltonian operators \hat{H}_{exc} and \hat{H}_{rec} will be used for description of the pulse sequence during excitation and reconversion period. To realize time reversal ([Yen83]) during the reconversion period the following condition has to be fulfilled:

$$\hat{U}_{rec} = \hat{U}_{exc}^+ = \hat{U}_{exc}^{-1} = e^{i\hat{H}_{exc}t} \quad \Rightarrow \quad \hat{H}_{rec} = -\hat{H}_{exc}. \quad (2.16)$$

This leads to the simple modification of the excitation pulse sequence during reconversion period, which can be done by the phase shift. Let us define an angle of the phase shift as ϕ with the phase propagator $\exp(-i\phi\hat{I}_z)$. The reconversion Hamiltonian in this case can be written as

$$\hat{H}_{rec} = e^{-i\phi\hat{I}_z} \hat{H}_{exc} e^{i\phi\hat{I}_z}. \quad (2.17)$$

Let us assume the excitation Hamiltonian defined by the irreducible spherical tensors ([Meh83, Sli92]) $\hat{H}_{exc} \cong A_{m,n} \hat{T}_{m,n}$, where $A_{m,n}$ contains all lattice variables, which are under the phase rotation of the pulse sequence invariant. In this notation the quantum number $n = -m, -m + 1, \dots, +m$ can be identified with the coherence order p and the rank of the tensors $m = 0, 1, \dots, 2L$ defined through total spin quantum number L , which represent the sum of the spin quantum numbers of the component nuclei (e.g. for two spins $I = \frac{1}{2}$, $L = 1$). If we use the transformation property for the spin operators $\hat{T}_{m,n}$ by $e^{-i\phi\hat{I}_z} \hat{T}_{m,n} e^{i\phi\hat{I}_z} = e^{-in\phi} \hat{T}_{m,n}$ (see [Ern87] p. 269 or [SR94] p. 108), we can express equation (2.17) as

$$e^{-i\phi\hat{I}_z} \left(A_{m,n} \hat{T}_{m,n} \right) e^{i\phi\hat{I}_z} = e^{-in\phi} A_{m,n} \hat{T}_{m,n}. \quad (2.18)$$

To fulfill the condition of the time reversibility of the reconversion Hamiltonian (see equation (2.16)), the condition for the phase shift ϕ can be directly seen from the above equation:

$$e^{-in\phi} = -1 \quad \text{if} \quad \phi = \frac{\pi}{|n|}. \quad (2.19)$$

To find a correct reconversion sequence for any excitation sequence is than very simple. For n -quantum coherence all phases of the r.f. pulses have to be shifted by an angle $\frac{\pi}{n}$ ³. In this manner one has to find for an experiment only the correct excitation sequence.

2.4 Static MQ experiment

In this section MQ r.f. pulse sequences for static solids will be described. We will concentrate to the excitation and detection of high-order MQ coherences in proton (¹H) systems. Coherences of very high order are usually possible where an extensive network of dipolar couplings exist. Typical example are strongly coupled abundant nuclear spin- $\frac{1}{2}$ systems like e.g. adamantane or hexamethylbenzene (HMB). In this systems the influence of a coupling between two spins on the development of the system depends on the time elapsed, with the value $d_{ij}^{II} \tau$ (see equation (1.27) and Figure 2.5) providing a measure of the effectiveness of a particular pair interaction at each instant. When excitation time τ is not enough long i.e. $d_{ij}^{II} \tau \ll 1$, the interaction between i and j spins is negligible. However, with increasing time τ more couplings become sufficiently large to contribute to the resulting spectrum. In addition, the strongly coupled spins, which determine the early time

³In this work 90° phase shift for $n = 2$ will be used as will be shown later.

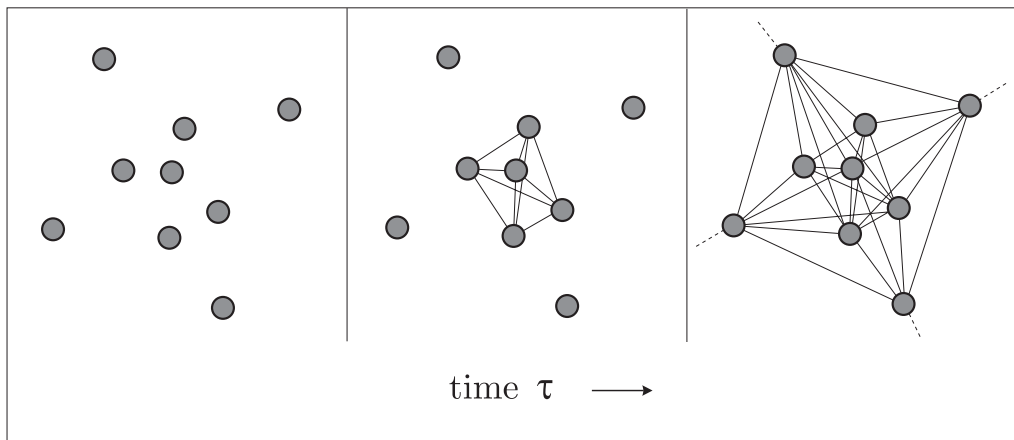


Figure 2.6: *Symbolic representation of the growth of a cluster sizes with time. Initially, the spins act independently, having had insufficient time to communicate via dipole-dipole interactions. As longer the excitation time τ as higher the probability for spins to interact between each other.*

development continue to influence the dynamics at later times. The growth of the so-called 'spin clusters' under the influence of a many body bilinear Hamiltonian is schematically shown in Figure 2.6. In general, for many number of coupled spins up to the effective 'size' of the system at time τ , can be excited. In the next part we will introduce some pulse sequences which can monitor the evolution of the spin clusters.

2.4.1 Time reversal pulse sequences

Already over 16 years ago, Yen and Pines ([Yen83]) demonstrated the possibility to detect MQ coherences in strongly coupled systems of spins- $\frac{1}{2}$ in solids. Up to now there are plenty of time reversal multiple-pulse sequences, which are able to do it (reader is referred to overview monographs [Bod81, Wei83, Mun87]). The methods are developed further as a tool for estimating the sizes of nuclear spin clusters in solids ([Bau85, Shy88]). General scheme for such experiments is shown in Figure 2.5.

To understand the effect of these sometimes complicated pulse sequences one has to solve the density operator equation (1.3) under the action of various pulses and evolution Hamilton operators. This will lead in most of the cases to the cumbersome calculations, which can be avoided by considering of the evolution of the initial density operator in the presence of an average Hamiltonian. Such a treatment of *Average Hamiltonian Theory* (see section 1.3) requires the pulse sequence to be periodic (and cyclic) so that it is sufficient to calculate the average Hamiltonian for a limited number of pulses and evolution intervals,

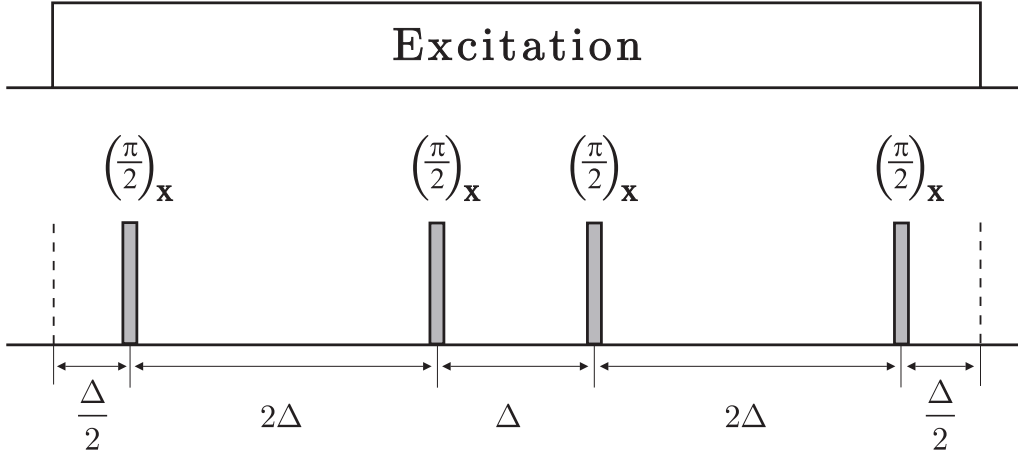


Figure 2.7: A pulse sequence for double quantum excitation for static case. It can be repeated for increasing excitation time τ .

so-called cycle. We will make a small example for calculating the average Hamiltonian in the case of the pulse sequence shown in Figure 2.7 where the cycle consist of four x -pulses. It will be shown that this pulse sequence generates double quantum (DQ) average Hamiltonian in the first order approximation. Two methods of calculations will be presented. One a little bit more sophisticated requiring more calculations and the second one with the pictorial representation of the toggling frame Hamiltonian ([Ern87]).

We start with the evolution of the density operator under the action of the pulse sequence (Figure 2.7) with the cycle time 6Δ . We will assume δ -pulses for simplicity. The density operator at the end of the cycle, for this pulse sequence, is given by

$$\hat{\rho}(6\Delta) = \hat{U}(6\Delta) \hat{\rho}(0) \hat{U}^{-1}(6\Delta) \quad (2.20)$$

with the time-evolution operator ('propagator') for the full cycle⁴

$$\hat{U}(6\Delta) = \hat{L}_z^{(\frac{1}{2})} \hat{P}_x \hat{L}_z^{(2)} \hat{P}_x \hat{L}_z \hat{P}_x \hat{L}_z^{(2)} \hat{P}_x \hat{L}_z^{(\frac{1}{2})}, \quad (2.21)$$

where $\hat{P}_x = e^{i\gamma B_1 \hat{I}_x t_{rf}}$ is the pulse operator and $\hat{L}_z^{(\frac{1}{2})} = e^{-i\hat{H}_z \frac{\Delta}{2}}$, $\hat{L}_z = e^{-i\hat{H}_z \Delta}$ and $\hat{L}_z^{(2)} = e^{-i\hat{H}_z 2\Delta}$ governs the evolution under the influence of the Hamiltonian \hat{H}_z , which can be the Hamiltonian for homonuclear dipolar coupling $\hat{H}_z = \hat{H}_{zz} = \hat{H}_D^{II}$ (see equation (1.28)) or in the case of chemical shift $\hat{H}_z = \omega_{CS} \hat{I}_z$ (see equation (1.22)). As initial density operator $\hat{\rho}(0)$, we use $\hat{\rho}(0) = c \hat{I}_z$ like in equation (1.38).

⁴Interactions are going from right to left but because of the symmetry of this particular pulse sequence it has no importance.

Note, that all Hamiltonians are characterized by spin operators so that the transformation of the spin operators by the pulses directly determines the transformation properties for the propagator $\hat{\mathbf{L}}_z$ ($\hat{\mathbf{P}}_{-x} = \hat{\mathbf{P}}_x^{-1}$)

$$\hat{\mathbf{P}}_x \hat{\mathbf{L}}_z \hat{\mathbf{P}}_{-x} = \hat{\mathbf{L}}_y \quad \text{and} \quad \hat{\mathbf{P}}_y \hat{\mathbf{L}}_z \hat{\mathbf{P}}_{-y} = \hat{\mathbf{L}}_x^-. \quad (2.22)$$

The corresponding transformation properties can be found also for $\hat{\mathbf{L}}_x$ and $\hat{\mathbf{L}}_y$. The minus sign in the superscript of the evolution operator in the second term of equation (2.22) reminds us that the corresponding spin operators have been transformed from $\hat{\mathbf{I}}_\alpha$ to $-\hat{\mathbf{I}}_\alpha$ ($\alpha = x, y, z$; e.g.: $\hat{\mathbf{H}}_{zz}^- = \hat{\mathbf{H}}_{zz}$). The only difference between $\hat{\mathbf{L}}_z$ and $\hat{\mathbf{L}}_y$ (or $\hat{\mathbf{H}}_z$ and $\hat{\mathbf{H}}_y$) is that the corresponding spin operators $\hat{\mathbf{I}}_z$ have been transformed to $\hat{\mathbf{I}}_y$. For homonuclear dipolar Hamiltonian we will use abbreviation⁵

$$\hat{\mathbf{H}}_{yy} = - \sum_{i < j} d_{ij}^{II} \frac{1}{2} (3 \cos^2 \vartheta_{ij} - 1) (3 \hat{\mathbf{I}}_y^i \hat{\mathbf{I}}_y^j - \vec{\mathbf{I}}^i \cdot \vec{\mathbf{I}}^j). \quad (2.23)$$

Inserting unity operator $\hat{\mathbf{1}} = \hat{\mathbf{P}}_{-x} \hat{\mathbf{P}}_x$ into equation (2.21) after each $\hat{\mathbf{L}}_z$ operator and performing the transformation according to equation (2.22) we obtain

$$\hat{\mathbf{U}}(6\Delta) = \hat{\mathbf{L}}_z^{(\frac{1}{2})} \hat{\mathbf{L}}_y^{(2)} \hat{\mathbf{P}}_x \hat{\mathbf{L}}_y \hat{\mathbf{P}}_x \hat{\mathbf{L}}_y^{(2)} \hat{\mathbf{P}}_x \hat{\mathbf{L}}_z^{(\frac{1}{2})} \hat{\mathbf{P}}_x, \quad (2.24)$$

where the pulse propagators have been shifted one step to the right. Repeating this procedure two more times results in

$$\hat{\mathbf{U}}(6\Delta) = \hat{\mathbf{L}}_z^{(\frac{1}{2})} \hat{\mathbf{L}}_y^{(2)} \hat{\mathbf{L}}_z^- \hat{\mathbf{L}}_y^{(2)-} \hat{\mathbf{L}}_z^{(\frac{1}{2})} \hat{\mathbf{P}}_x \hat{\mathbf{P}}_x \hat{\mathbf{P}}_x \hat{\mathbf{P}}_x, \quad (2.25)$$

where the evolution and pulse propagators have been separated. Realizing that the four $(\frac{\pi}{2})_x$ pulses corresponds to a 360° rotation and thus can be omitted (more formally using that the pulse sequence is cyclic, i.e. $\hat{\mathbf{U}}_{rf} = \pm 1$ for the pulse cycle, where $\hat{\mathbf{U}}_{rf}$ is the propagator corresponding to all pulses), we are left with a propagator from which the pulses are removed. This can be interpreted such that we transform from the conventional rotating frame to a frame fixed to the pulses, so-called the toggling frame. We therefore view the evolution Hamiltonian from this frame, which accounts for the change from $\hat{\mathbf{L}}_z$ to $\hat{\mathbf{L}}_y^-$ in two of the evolution intervals.

To analyze equation (2.25) further, let us make an approximation for short times Δ . Expanding the exponential operators $\hat{\mathbf{L}}_z$ and $\hat{\mathbf{L}}_y$, multiplying the resulting terms and

⁵For $\hat{\mathbf{H}}_{xx}$ spin operators $\hat{\mathbf{I}}_y^i \hat{\mathbf{I}}_y^j$ are replaced by $\hat{\mathbf{I}}_x^i \hat{\mathbf{I}}_x^j$.

sorting them according to their order we are getting that

$$\hat{U}(6\Delta) = 1 - i \left(\hat{H}_z + \hat{H}_z^- + 2(\hat{H}_y + \hat{H}_y^-) \right) \Delta + \text{higher orders} \approx e^{-i \hat{H} 6\Delta}. \quad (2.26)$$

Exact calculation of the above equation will lead to so-called the Magnus expansion (see equations (1.54 - 1.56)). The first order approximation corresponds to the linear terms and can be written as

$$\hat{H}^{(0)} 6\Delta = \left(\hat{H}_z + \hat{H}_z^- + 2(\hat{H}_y + \hat{H}_y^-) \right) \Delta. \quad (2.27)$$

This lowest order of approximation is sufficient only for very short Δ values. We will not deal with higher-order terms explicitly and only note that they contain commutators between the Hamiltonians at different times. For two-spin system these commutators are zero and our zero order treatment is exact. Whereas for a multiple-spin Hamiltonian higher-orders have to be calculated to obtain a satisfactory description of the pulse sequence. However, the zero-order average Hamiltonian always has to be derived as a first step, even if an analysis of higher-order terms is performed. The higher-order correction terms will be in this work considered only in the form of symmetry rules for the pulse sequence.

For calculation of the zero order homonuclear dipolar Hamiltonian \hat{H}_D^{II} with its bilinear form so that $\hat{H}_z = \hat{H}_z^- = \hat{H}_{zz}$, we will obtain from equation (2.27)

$$\hat{H}_D^{(0)} = \frac{1}{3} \left(\hat{H}_{zz} + 2\hat{H}_{yy} \right) = \frac{1}{3} \left(\hat{H}_{yy} - \hat{H}_{xx} \right). \quad (2.28)$$

For the last step, so-called the *magic-zero condition*

$$\hat{H}_{xx} + \hat{H}_{yy} + \hat{H}_{zz} = 0 \quad (2.29)$$

has been used, which can be easily verified. It can be shown that equation (2.28) corresponds to the products of the raising and lowering operators ([Bau85]) $\left\{ \hat{I}_+^i \hat{I}_+^j + \hat{I}_-^i \hat{I}_-^j \right\}$ for two spins I^i and I^j , which represent \pm DQ coherence in the case of the two spin interaction.

The zero order chemical shift average Hamiltonian over the full cycle can also be calculated from equation (2.27) as

$$\hat{H}_{CS}^{(0)} = \frac{1}{6} \left(\hat{I}_z - \hat{I}_z + 2(\hat{I}_y - \hat{I}_y) \right) = 0. \quad (2.30)$$

Thus this sequence removes chemical shift (or offset terms) in the first order approximation.

Now the effect of such a 'pure' DQ zero-order average Hamiltonian (equation (2.28)) for two spin system on the initial density operator has to be calculated. It follows from its calculation for dipolar coupled two spins I^i and I^j under the initial density operator $\hat{\rho}(0) = c(\hat{\mathbf{I}}_z^i + \hat{\mathbf{I}}_z^j)$ that

$$\begin{aligned} \hat{\rho}(\tau_c) &= c \left(\hat{\mathbf{I}}_z^i + \hat{\mathbf{I}}_z^j \right) \cos [D^{ij} \tau_c] + i c \left(\hat{\mathbf{I}}_+^i \hat{\mathbf{I}}_+^j - \hat{\mathbf{I}}_-^i \hat{\mathbf{I}}_-^j \right) \sin [D^{ij} \tau_c] \quad (2.31) \\ D^{ij} &= d_{ij}^{II} \frac{1}{2} (3 \cos^2 \vartheta_{ij} - 1) . \end{aligned}$$

The cycle time is $\tau_c = 6\Delta$ in the case of δ -pulses. From equation (2.31) it can be directly seen that the second coefficient represents to DQ coherence and thus the pulse sequence shown in Figure 2.7 excite DQ transitions. The first part of the mentioned equation corresponds to the longitudinal magnetization and without additional cycling of the pulses it can not be removed out from the resulting spectrum. For more detailed discussion about equation (2.31) see section 2.2.

So far, we have concentrated on the zero-order analysis, which is not each time sufficient. For optimizing multiple-pulse sequences, however, it is useful to be aware of some few symmetric principles for elimination of higher-order terms. The so-called 'super' cycles that is, well designed combination of the different variants of the basic cycles can be used for this purpose. The design of such super-cycles is possible when the zero-order chemical shift (or offset terms) vanishes for a basic cycles. Then higher-order effects left over by the basics cycles are additive and thus when generated with the opposite sign in two following periods will cancel each other. Odd-order correction terms in the Magnus expansion, for instance, can be cancelled using super-cycles that are symmetric with respect to the toggling-frame states ([Hae76]). Four pulse sequence shown in Figure 2.7 fulfills the condition for the symmetric cycle for the toggling-frame states as will be shown in the next section.

Finite pulse lengths can also contribute to the resulting spectrum in the detection period and therefore it is useful to eliminate their effects. This can be done by designing the reflection symmetric pulse sequences. Our four pulse sequence than does not fulfill this condition and has to be extended as will be shown in section 2.4.1.2.

2.4.1.1 Determining toggling-frame states for four pulse sequence

For analysis of multiple-pulse sequences under the average Hamiltonian theory toggling frame states have to be calculated. Let us assume for the moment infinite narrow r.f. pulses,

represented by the transformation $\hat{P}_{\alpha_1}, \hat{P}_{\alpha_2}, \dots, \hat{P}_{\alpha_n}$ ($\alpha = \pm x, \pm y$) and separated by free precession periods. Each pulse rotates the toggling frame into a new position, where the toggling frame Hamiltonian $\hat{\tilde{H}}(t)$ (see equation (1.45)) remains constant. For the interval Δ_k between two pulses k and $k + 1$ it can be then written $\hat{\tilde{H}}(t) = \hat{\tilde{H}}_{(k)}$ and the toggling Hamiltonian can be calculated by stepwise transformations

$$\begin{aligned}\hat{\tilde{H}}_{(0)} &= \hat{H}_{int} \\ \hat{\tilde{H}}_{(1)} &= \hat{P}_{\alpha_1}^{-1} \hat{H}_{int} \hat{P}_{\alpha_1} \\ \hat{\tilde{H}}_{(2)} &= \hat{P}_{\alpha_1}^{-1} \hat{P}_{\alpha_2}^{-1} \hat{H}_{int} \hat{P}_{\alpha_2} \hat{P}_{\alpha_1} \\ &\vdots\end{aligned}\quad (2.32)$$

where $\hat{H}_{int} = \hat{H}_z$ represents the secular Hamiltonian for particular interaction. It is important to note an unexpected order of the transformation in equation (2.32). All previous pulses are arranged in reverse order and appear with reversed sense of rotation ([Ern87]).

The zero-order average Hamiltonian is obtained from a weighted sum

$$\hat{\tilde{H}}^{(0)} = \frac{1}{\tau_c} \sum_{k=0}^n \Delta_k \hat{P}_{\alpha_1}^{-1} \dots \hat{P}_{\alpha_k}^{-1} \hat{H}_{int} \hat{P}_{\alpha_k} \dots \hat{P}_{\alpha_1}. \quad (2.33)$$

This analysis enables us to make the detailed description of a pulse sequence. Determination of the toggling frame states are also the basics for calculating average Hamiltonians of the higher orders, which leads to the Magnus expansion series (see section 1.3). Usually multiple-pulse sequences are designed to remove higher order terms (or to suppress them to have negligible influence) and then only zero-order average Hamiltonian became of importance.

According to equation (2.32) the graphical representation of the toggling frame states can be done ([Haf98]). It is based on simple rotations of the spin operators. Rotations in the spin space can be performed quite easily, either by a suitable computer program, or by the help of a cube that is rotated. This graphical determination of the toggling frame states provide us much simple and intuitively more appealing model than sometimes cumbersome calculations presented in the previous section. A sketch of such a cube, which serves as a simple model for the toggling frame is shown in Figure 2.8. Each of its sides is labelled by the corresponding operator \hat{I}_α , where $\alpha = \pm x, \pm y, \pm z$, so that a right-handed coordinate system is built. The cube is placed on a plane, where x and y axis are drawn indicating the orientation of the corresponding r.f. pulses. In the initial state this 'magic cube' is

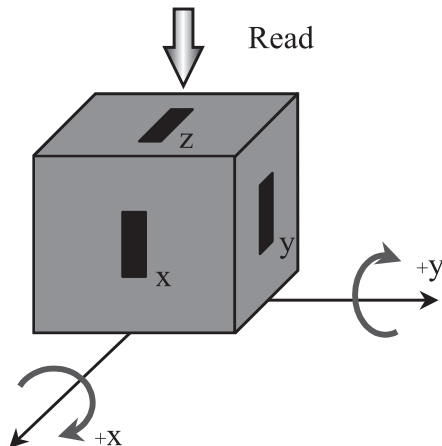


Figure 2.8: The 'magic cube', a convenient tool for determining toggling-frame states \hat{I}_x , \hat{I}_y , \hat{I}_z for the given pulse sequence. The cube is oriented so that the initial state \hat{I}_z is pointing upwards. The cube is rotated around the two fixed axes x or y according to the pulse sequence. The spin operator that is pointing upwards for each rotation step reflects the toggling-frame state for the corresponding time interval.

oriented such, that \hat{I}_z operator is up and the \hat{I}_x and \hat{I}_y operators are pointing in the direction of the corresponding axes as shown in the drawing. Now, the investigated pulse sequence can be analyzed pulse by pulse in the straightforward way by simple rotating the cube around the two fixed axes in accordance with the pulse sequence. In our case the rotations have left handed sense. It hangs on the definition of the $\vec{B}_1(t)$ field (see equation (1.14)). The toggling-frame state for each rotational step is then determined by the operator, which is pointing upwards.

Using this simple cube model the four pulse sequence introduced in the previous section can be analyzed. Corresponding toggling frame states for the dipolar interaction and the chemical shift interaction are shown in Figure 2.9. After that, according to equation (2.33), zero-order average Hamiltonian can be directly calculated. It can be simply shown that average Hamiltonians for the particular interaction have the same form as in equations (2.28) and (2.30). Reflection symmetry of a cycle to the toggling frame states can be easily recognized from Figure 2.9.

It should be stressed, that such a simple 'magic cube' formalism for determining toggling frame states and follow-up zero-order average Hamiltonian can be used only in the case of δ -pulses. For pulses of finite length equation (2.33) is not more valid and has to be extended by the duration of the pulses, where toggling frame changes continuously.

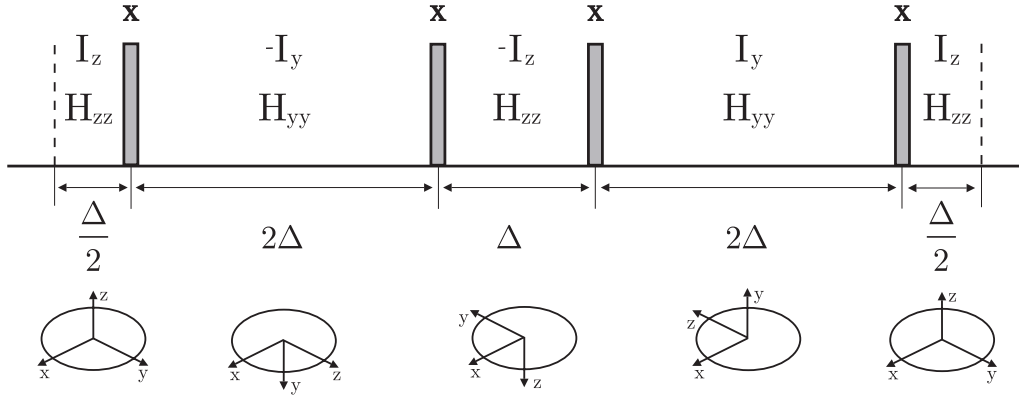


Figure 2.9: The four pulse sequence for DQ excitation with the given toggling frame states for chemical shift and dipolar interaction. The rotation of the coordinate system, known as toggling frame is schematically drawn.

It can be calculated that for our four pulse sequence the contribution of this parts to the average Hamiltonian is additive and thus lead even in the first order approximation to the incorrect results. This imperfections can be avoided by adding additional period of the pulses shifted by 180° as will be shown in the next section.

2.4.1.2 Eight pulse sequence

Most extensively used pulse sequence for exciting multiple quantum coherences in static solids was at the beginning of eighties in the group of A. Pines, eight pulse sequence. With its two versions adopted from J. Baum et al. ([Bau85]) it is shown in Figure 2.10. Both pulse sequences consist of eight $\frac{\pi}{2}$ -pulses of duration t_p separated by delays Δ and $\Delta' = 2\Delta + t_p$. On contrary to the previous section where δ -pulses were assumed, period Δ' was enlarged by the duration of the $\frac{\pi}{2}$ -pulse, t_p , for proper zero-order average Hamiltonian. These pulse sequences can excite even order coherences for homonuclear dipolar coupling and their zero-order even-quantum average Hamiltonian is derived as ([War80, Bau85])

$$\hat{\mathbf{H}}_{D,8p}^{(0)} = -\sum_{i<j} D_{ij} \left(\hat{\mathbf{T}}_{2,2}^{ij} + \hat{\mathbf{T}}_{2,-2}^{ij} \right) \quad (2.34)$$

$$D_{ij} = \frac{\mu_0 \hbar}{4\pi} \frac{\gamma^2}{r_{ij}^3} \frac{1}{2} (3 \cos^2 \vartheta_{ij} - 1) .$$

Equation (2.34) represents for two spin system 'pure' DQ operator. The cycle time τ_c is equal to $12(t_p + \Delta)$ for both pulse sequences. Due to their reflection symmetry the part, where toggling frame changes continuously (during r.f. pulses), from the zero-order

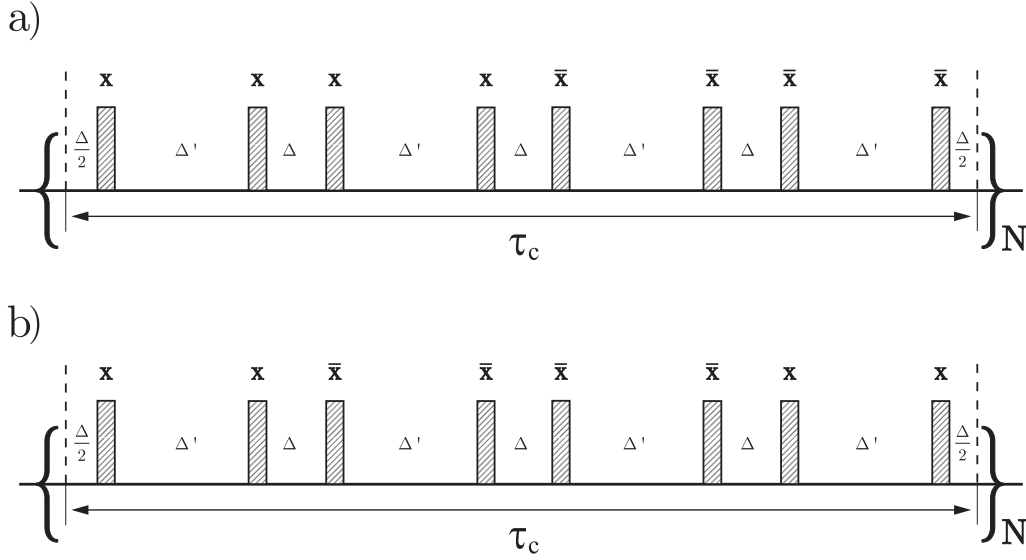


Figure 2.10: Two time reversal pulse sequences for exciting multiple quantum coherences for static solids. Excitation and reconversion time can be increased by repeating of the pulses N times. In the case of δ -pulses $\Delta' = 2\Delta$, but for finite pulse length t_p it has to be increased to $\Delta' = 2\Delta + t_p$.

average Hamiltonian is removed and in addition also $\hat{\mathbf{H}}_{D,sp}^{(1)} = 0$ (equation (1.55)). Pulse sequence shown in Figure 2.10a is preferred whenever resistance to resonance offset effects during excitation and reconversion is particularly important. On the other hand pulse sequence in Figure 2.10b is more appropriate in cases when r.f. field inhomogeneity is a serious problem. In this work experimental results were made with pulse sequence b). It can be seen (see section 2.4.1) that chemical shift interaction (or offset terms) are removed from the average Hamiltonian in the case when $\|\hat{\mathbf{H}}_D\| \gg \|\hat{\mathbf{H}}_{CS}\|$, which is a limitation for using eight pulse sequence. To avoid relaxation of the multiple quantum signal during excitation and reconversion period the cycle time τ_c has to be enough small, i.e. $\|\hat{\mathbf{H}}_D^{(0)}\| \tau_c \ll 1$. Beyond this condition overall excitation time $\tau = N\tau_c$ has to be comparable with the coupling strength, i.e. $\|\hat{\mathbf{H}}_D^{(0)}\| \tau \geq 1$.

2.4.1.3 Thirty-two pulse sequence

In some cases eight pulse sequence introduced in section 2.4.1.2 is not enough efficient to excite MQ coherences in static solids. As was recently proposed by O.N. Antzugin ([Ant99]) in systems where homonuclear dipole-dipole coupling strength is in the order of chemical shift anisotropy (CSA) or higher, CSA Hamiltonian $\hat{\mathbf{H}}_{CSA}$ interferes with coherence averaging of dipolar Hamiltonian $\hat{\mathbf{H}}_D$ and produce large CSA/dipole-dipole

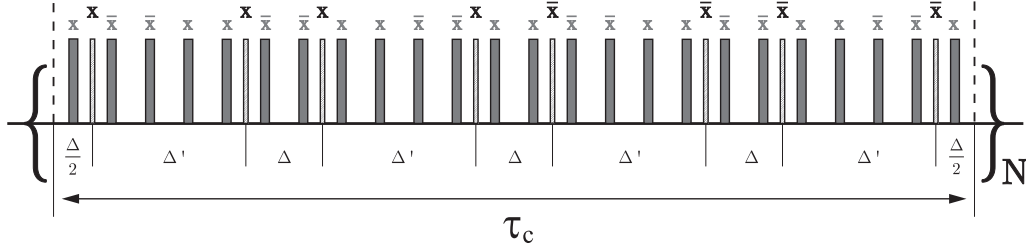


Figure 2.11: Thirty-two pulse sequence used in excitation and reconversion period for exciting MQ coherences in the systems where $\|\hat{\mathbf{H}}_{CSA}\| \lesssim \|\hat{\mathbf{H}}_D\|$. The cycle with characteristic time τ_c consist of eight $\frac{\pi}{2}$ -pulses (see also Figure 2.10a) centered about delays $\Delta = \frac{1}{16} \tau_c$ and $\Delta' = 2\Delta = \frac{1}{8} \tau_c$. Twenty-four π pulses (full rectangles), inserted to average out anisotropic chemical shifts on a time scale of $\frac{1}{24} \tau_c$, are centered about times $\frac{2m+1}{48} \tau_c$, $m = 0, 1, 2, \dots, 23$. The π pulses phases follow the pattern $x, -x, -x, x$, repeated six times.

cross terms in average Hamiltonian. For this reason eight pulse sequence was improved by inserting twenty-four additional π -pulses into each cycle to average out chemical shifts. This pulse sequence is shown in Figure 2.11. Twenty-four pulses are inserted on the time scale $\tau_{echo} = \frac{1}{24} \tau_c$ and cycle time is chosen so that the conditions $\|\hat{\mathbf{H}}_D\| \tau_c < 1$ and $\|\hat{\mathbf{H}}_{CSA}\| \tau_{echo} < 1$ are accomplished.

In the next sections two kind of experiments for exciting MQ coherences for studying static solids will be explained. Some of the basic were already made in section 2.3.

2.4.2 Separation of MQ coherences

Until now no method was explicitly mentioned for separating of MQ coherences. DQ propagator prepared by time reversal pulse sequences (see e.g. section 2.4.1.2) can excite for the system with more coupled spins also quantum coherences of higher orders. These coherences usually merge together (e.g. in Adamantane in the case of on-resonance excitation). To separate them some methods listed below can be used:

- Separation of quantum-orders by magnetic field variation.

Changing of the static magnetic field ΔB_0 will lead to the change of the Larmor frequency $\Delta\omega_L = \gamma_i \Delta B_0$ of spin I^i . In the case of homonuclear p -quantum coherence the resulting frequency will be proportional to the sum of $\Delta\omega_L = \sum_{i=1}^p \gamma_i \Delta B_0 = p \cdot \gamma_I \Delta B_0$. During evolution time t_1 such a coherence evolves with different frequencies corresponding to different quantum orders and can be separated by the Fourier transformation. This technique allow us to be on-resonance while exciting

MQ coherences but requires on the other hand spectrometer, which is able to switch rapidly magnetic field with a good homogeneity. This is usually a big problem and for our spectrometer not applicable.

- Separation of quantum-orders by off-resonance excitation.

By off-resonance excitation of MQ coherences, where the resonance offset is defined by $\Delta\omega_{\text{off}}$, the p -quantum coherence is shifted by $p \cdot \Delta\omega_{\text{off}}$, written in the density matrix formalism as

$$\hat{\rho}(\tau, t_1) = \sum_p \hat{\rho}^p(\tau, t_1) e^{-ip\Delta\omega_{\text{off}} t_1}. \quad (2.35)$$

This phenomenon can also be used for separating of different orders of coherences. It has to be noted that also line-width of the quantum orders is proportional to the increasing of the order. To resolve higher-quantum orders is than necessary to by strongly out off resonance. On the other hand offsets can influence also average Hamiltonian during excitation and reconversion period and this can cause problems if pulse sequence is not designed to remove these terms. If resonance offsets are very high, compensation in most of the cases does not work properly and unwanted artifacts can appear in the spectrum. This leads to decreasing of the resolution of the particular order of coherence. To get a sufficient resolution a lot of t_1 increments has to be done, which rapidly increase measuring time. Some of the examples for separation of quantum orders by off-resonance excitation can be found in M. Munowitz et al. ([Mun87]).

- Separation of quantum orders by phase change.

Shifting of the pulses in the excitation period by an angle $\Delta\phi$ from the pulses in the reconversion period leads also to the separation of the quantum orders. p -quantum coherence will by then shifted by $p \cdot \Delta\phi$. This effect can by also written using density matrix formalism as

$$\hat{\rho}(\tau, t_1) = \sum_p \hat{\rho}^p(\tau, t_1) e^{-ip\phi}. \quad (2.36)$$

It can be seen that this method provides separation of different orders of coherence even when no evolution during t_1 presents (e.g. on-resonance excitation). Either unwanted broadening of the higher orders caused by off-resonance excitation is removed. Changing of the phase allow us to detect maximum $\pm p_{\text{max}}$ orders

of coherence if the size of the increment is determined according to the relation $\Delta\phi = \pi/p_{\max}$ ([Yen83]).

In this work the last method for separating of orders of coherences was used. If on-resonance excitation is not possible due to the complicated structure of the sample the second method will also influence the spectrum. In these cases both effects, namely artificial phase change and off-resonance excitation, coexist and $\Delta\phi$ and Δt_1 must be chosen such that aliasing and overlapping of the coherences is avoided within the available bandwidth equal to $1/\Delta t_1$.

Two experimental methods used in this work for exciting and detecting different orders of coherences in static solids will be presented. The first one commonly called *time-proportional phase incrementation* (TPPI) and the second one called 'spin-counting' where no evolution during t_1 take place ($t_1 = 0$).

2.4.3 TPPI MQ experiment

To separate coherences of different orders *time-proportional phase incrementation* (TPPI) method can be used. How to realize such an experiment is schematically shown in Figure 2.12. This method allows us to excite and resolve desired orders of coherence without introducing the resonance offset. The r.f. pulses of the excitation period are shifted in addition to the r.f. pulses in reconversion period synchronically with incrementing of time t_1 , i.e. $\phi = \Delta\omega_\phi t_1$ ($t_1 = 0, \Delta t_1, 2\Delta t_1, \dots$). Fourier transformation of the signal $S_\alpha = \text{Tr} \left\{ \hat{I}_\alpha \hat{\rho} \right\}$ with respect to t_1 distributes the different orders over the bandwidth in ω_1 dimension equal to $\frac{1}{\Delta t_1}$. Adjacent orders are therefore separated by the apparent offset frequency $\Delta\omega_\phi = \frac{\Delta\phi}{\Delta t_1}$. The number of orders detected is $\pm p_{\max}$ and is determined by the size of the phase increment so that $\Delta\phi = \frac{\pi}{p_{\max}}$. It means e.g. for $p_{\max} = 4$ maximum four quantum orders of coherences can be seen in the spectrum. Important is also to chose Δt_1 and $\Delta\phi$ so that all signals from different coherence orders fit into the available bandwidth ($\frac{1}{\Delta t_1}$) to prevent aliasing and overlapping of the lines in the spectrum.

The demonstration of the excitation of MQ coherences was made on the polycrystalline Adamantane ($\text{C}_{10}\text{H}_{16}$). Adamantane at room temperature forms a plastic crystal in which the nearby spherical molecules tumble rapidly and isotropically. The motion averages all intra-molecular dipolar couplings to zero, but does not eliminate inter-molecular couplings. However, the motion leaves only one distinct coupling between every pair of molecules,

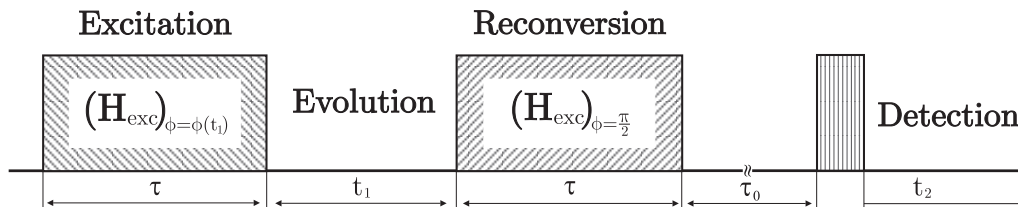


Figure 2.12: General form of pulse sequences for 2D MQ NMR spectroscopy for static solids. Separation of p -quantum orders is accomplished by shifting the excitation pulses by an amount $\phi = \Delta\omega_\phi t_1$ (TPPI, see text). Time reversal is made by shifting excitation pulses by $\frac{\pi}{2}$ during reconversion period: $\hat{H}_{rec} = (\hat{H}_{exc})_{\phi=\pi/2} = -\hat{H}_{exc}$ (see also section 2.3.1). The delay τ_0 between reconversion period and detection pulse can be included to allow dephasing of undesirable coherences. This delay should be not so long to prevent unwanted magnetization exchange during this time.

thereby reducing the Adamantane molecule to a point dipole source containing 16 spins. The molecules pack into face-centered-cubic lattice, with each Adamantane molecule surrounded by 12 neighbours at a distance of 6.60 Å, 6 more at 9.34 Å, and additional 16 at 11.4 Å ([Now45]).

Experimental results of ^1H MQ spectrum of polycrystalline Adamantane can be found in Figure 2.13. Experiment was made with eight pulse sequence presented in Figure 2.10b (see page 42) which was applied during excitation and reconversion period. Separation of different orders has been accomplished by TPPI, so that $\Delta\phi$ and Δt were chosen as $\Delta\phi = 8^\circ$ and $\Delta t_1 = 0.1 \mu\text{s}$, respectively, to prevent aliasing and overlapping of adjacent coherence orders. The basic eight pulse sequence cycle τ_c was repeated $N = 8$ times to get the overall excitation time $\tau = 384 \mu\text{s}$. Time spectrum was transformed by the conventional Fourier transformation to get the resulting spectrum shown in Figure 2.13. Since coherences of $+p$ and $-p$ are equally probable, the spectrum is naturally symmetric about $p = 0$. To obtain then all the information available only one-half of the spectrum is necessary to be displayed. Up to 22 even order coherences can be seen.

In some cases we are not interested to have the information about the line shapes of MQ coherences and so time evolution between excitation and reconversion pulses (see Figure 2.12) can be simply omitted ($t_1 = 0$). This kind of experiment will be presented in the next section.

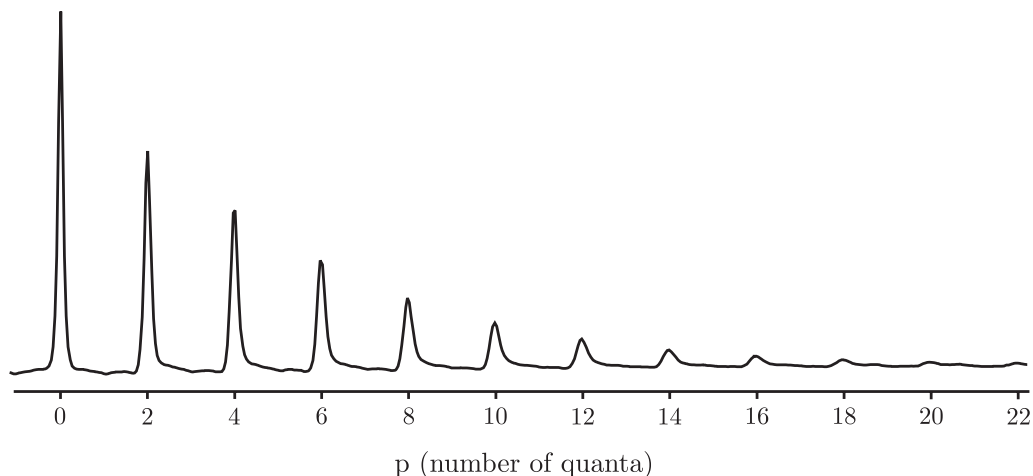


Figure 2.13: 400MHz ^1H multiple quantum spectrum of polycrystalline Adamantane at room temperature. Eight pulse sequence (Figure 2.10b) was used to excite up to 22 ($p_{max} = 22$) order of coherences with excitation time $\tau = 384 \mu\text{s}$. The basic cycle time τ_c was chosen $48 \mu\text{s}$ ($t_p = 3.2 \mu\text{s}$, $\Delta = 0.8 \mu\text{s}$, and $\Delta' = 4.8 \mu\text{s}$). Separation of different orders of coherences has been made by TPPI (for details see text). A delay of $\tau_0 = 1.6 \text{ms}$ was included after reconversion period to allow unwanted transients to decay away from the spectrum. The z-component of magnetization is monitored by $\frac{\pi}{2}$ detection pulse with the phase $\pm x$ which is cycled to remove spectrometer offset.

2.4.4 Spin counting MQ experiment

Time reversal MQ experiment shown in the previous section where TPPI method for exciting coherences of very high orders has been used, is very time consuming. One has to realize enough time t_1 increments to get the sufficient resolution of the adjacent MQ coherences. In such an experiment the important information about growing of the spin clusters is contained in the integrated intensities of the MQ orders, rather than in the different frequencies occurring within each order. Shykind et al. ([Shy88]) showed that even integration of individual coherence orders is in most of the cases not necessary for obtaining the cluster sizes. In these cases time evolution from MQ experiments can be simply omitted ($t_1 = 0$). Measuring time than will be rapidly decreased from e.g. 12 hours (with TPPI) to couple of tens minutes (without TPPI). This kind of experiment will be called "spin counting" experiment in this work (similar like in literature).

The basic scheme of MQ spin counting experiment is shown in Figure 2.14. Reconversion period follows immediately excitation period without supplementary evolution time t_1 . The separation of quantum orders is made by changing of r.f. pulse phases during the excitation period while phases of the r.f. pulses in the reconversion period are holding

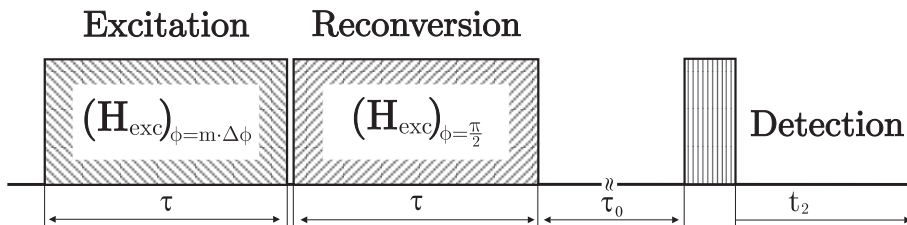


Figure 2.14: Design of the spin counting experiment. Pulses during excitation period are shifted according the rule $\phi = m \cdot \Delta\phi$ with $m = 0, 1, \dots, q - 1$ in the same way like in TPPI experiment (more details can be found in the text and in the description under Figure 2.12).

constant. The phase change about ϕ of the r.f. pulses will lead to the $p \cdot \phi$ phase change for desired p -quantum order which can be written using density matrix formalism as (see e.g. equation (2.36))

$$\hat{\rho}(\tau) = \sum_p \hat{\rho}^p(\tau) e^{-ip\phi}. \quad (2.37)$$

Similar like in TPPI experiment (see section 2.4.3) the phases of excitation pulses will be changed as $\phi = m \cdot \Delta\phi$ where $\Delta\phi = \frac{\pi}{p_{max}}$ is determined by the maximum p_{max} quantum order of visible coherences in the spectrum. Because the signal is strictly periodic with the period 2π it is enough to vary the phase ϕ only in the range $0 \dots 2\pi$. Hence number of phase increments q ($m = 0, 1, \dots, q - 1$) has to be chosen as $q = k \frac{2\pi}{\Delta\phi}$ where k ($k = 1, 2, \dots$) represents periodicity. Additionally, to realize the numerical Fourier transformation (*fast fourier transform*, FFT) of the periodic function, k and p_{max} have to fulfill the condition $k \cdot p_{max} = 2^j$ ($j \in \mathbf{N}$) to get the correct results. Experimental results of spin counting experiment can be found in section 3.5.2.

2.5 MAS MQ experiment

On contrary to the static MQ experiments MAS provides much higher spectral resolution for studying abundant spins in solids. MAS effectively suppress dipole-dipole interaction (see section 1.6) as well as chemical shift anisotropy (CSA) interaction ([Meh83]). Three possible strategies can be used while combining more quantum NMR methods with rotation of the sample at magic angle:

- **quasi-static excitation:** Conventional static multiple-pulse sequences (see sections 2.2 and 2.4.1) can be used to excite MQ coherences with the limitation for excitation time $\tau \leq 0.5\tau_r$. This strong condition where excitation time can not exceed

half of the rotor period τ_r , limits the use of this method for slow spinning speeds. Dipolar coupling is in this case still not sufficiently averaged by MAS ($\omega_r \leq \|\hat{\mathbf{H}}_D\|$) so effective high resolution is not achieved. This method leads to the compromise between an optimal spectrum resolution and the enough long excitation time τ for detecting higher MQ coherences. Using quasi-static method MQ coherences in liquid samples can be excited with the help of e.g. three pulse sequence.

- MAS synchronized excitation:** If the spinning frequency becomes high enough to resolve averaged dipolar interaction ($\omega_r \gg \|\hat{\mathbf{H}}_D\|$) time reversal pulse sequences used for static samples (see section 2.4.1) will not more effectively excite MQ coherences in solids. MAS during excitation and reconversion periods causes a 'self-time reversal', and MQ coherences disappear after each full rotor period⁶. The solution suggested by Meier and Earl ([Mei86]) to prevent this process of 'self-time reversal' involves phase switching the original pulse sequences every half rotor period. The average Hamiltonian in a multiple-pulse sequence has been manipulated such that its sign has been changed synchronously with the spinner rotation. However, this method is necessarily limited to situations in which the spinning rate is sufficiently slow to allow at least two cycles of the multiple-pulse sequence to fit into a single rotor period ($2\tau_c \leq \tau_r$). This method is therefore restricted to samples with small dipolar couplings e.g. for studying labelled pairs of ^{13}C nuclei ([Mei87]).
- fast MAS excitation (rotor synchronized):** An alternative approach to the second method proposed by Meier and Earl will be used in this work where cycle time τ_c is a whole number of rotor periods ($\tau_c = n \cdot \tau_r$; $n = 1, 2, \dots$). This leads to MQ experiments suitable even at very fast MAS speeds. In some cases these high spinning speeds are required to obtain high-resolution spectra for abundant spins in solids. Under the fast MAS conditions ($\|\hat{\mathbf{H}}_D\| \ll \omega_r$) where spectral lines are successfully narrowed dipole-dipole coupling is averaged to zero $\langle \hat{\mathbf{H}}_D \rangle \rightarrow 0$ which act like a disadvantage. Consequently recoupling of the dipolar coupling is necessary. This can be done by a rotor synchronized recoupling pulse sequences like e.g. DRAMA, BABA, C7, ... (see section 2.5.1). For strong coupled spin systems ($\omega_D/2\pi \gg 10$ kHz) recoupling pulse sequences are already not so often used because higher terms of effective average Hamiltonians reduced by this sequences in the

⁶This is a consequent of the fact that the dipolar interaction has an isotropic value of zero.

Magnus expansion (see section 1.3) can have unexpected effects during recoupling. For rigid solids where $\omega_D/2\pi \simeq 50$ kHz this method is not more useful because of the limitation in MAS spinning speeds (up to now $\omega_r/2\pi \simeq 40$ kHz have been reached). Due to the synchronization of the r.f. pulses to the spinning frequency the excitation time τ can be only the whole number of the rotor period τ_r (except C7) which is in some cases also disadvantage.

In the following part we will introduce some recoupling pulse sequences which are suitable for qualitative measuring of dipolar couplings for abundant spins in solids. Some of them can be effectively used for monitoring the evolution of the spin clusters under MAS as will be shown in section 2.5.3.

2.5.1 Recoupling pulse sequences

In recent years a lot of recoupling pulse sequences were developed for measuring dipole-dipole couplings under MAS for solids. High spinning speeds are in most of the cases prerequisite for obtaining high resolution spectra in solids. Recoupling pulse sequences can be divided in principle into two categories.

The first one is dealing with high power r.f. pulses which are for calculating average Hamiltonian operators of particular pulse sequence described via δ -pulses. Such a treatment was in more details introduced in section 2.4.2 for static solids. Duration of the r.f. pulses t_p has to be for these pulse sequences much smaller compared to the rotational period τ_r . Consequently with increasing spinning speeds higher r.f. powers and shorter r.f. pulses are required. This is the strong demand for a very good spectrometer if spinning speeds exceed $f_r > 20$ kHz.

In the second category are recoupling pulse sequences working with relatively long r.f. pulses (*spinlock*-pulses) where duration of the pulses is fixed to the rotor period. In other words, the r.f. field strength witch leads to the precession of the spins I in the rotating frame with the angular frequency $\omega_1 = \gamma_I B_1$ has to be a whole number of the rotational angular frequency ω_r ($\omega_1 = n \cdot \omega_r$; $n = 1, 2, \dots$). For calculating average Hamiltonians, periods of r.f. pulses where toggling-frame Hamiltonians⁷ are changing continuously have to be assumed. In general these pulse sequences are sensitive to the homogeneity of the r.f. field as well as to the sufficiently fast changing of the phases between pulses.

⁷Frame where Hamiltonians of the spin system are expressed in the interaction frame of the r.f. field (see also equation (1.45)).

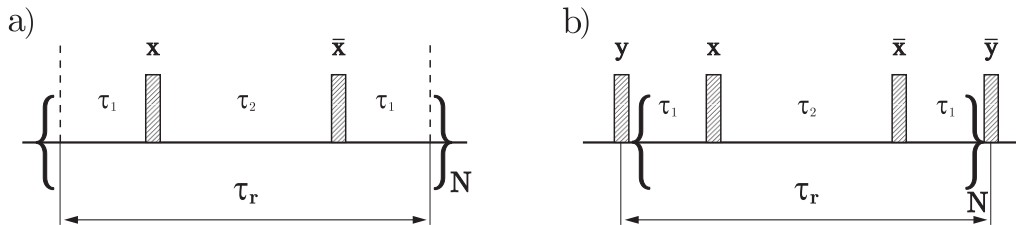


Figure 2.15: Rotor synchronize DRAMA pulse sequence. a) Original pulse sequence which leads to the recoupling of the dipolar coupling under MAS. b) The second variant where DQ average Hamiltonian is prepared after finishing of full rotor cycle τ_r ($\tau_1 = \tau_r/4$, $\tau_2 = 2\tau_1$). Overall excitation time τ can be manipulated through integer number N ($\tau = N\tau_r$).

Their efficiency is generally higher (e.g. for C7 [Lee95] or for MELODRAMA [Sun94]) than for that with 'delta-pulses'.

We will concentrate in this work to the MQ recoupling pulse sequences working with short 'delta-pulses' like DRAMA or BABA, and for that with *spin-lock* pulses like C7 or POST-C7 ([Hoh98]). In the next part these pulse sequences will be explained in more details.

2.5.1.1 DRAMA

The oldest pulse sequence which was able to recover dipole-dipole coupling under fast MAS was DRAMA (*dipolar recovery at the magic angle*) proposed by R. Tycko and G. Dabbagh [Tyc90]. It is shown in Figure 2.15a. Because this simple version consisting of two 90° -pulses was not able to efficiently recover homonuclear dipolar coupling several improvements were made in the case of ^{13}C NMR spectroscopy ([Tyc91, Tyc93]). Extending of the original pulse sequence by two additional pulses shifted by 90° phase from the original ones and positioning them at the beginning and at the end of the cycle interval as it is shown in Figure 2.15b even quantum order selective dipolar Hamiltonian can be derived. This pulse sequence was successfully applied for proton ^1H systems under fast MAS by H. Geen et al. [Gee94]. It was shown ([Gee95]) that it generates 'pure' double quantum (DQ) average Hamiltonian for homonuclear dipole-dipole coupling in samples where CSA and resonance offsets can be neglected.

Assuming isolated spin pair coupled via dipole-dipole interaction toggling-frame states for DRAMA can be determined as can be seen from Figure 2.16 (more details see section 2.4.1.1). Because the geometrical part $R_{2,0}^{ij}$ of the dipolar Hamiltonian

(equation (1.60)) becomes time dependent under MAS as was shown in equation (1.74) we will define for better understanding of the pulse sequence rotor-modulated functions

$$F_{S1} = \sin(\omega_r t) , F_{C1} = \cos(\omega_r t) , F_{S2} = \sin(2\omega_r t) , F_{C2} = \cos(2\omega_r t). \quad (2.38)$$

These functions can be used for an intuitive description of the modulation of a particular Hamiltonian by equation (1.74) under MAS. Combining now toggling frame Hamiltonians prepared after each pulse in DRAMA pulse sequence with the rotor modulated functions it can be directly shown that DQ average Hamiltonian (more details see section 2.4.1)

$$\hat{\mathbf{H}}_{D, DRAMA}^{(0)} \approx \frac{1}{2} \left(\hat{\mathbf{H}}_{xx} - \hat{\mathbf{H}}_{yy} \right) \quad (2.39)$$

is recoupled in F_{C1} component (see Figure 2.16). It can be simply proven that average Hamiltonian presented in equation above represents 'pure' DQ operator for a system with two coupled spins. It is clear that this simple description can be used only for the intuitive understanding of the pulse sequence. Detailed theoretical analysis made by R. Graf et al. [Gra97b] (can be proven by assuming equations (1.74), (1.61), (1.59) and (1.45), (1.54)) shows that zero-order average Hamiltonian for homonuclear coupling in the limit of δ -pulses is given by

$$\hat{\mathbf{H}}_{D, DRAMA}^{(0)} = - \sum_{i < j} \frac{3}{\pi \sqrt{2}} d_{ij}^{II} \sin(2\vartheta_{ij}) \cos(\psi_{ij} + \omega_r t^0) \left(\hat{\mathbf{T}}_{2,2}^{ij} + \hat{\mathbf{T}}_{2,-2}^{ij} \right). \quad (2.40)$$

d_{ij}^{II} represents the dipolar coupling constant defined by equation (1.27) and $\hat{\mathbf{T}}_{2,\pm 2}^{ij}$ are irreducible tensor operators (see Appendix A) describing \pm DQ coherence. The Euler angles $(\varphi_{ij}, \vartheta_{ij}, \psi_{ij})$ relate the principal axes of dipolar coupling tensor to the reference frame fixed on the rotor (more details see section 1.6). $\omega_r t^0$ describes modulation of the ψ_{ij} angle with the initial position of the rotor represented by time point t^0 at which the pulse sequence is initiated. It is especially important during reconversion period.

Introducing CSA or resonance offset terms written in the general form $\hat{\mathbf{H}}_z = \Omega \hat{\mathbf{I}}_z$, zero order average Hamiltonian can be calculated for these interaction. Non zero contribution to the average Hamiltonian will be found only in the F_{C1} component of the rotor-modulated function (see Figure 2.16) and it can be written as

$$\hat{\mathbf{H}}_{\Omega, DRAMA}^{(0)} \approx \frac{1}{2} \Omega \left(\hat{\mathbf{I}}_x + \hat{\mathbf{I}}_y \right). \quad (2.41)$$

This term represents an unwanted contribution to the signal. This version of DRAMA therefore does not lead to the correct results if CSA or resonance offset can not be neglected

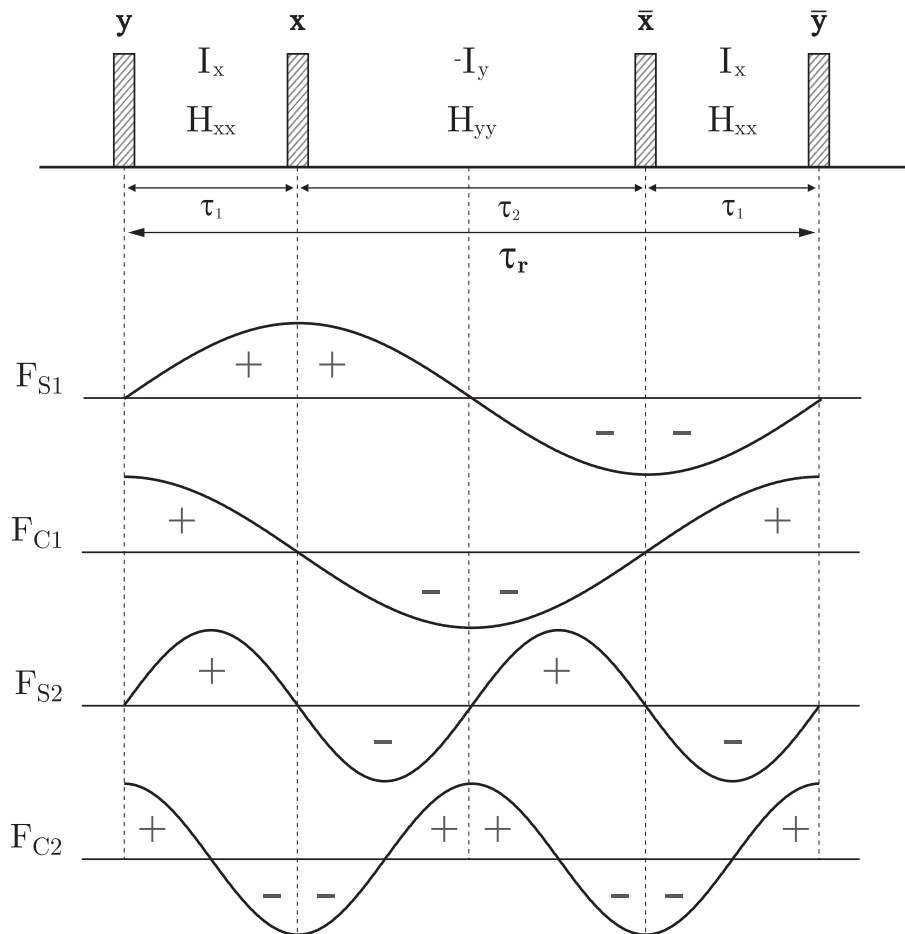


Figure 2.16: DRAMA pulse sequence reflected by the four rotor-modulated functions (see equation (2.38) and equation (1.74)). Toggling frame Hamiltonians for each interval between pulses are indicated for CSA (or resonance offsets) and dipolar interaction respectively. These states are weighted by the areas under the rotor-modulated function for the time during which they are present. Positive or negative contributions of the toggling Hamiltonians to the average Hamiltonian are indicated with sign + or -. In this way, a non-vanishing DQ average Hamiltonian $\hat{H}_{DQ} = \hat{H}_{xx} - \hat{H}_{yy}$ is created only in F_{C1} component. As can be seen average Hamiltonian in other components is cancelled. CSA interaction (or resonance offset terms) are not removed from the average Hamiltonian and can contribute to the resulting spectrum (more details see text).

(e.g. if sample has more than one isotropic components). Several attempts to compensate these unwanted signals were made for the DRAMA pulse sequence ([Tyc91, Tyc93]). They lead to complicated pulse sequences with long cycle times which are in experiment hard to handle. It will be shown that other compensated pulse sequences like BABA and C7 are much more efficient.

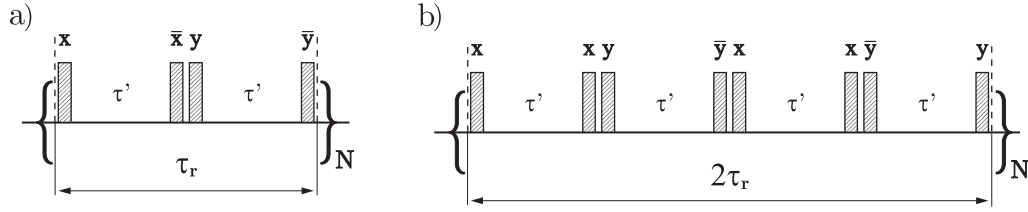


Figure 2.17: Rotor synchronize BABA pulse sequence. a) Original version where timing is set to $\tau' = \tau_r/2$ in the δ -pulses limit. b) Improved version where resonance offsets and CSA are averaged out in the zero-order average Hamiltonian during two full rotor periods $2\tau_r$. Overall excitation time can be manipulated through integer number N ($\tau = N \cdot \tau_r$ or $\tau = N \cdot 2\tau_r$).

2.5.1.2 BABA

BABA pulse sequence has been developed on the basis of Meier-Earl [Mei86] synchronization scheme setting the r.f. pulses *back-to-back*. Initially the pulse sequence $(-\frac{\Delta}{2} - (\frac{\pi}{2})_x - \tau' - (\frac{\pi}{2})_{-x} - \Delta - (\frac{\pi}{2})_y - \tau' - (\frac{\pi}{2})_{-y} - \frac{\Delta}{2})$ acting in the presence of fast MAS has been regarded [Som95]. Considering δ -pulses DQ average Hamiltonian is prepared for this pulse sequence if the synchronization is accomplished as $\tau' = \tau_r/2$ and $\Delta \rightarrow 0$. The basic version of BABA pulse sequence is shown in Figure 2.17a. As will be shown later this simplest version acting on the one rotor cycle does not remove CSA terms and is also sensitive to the resonance offsets like DRAMA pulse sequence. Improved version proposed by Feike et al. [Fei96a] which is shown in Figure 2.17b can solve this problem. Full compensation can be achieved during two rotor cycles.

Similar like for DRAMA (section 2.5.1.1) pulse sequence the zero order average Hamiltonian in the Magnus expansion can be intuitively estimated using toggling frame states modulated with the rotor functions defined by equations (2.38). Toggling frame Hamiltonians for basic version of BABA pulse sequence are shown in Figure 2.18. It can be simply seen from the drawing that zero-order average Hamiltonian for homonuclear dipolar coupling in the δ -pulse limit ($\Delta = 0$, $\tau' = \tau_r/2$) is found in the F_{S1} rotor-modulated function as

$$\hat{\mathbf{H}}_{D,BABA}^{(0)} \approx \frac{1}{2} \left(\hat{\mathbf{H}}_{yy} - \hat{\mathbf{H}}_{xx} \right). \quad (2.42)$$

It is the same average Hamiltonian as for DRAMA (see equation (2.39)) pulse sequence (except sign⁸). More detailed calculations shows the exact value of the zero order average

⁸Sign is not important in this intuitive approximation. It can be changed by proper time integration of the geometrical function $R_{2,0}(t)$ (see equation (1.74)) over the full cycle of the pulse sequence.

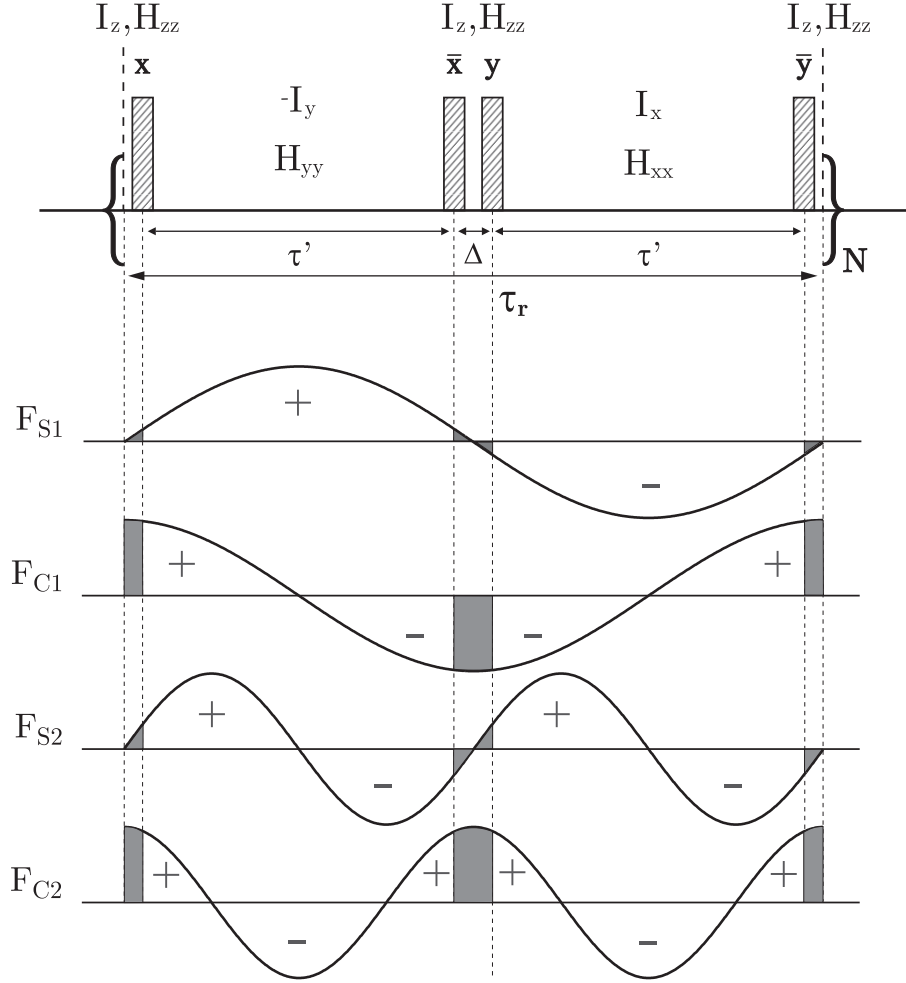


Figure 2.18: Basic version of BABA pulse sequence reflected by four rotor-modulated functions (see also description under Figure 2.16). Non vanishing DQ average dipolar Hamiltonian $\hat{\mathbf{H}}_{DQ} = \hat{\mathbf{H}}_{yy} - \hat{\mathbf{H}}_{xx}$ is created in F_{S1} rotor function. In other components it is averaged out. CSA terms or resonance offsets written in the general form $\hat{\mathbf{H}}_z = \Omega \hat{\mathbf{I}}_z$ can contribute to the resulting zero-order average Hamiltonian also in F_{S1} rotor function and can be written as $\hat{\mathbf{H}}_{\Omega}^{(0)} \approx -\frac{1}{2} \Omega (\hat{\mathbf{I}}_x + \hat{\mathbf{I}}_y)$. Shaded areas represent error term arising from finite switching delays Δ between pulses in the case of δ -pulses (more details see text).

Hamiltonian in the δ -pulse limit approximation ([Fei96a]) as

$$\hat{\mathbf{H}}_{D, BABA}^{(0)} = - \sum_{i < j} \frac{3}{\pi \sqrt{2}} d_{ij}^{II} \sin(2\vartheta_{ij}) \cos(\psi_{ij} + \omega_r t^0) \left(\hat{\mathbf{T}}_{2,2}^{ij} + \hat{\mathbf{T}}_{2,-2}^{ij} \right). \quad (2.43)$$

This result exactly correspond to zero-order average Hamiltonian for DRAMA pulse sequence (equation (2.40)). Both pulse sequences then excite even order MQ coherences with the same efficiency. This is limited to the short excitation times (1 – 2 rotor periods) and the samples with the small chemical shifts ([Fei96b]). An advantage of BABA pulse

sequence is in the second variant (Figure 2.17b) where CSA and resonance offsets are compensated (detailed analysis see [Fei96a]). Error terms arising from finite pulse lengths can be compensated by shifting of the all pulses in BABA pulse sequence about 180° in the next full cycle. This lead to the reducing of the zero-order average Hamiltonian presented in equation (2.43) by the small amount. Therefore, very short r.f. pulses are prerequisite for both BABA and DRAMA pulse sequences.

We will now shortly discuss the problem of the switching of the phases between pulses for BABA pulse sequence. It is known that such a delay Δ is needed for each pulse after setting the phase of the pulse until the phase settle. Design of the BABA pulse sequence force us to think about this problem, which was not the case of DRAMA pulse sequence where no pulses were so close together. Error contributions to the zero-order average Hamiltonian for the original version of BABA pulse sequence are representing by the shadow areas of each rotor-modulated function (see Figure 2.18). For simplicity δ -pulses has been assumed. As can be seen from the drawing non-zero component to the average Hamiltonian appear only from F_{C2} component of the rotor-modulated function. It can be calculated in the limit of $\Delta \ll \tau_r$ that contributions from the finite switching delay (FSD) to the homonuclear dipolar Hamiltonian have the form:

$$\hat{\mathbf{H}}_{D, FSD}^{(0)} \approx \frac{3\Delta}{\tau_r} \hat{\mathbf{H}}_{zz}. \quad (2.44)$$

Error terms to the zero-order CSA (or resonance offsets) average Hamiltonian $\hat{\mathbf{H}}_z = \Omega \hat{\mathbf{I}}_z$ can also be calculated by

$$\hat{\mathbf{H}}_{\Omega, FSD}^{(0)} \approx \frac{\Delta}{\tau_r} \left(2\Omega \hat{\mathbf{I}}_z + \Omega \hat{\mathbf{I}}_y - \Omega \hat{\mathbf{I}}_x \right). \quad (2.45)$$

Same analysis can be applied for the full compensated BABA pulse sequence shown in Figure 2.17b. It will be found that contributions to the zero-order homonuclear dipolar Hamiltonian and CSA (or resonance offsets) average Hamiltonian can be written

$$\hat{\mathbf{H}}_{D, FSD}^{(0)} \approx \frac{6\Delta}{\tau_r} \hat{\mathbf{H}}_{zz} \quad , \quad \hat{\mathbf{H}}_{\Omega, FSD}^{(0)} = 0, \quad (2.46)$$

respectively. Full compensation of the CSA terms and resonance offsets is directly seen from equation above even when small phase-switching delays Δ are presented. It is important to note that homonuclear contribution to the average Hamiltonian was not removed but doubled. This error is than increased proportionally with increasing number of cycles N . It can not be removed even by shifting of the phases of the pulses by 180° in the

next full cycle which eliminates the error terms arising from finite pulse length. Beside the fact that this effect is additive it is very small because $\Delta < 0.5 \mu\text{s}$ in commercial spectrometers and even for very high spinning speeds $f_r = 40 \text{ kHz}$ can be neglected. In addition it contribute to the zero-quantum coherence (from equation 2.44: $\hat{H}_{zz} \approx \hat{T}_{2,0}$) and can be separated from the DQ spectra by TPPI as will be shown in sections 2.5.2 and 2.5.3.

2.5.1.3 C7

C7 pulse sequence belongs to the second category of the recoupling pulse sequences. It works with relatively long r.f. pulses (*spinlock*-pulses) with duration fixed to the rotor period despite δ -pulses sequences like DRAMA and BABA. It is a full compensated pulse sequence first time proposed by Y.K. Lee et al. [Lee95]. The name of the C7 is derived from the sevenfold-symmetric phase shift scheme acting on the two rotor periods $2\tau_r$. It provides homonuclear dipolar recoupling with better efficiency than previous pulse sequences and is much less sensitive to higher resonance offsets and CSA terms. It was shown by Y.K. Lee et al. that its efficiency is around two times higher for ^{13}C systems with large chemical shifts (both isotropic and anisotropic) than DRAMA pulse sequence.

The ^1H version of C7 pulse sequence is shown in Figure 2.19. Seven elements ($C_{\phi'}$) are timed to occupy two rotational periods. Neighbouring elements differ in phase by $\Delta\phi' = \frac{2\pi}{7}$ always rotating in the same sense. In the simplest version ([Lee95]) each element $C_{\phi'}$ consists of two r.f. pulses (see Figure 2.19a), both with r.f. phases differing by π . The strength of the r.f. field B_1 has to be adjusted in order to be equal seven times the spinning frequency $\omega_{B_1} = 7\omega_r$. This condition leads to the 2π flip angle of the r.f. pulse. Then, each element can be described in the conventional notation by $C_{\phi'} = (2\pi)_{\phi'}(2\pi)_{\phi'+\pi}$. The duration of the $C_{\phi'}$ element can be simply estimated as $\frac{2\tau_r}{7}$. As was shown in reference [Lee95] zero-order homonuclear dipolar average Hamiltonian for C7 can be calculated as⁹

$$\hat{H}_{D,C7}^{(0)} = \sum_{k<l} \left\{ \omega_{kl} \hat{T}_{2,2}^{kl} + \omega_{kl}^* \hat{T}_{2,-2}^{kl} \right\}, \quad (2.47)$$

where

$$\omega_{kl} = \frac{343(i + e^{i\pi/14})}{520\pi\sqrt{2}} d_{kl}^{II} \sin(2\vartheta_{kl}) e^{i(\omega_r t^0 - \psi_{kl})}. \quad (2.48)$$

⁹We will change indexation for this section from traditional ij to kl to clearly distinguish between indexes and imaginary number i .

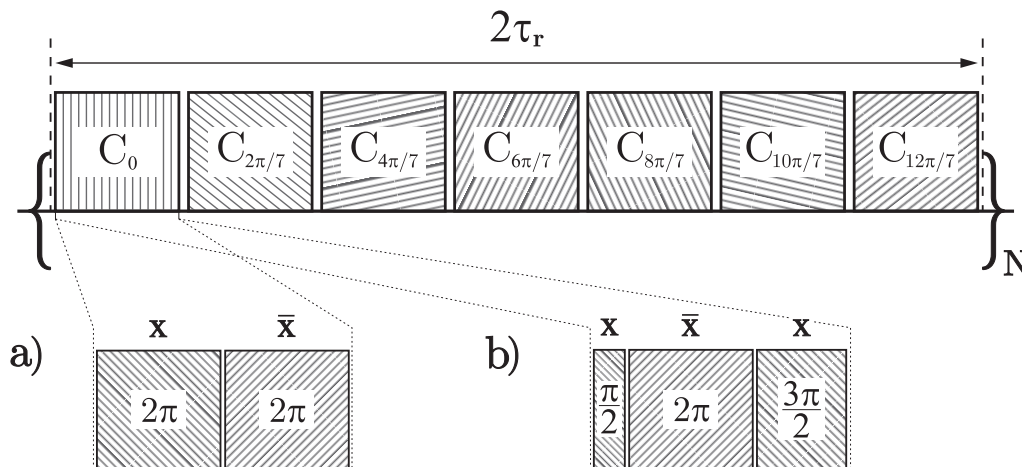


Figure 2.19: *C7 pulse sequence. Seven fold-symmetric r.f. pulse scheme timed on two rotor periods $2\tau_r$ leads to the compensation of all unwanted interactions (more details see text). Each element with duration $\tau_c = 2\tau_r/7$ differs in the phase from the previous one by $2\pi/7$. In the basic version a) each element consists of two 2π r.f. pulses differing in the phase by π . The second version b) called POST C7 having three pulses in the base element is even much less sensitive to resonance offsets (see text). Overall excitation time τ can be changed by integer number N ($\tau = N \cdot 2\tau_r$). It was shown by [Lee95] that even incomplete C7 cycles ($\tau = n \cdot \tau_c$, $n \geq 7$) generates DQ average Hamiltonian. The full compensation is established only after full sevenfold cycle ($n = 7N$).*

Detailed explanation of the symbols in equation above can be seen under equation (2.40). t_0 represents the time point at which the pulse sequence is initiated. It is especially important during reconversion period because it indicates the phase of the DQ Hamiltonian. On contrary to DRAMA and BABA pulse sequences magnitude of zero-order dipolar average Hamiltonian (equation (2.48)) does not depend on the angle ψ_{kl} and leads to the higher efficiency of C7 pulse sequence especially in powders. C7 shown in Figure 2.19a compensate isotropic resonance offsets and r.f. inhomogeneity to first-order in the Magnus expansion.

In Figure 2.19b the second variant of C7 is shown. It was named as POST C7 [Hoh98] (*permutationally offset stabilized C7*). Theoretical and experimental analysis performed by M. Hohwy et al. [Hoh98] shows that POST C7 is even less sensitive to the resonance offsets as original version of C7. POST C7 consist of three pulses in the base element $C_{\phi'} = (\frac{\pi}{2})_{\phi'}(2\pi)_{\phi'+\pi}(\frac{3\pi}{2})_{\phi'}$ (see Figure 2.19b). The zero-order homonuclear dipolar average Hamiltonian of POST C7 is identical with C7 (see equations (2.47)–(2.48)). It is supposed to eliminate isotropic resonance offsets up to fourth-order in the Magnus

expansion and isotropic resonance offsets/r.f. inhomogeneity up to third-order. It also removes the effects of CSA in the zero-order expansion similar like C7.

Comparing C7 with other recoupling pulse sequences of the same kind like HORROR (*homonuclear rotary resonance*, [Nie94]) it provides better experimental results with higher efficiency. The basic version of C7 was also used in ^{31}P NMR spectroscopy to obtain high resolution spectra in powders ([Dol97]). Besides POST C7 other compensation schemes were designed [Rie98] which might lead to even greater efficiencies. In this work most of the experiments were performed with POST C7 because of sufficiently high compensation.

2.5.2 Two-dimensional MQ experiment

General form of the pulse sequence scheme for two-dimensional (2D) MQ experiment under MAS is shown in Figure 2.20. It is nearly identical with the design of 2D MQ experiment for static solids (see Figure 2.12) with an exception of rotor synchronization for the pulses during excitation and reconversion period. Synchronization of the detecting pulse ($n_0\tau_r$) is not a prerequisite for this kind of experiment, but it was used in this work.

Separation of different orders of coherence is accomplished by TPPI similar like in section 2.4.3. Time reversal during reconversion period is made by shifting of the r.f. pulses by $\frac{\pi}{2}$ in comparison to the pulses acting during excitation period (for details see section 2.3.1). Pulse sequences used in this work can be described by average Hamiltonian representing 'pure' DQ operator for the two spins- $\frac{1}{2}$ system and can be written in the general form as (see also sections 2.5.1.1 - 2.5.1.3)

$$\hat{\mathbf{H}}_{DQ} = \sum_{i < j} \left\{ \omega_{ij}(\vartheta, \psi, t^0) \hat{\mathbf{T}}_{2,2}^{ij} + \omega_{ij}^*(\vartheta, \psi, t^0) \hat{\mathbf{T}}_{2,-2}^{ij} \right\}. \quad (2.49)$$

The complex term ω_{ij} corresponds to the amplitude and to the phase of the DQ Hamiltonian. It depends on Euler angles (ϑ, ψ) and on the starting time point t^0 of the particular pulse sequence (see e.g. equation (2.40)). DQ Hamiltonian shown in equation (2.49) can excite even order of coherences under ideal conditions ([War80]).

TPPI in 2D MQ experiment (Figure 2.20) is performed by the phase change of the r.f. pulses during excitation period synchronically with increasing evolution time t_1 as: $\phi = \phi(t_1) = \Delta\omega_\phi t_1$ ($t_1 = 0, \Delta t_1, 2\Delta t_1, \dots$). Such a phase change gives rise to the transformation of the DQ spin operator $\hat{\mathbf{T}}_{2,\pm 2}$ as ([Ern87, SR94])

$$e^{-i\phi\hat{\mathbf{I}}_z} \hat{\mathbf{T}}_{2,\pm 2} e^{i\phi\hat{\mathbf{I}}_z} = e^{\mp i 2\phi} \hat{\mathbf{T}}_{2,\pm 2}. \quad (2.50)$$

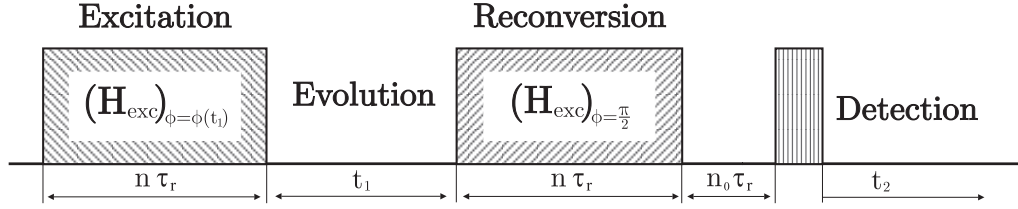


Figure 2.20: Design of the 2D single channel (in t_1 dimension) MQ experiment under MAS. Rotor synchronized pulse sequences like DRAMA, BABA and C7 can be used in the excitation and reconversion periods, respectively. n represent symbolically rotor synchronization ($n = 1, 2, \dots$). Separation of different orders is made by TPPI (see text). A period $n_0\tau_r$ ($n_0 = 1, 2, \dots$) is inserted between the reconversion and detection period to allow undesired coherences to dephase.

Simply speaking it evokes changing of the phase for DQ coherence by an angle 2ϕ . Inserting equation (2.50) in to equation (2.49) the DQ average Hamiltonian during excitation period is derived and is holds

$$\hat{\mathbf{H}}_{DQ}^{exc} = \sum_{i < j} \left\{ \omega_{ij}(\vartheta, \psi, t^0 = 0) e^{-i2\phi(t_1)} \hat{\mathbf{T}}_{2,2}^{ij} + \omega_{ij}^*(\vartheta, \psi, t^0 = 0) e^{i2\phi(t_1)} \hat{\mathbf{T}}_{2,-2}^{ij} \right\}. \quad (2.51)$$

Initial position of the rotor has for $\hat{\mathbf{H}}_{DQ}^{exc}$ no importance and can be set to zero: $t^0 = 0$. The response of the spin system to the excitation Hamiltonian (equation (2.51)), in the case of spin pairs, is simplified by the fact that DQ coherence does not evolve under the influence of the dipolar coupling (see also equation (2.11) and equation (1.75)) since $[\hat{\mathbf{H}}_D(t), \hat{\mathbf{H}}_{DQ}^{exc}] = 0$.

The influence of the sample rotation to the resulting signal is described by reconversion Hamiltonian. Its DQ form where rotor modulation is present during evolution time t_1 is written as (see also equations (2.40), (2.43), (2.47))

$$\hat{\mathbf{H}}_{DQ}^{rec} = - \sum_{i < j} \left\{ \omega_{ij}(\vartheta, \psi, t^0 = t_1) \hat{\mathbf{T}}_{2,2}^{ij} + \omega_{ij}^*(\vartheta, \psi, t^0 = t_1) \hat{\mathbf{T}}_{2,-2}^{ij} \right\}. \quad (2.52)$$

The minus sign in the prefactor of this Hamiltonian is the result of the $\frac{\pi}{2}$ -phase shift of the pulses of the reconversion period compared with the excitation period.

This kind of experiment, where pulse sequence is characterized by the DQ operator excites even-order coherences which are distributed over the bandwidth in ω_1 dimension equal to $\frac{1}{\Delta t_1}$. TPPI separate adjacent orders of coherences by the apparent offset frequency $\Delta\omega_\phi = \frac{\Delta\phi}{\Delta t_1}$ ¹⁰, where the phase increment is: $\Delta\phi = \frac{\pi}{p_{max}}$. The highest quantum order detected is $\pm p_{max}$. In addition each order is modulated by the spinning frequency ω_r

¹⁰For neighbouring even quantum orders is the offset frequency than $2 \cdot \Delta\omega_\phi$.

which leads to the supplementary offset to the p -quantum coherence offset ($p \cdot \Delta\omega_\phi$). This results in the sideband spectrum for each p -quantum order (especially for DQ sideband pattern see section 3.2). This can lead to the very complicated spectrum where a lot of sidebands originating from the neighbored quantum orders overlap. Care has to be taken to choose proper Δt_1 , $\Delta\phi$ and spinning frequency ω_r to prevent overlapping and aliasing of the sidebands from different orders. Selective excitation ([War79, War80, War81]) or DQ filtering (see section 4.3) may be the solution to this problem.

Due to the fact that 2D MAS experiment is quite time consuming and for strong coupled systems of spins- $\frac{1}{2}$, $\Delta\phi$ (p_{max}) has to be chosen small (high) enough which decrease the resolution of the Fourier spectrum and thus more t_1 increments has to be made, we where concentrated to systems with relatively weak couplings (see section 3.3).

2.5.3 Spin counting MQ experiment

Spin counting experiment already described in section 2.4.4 can be realized under MAS conditions. It is particularly important for systems with strong couplings where also higher order coherences may be expected and line shapes are not of interest. It was shown by H. Geen et al. [Gee99] that such an experiment can be used for studying spin clusters under MAS on Adamantane. Their results show an agreement with the result from the traditional experiment provided on static solids [Bau85] where eight pulse sequence (see section 2.4.1.2) was used.

The general scheme of MQ spin counting experiment is shown in Figure 2.21. Evolution time t_1 between excitation and reconversion period is simply omitted ($t_1 = 0$). Excitation and reconversion periods are strictly rotor synchronized in the same way like in section 2.5.2. Phase of the r.f. pulses acting during excitation period are changed in the similar way like in TPPI experiment $\phi = m \cdot \Delta\phi$, where $\Delta\phi = \frac{\pi}{p_{max}}$ is related to the maximum observed coherence order p_{max} in the spectrum. DQ average Hamiltonian during excitation period for pulse sequences like DRAMA, BABA and C7 (see sections 2.5.1.1, 2.5.1.2 and 2.5.1.3) according to their general form presented by equation (2.49) can be written as (see also equation (2.50))

$$\hat{\mathbf{H}}_{DQ}^{exc} = \sum_{i < j} \left\{ \omega_{ij}(\vartheta, \psi, t^0 = 0) e^{-i2m \cdot \Delta\phi} \hat{\mathbf{T}}_{2,2}^{ij} + \omega_{ij}^*(\vartheta, \psi, t^0 = 0) e^{i2m \cdot \Delta\phi} \hat{\mathbf{T}}_{2,-2}^{ij} \right\}. \quad (2.53)$$

DQ coherence will be thus shifted by the amount $2\Delta\phi$ in each step of m . Starting time point of the pulse sequence t^0 is for excitation period not relevant and can be set to zero

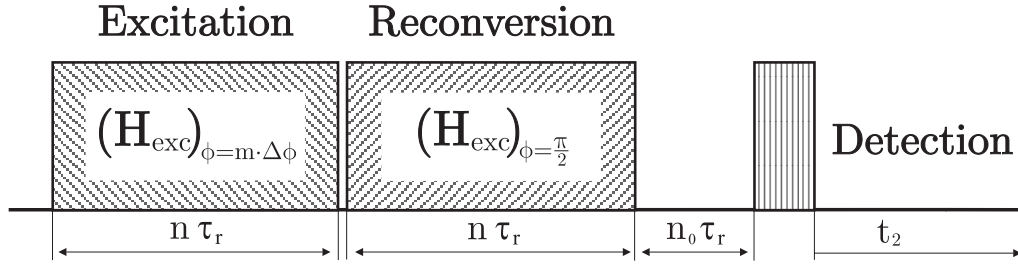


Figure 2.21: Spin counting MQ experiment under MAS. Reconversion period follows immediately excitation period and both are rotor synchronized. R.f. pulses acting during excitation period are shifted as follows: $\phi = m \cdot \Delta\phi$, where $m = 0, 1, \dots, q - 1$ (more details see text). Undesired coherences are dephased during purging period $n_0\tau_r$ ($n_0 = 1, 2, \dots$).

like in section 2.5.2.

During reconversion period higher order coherences are reconverted to longitudinal magnetization. In spin counting experiment reconversion period follows immediately excitation period resulting in the initial phase to be the same like for the excitation Hamiltonian ($t^0 = n \cdot \tau_r \equiv t^0 = 0$)¹¹. This can be simply written as:

$$\hat{H}_{DQ}^{rec} = - \sum_{i < j} \left\{ \omega_{ij}(\vartheta, \psi, t^0 = 0) \hat{T}_{2,2}^{ij} + \omega_{ij}^*(\vartheta, \psi, t^0 = 0) \hat{T}_{2,-2}^{ij} \right\}. \quad (2.54)$$

Minus sign presented in above equation takes care for the time reversibility of the reconversion Hamiltonian.

Calculating of the intensity of the signal resulting from two successive periods excitation and reconversion it will be found that it arise in longitudinal magnetization (see also appendix C). DQ part of that signal is modulated by the $\cos(2\Delta\phi \cdot m)$ (see section 3.2) term. Presence of the cosine factor shows that negative and positive frequencies can not be distinguished corresponding to the single-channel detection ([SR94]). Fourier transformation according to m will shift DQ signal by the frequency $2\Delta\phi \cdot f_{sw}$, where f_{sw} is the half spectral width. In general each p -quantum order will be shifted by $p\Delta\phi \cdot f_{sw}$. Because effective average Hamiltonian representing by equations (2.53) and (2.54) is a "pure" DQ one ([War80]) it can excite only even orders of coherence. Therefore, visible coherences will be $p = 0, 2, 4, 6, \dots, \leq p_{max}$.

It is important to note that the p -quantum signal consequent upon spin counting experiment is strictly periodic with the period 2π . Hence it is enough to vary the phase

¹¹Reconversion Hamiltonian is rotor modulated (see e.g. equations (2.43)) and thus any changes in the phase by 2π are not relevant.

ϕ only in the range $0 \dots 2\pi$. Number of phase increments q can not be varied arbitrary ($m = 0, 1, \dots, q - 1$). Only complete phase cycles can be sampled and thus q has to fulfil condition $q = k \cdot 2p_{max}$, where k ($k = 1, 2, \dots$) represent periodicity. In addition numerical Fourier transformation (*fast fourier transform*, FFT) requires 2^j ($j \in \mathbf{N}$) data sets and thus $k \cdot p_{max} = 2^j$ for obtaining correct results. Experimental results on Adamantane will be presented in section 3.4.

Chapter 3

Measuring of Homonuclear Dipole-Dipole couplings

In this chapter a various NMR r.f. pulse techniques will be used and compared for measuring dipole-dipole couplings in amorphous polymers. If chemical shift anisotropies (CSA) can be neglected with comparison to the dipolar coupling strength as well as B_1 field inhomogeneities the simple r.f. pulse experiment under MAS can be used for estimating dipolar couplings. Already existing theoretical analysis valid for fast spinning regime ([Got96, Gra97a]) are extended for moderate spinning speeds in section 3.1. As an experimental example hexamethylbenzene (HMB) has been chosen for evaluating the dipolar coupling. In sections 3.2 and 3.3 high resolution multiple-pulse sequences like C7, POST C7, BABA and DRAMA which are suitable for site selective measuring of the dipolar couplings under fast MAS are compared. Their efficiencies are studied with connection to elastomers. Initial part of the build-up curves is used to evaluate the relative residual dipolar couplings in more complicated systems like natural rubber in section 3.3.2. In section 3.4 the high resolution MAS spin counting experiment is presented. POST C7 pulse sequence (see section 2.5.1.3) has been used to measure the sizes of the dipolar spin clusters in adamantane. It is shown that POST C7 provides comparable results to the already existing measurements performed by Geen et al. ([Gee99]) with C7 pulse sequence. In the last section (section 3.5) double quantum (DQ) as well as multiple quantum (MQ) coherences on static solids are presented. DQ filtering techniques (see section 4.3) are applied for eight pulse sequence and for thirty-two pulse sequence, respectively. Both pulse sequences can be used for measuring relative dipolar couplings. Their efficiencies with

respect to elastomers are compared in section 3.5.1. In section 3.5.2 MQ spin counting experiment on elastomers is presented. Up to the 6-th order of coherence has been measured in high crosslinked polybutadiene rubber with thirty-two pulse sequence which was up to now not reported on elastomers.

3.1 Single Quantum MAS experiment

In this section dipolar coupling will be measured from a single quantum (SQ) MAS experiment. Theoretical bases for simple one pulse MAS experiment were already done in section 1.6. Two spin- $\frac{1}{2}$ system coupled via dipole-dipole coupling was chosen to simulate the NMR signal (see equation (1.83)). Neglecting CSA terms it was shown that MAS generate a symmetric SQ spinning sidebands spectrum (see Figure 1.4). Comparing intensities of the spinning sidebands dipolar coupling strength d_{ij}^{II} can be calculated ([Gra97a, Fil97]). For moderate spinning speeds when $\omega_r \simeq d_{ij}^{II}$ an approximate solution of the equation (1.83) will be presented. It was found by our computer simulation that approximation up to the 6-th order is sufficient for this spinning regime.

For rapid spinning case ($\omega_r \gg d_{ij}^{II}$) equation (1.83) describing the signal from the dipolar coupled spin- $\frac{1}{2}$ pair can be formally solved. The cosine function may be expanded into the Taylor series and only up to the second-order coefficients will be considered. Calculating the powder average through angles ϑ, ψ it can be found the approximate solution

$$\tilde{S}_y^{MAS}(t) = 1 - \underbrace{\frac{27}{80}\mu^2}_{\text{Central line}} + \underbrace{\frac{3}{10}\mu^2 \cos(\omega_r t)}_{\text{1. Order sidebands}} + \underbrace{\frac{3}{80}\mu^2 \cos(2\omega_r t)}_{\text{2. Order sidebands}} \quad (3.1)$$

with the parameter $\mu = d_{ij}^{II}/\omega_r$. Detailed derivation of the equation above can be found in Graf thesis ([Gra97a], Appendix A). Assuming the integral intensity of the first sideband I_{s1} and the integral intensity of the central line I_0 the dipolar coupling can be calculated by the help of equation (3.1) as

$$d_{ij}^{II} = \omega_r \sqrt{\frac{20 I_{s1}/I_0}{3 + \frac{27}{4} I_{s1}/I_0}} \quad (3.2)$$

This simple two spin system approximation can not be used if the MAS spectrum is asymmetric which can be caused by spectrometer problems or by the influence of an anisotropic coupling (e.g. B_1 field inhomogeneity, CSA). The restriction for the second order approximation can be made according to Filip et al. ([Fil97]) calculations as $\mu \leq 0.5$ ($\omega_r \geq 2d_{ij}^{II}$). This restriction can be therefore considered as a condition for very fast

spinning limit. For smaller μ the difference between the exact and the approximate result became negligible for two spin system. In general the dipolar coupling can be also calculated from the integral intensity of the second order sideband (see equation (3.1)) but for the fast spinning case ($\mu \leq 0.5$) the intensity is at least 200 times smaller than the intensity of the central line and thus due to the big experimental error of evaluating the integral it has no use.

For moderate spinning speeds the error introduced by the considering only the second-order terms increasing rapidly as μ approaches the value $\mu = 1$ (Neglecting terms of order four and higher an error of 25% is introduced to calculate ratio $\frac{\text{1.-order sideband}}{\text{central line}}$ when $\mu = 1$). The extension to higher orders is necessary to get sufficient precise results. In moderate spinning regime ($\mu \lesssim 1$) the expansion until 6-th order of equation (1.83) is sufficiently enough. Integral intensities of the central line I_0 , 1.-order sideband I_{s1} and 2.-order sideband I_{s2} for powder sample were calculated and result can be written in following form

$$\begin{aligned} I_0/I_{st} &= 1 - \frac{27}{80} \mu^2 + \frac{2043}{35840} \mu^4 - \frac{89343}{16400384} \mu^6 \\ I_{s1}/I_{st} &= \frac{3}{20} \mu^2 - \frac{153}{4480} \mu^4 + \frac{10611}{2928640} \mu^6 \\ I_{s2}/I_{st} &= \frac{3}{160} \mu^2 + \frac{9}{2560} \mu^4 - \frac{241623}{328007680} \mu^6. \end{aligned} \quad (3.3)$$

The intensities are normalized by the integral intensity of the static NMR spectrum I_{st} . Due to the symmetry of the sideband spectrum (see e.g. Figure 1.4) only integral intensities of the one half of the spectrum are represented by symbols I_{s1} and I_{s2} . From set of equations (3.3) dipolar coupling can be directly determined similar like in equation (3.2). Three different solutions can be found comparing intensities of I_{s1}/I_0 , I_{s2}/I_0 and I_{s2}/I_{s1} . Due to the small intensity of the 2.-order sideband (I_{s2}) which brings a big experimental error in evaluating of the integral, only first solution (I_{s1}/I_0) will be considered for evaluating dipolar coupling d_{ij}^{II} .

If the sample has transverse isotropy the similar formula like equation (3.3) can be derived for the ϑ angle dependence. The expansion until 4-th order for such a case can be found elsewhere ([Fil97]).

According to equation (3.3) the dipolar coupling d_{ij}^{II} was calculated combining expression for the 1.-order sideband and the central line in hexamethylbenzene (HMB). MAS spectra of HMB for different rotational frequencies are shown in Figure 3.1. It has to be noted that HMB is not the ideal two spin system sample. The molecule itself rotate very

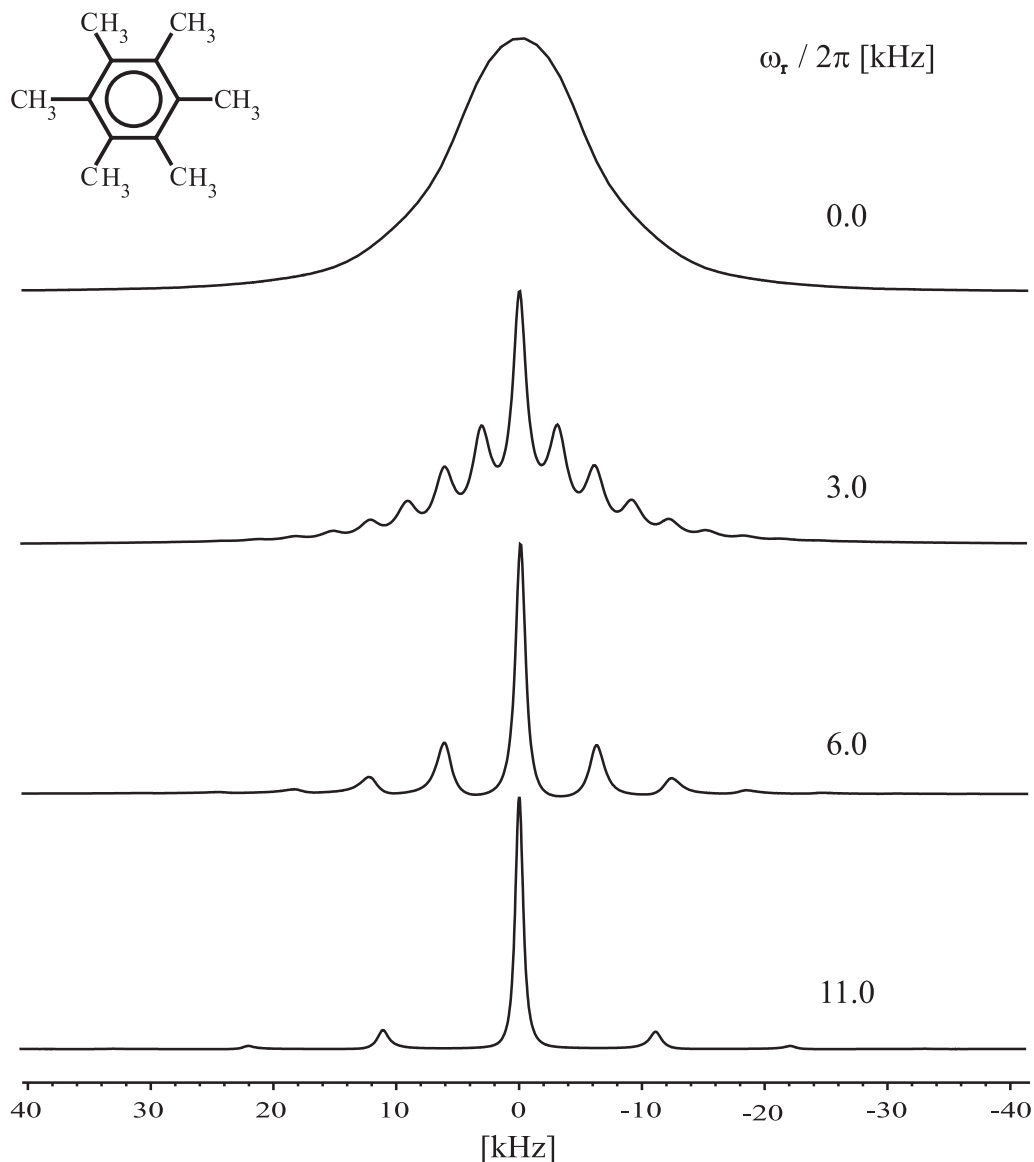


Figure 3.1: ^1H MAS spectra of hexamethylbenzene (HMB) measured at different rotational frequencies ω_r at room temperature. Spectra are normalized to the same amplitude.

fast and intra-molecular dipolar coupling between protons (^1H) in the same molecule are averaged out. Only the spin-spin interactions between molecules (inter-molecular) still remains. Thus, only 'effective' dipolar coupling could be measured. The last spectrum in Figure 3.1, where sample was rotating around the rotor axis under MAS conditions with the frequency $\omega_r/2\pi = 11$ kHz, was chosen to evaluate the coupling. The 'effective' dipolar coupling until the 6-th order approximation was estimated as $d_{ij,ef} = 2\pi \times 8.8$ kHz.

3.2 DQ sideband pattern under MAS

In this section the main difference between δ -pulses sequence (DRAMA/BABA) and spin-lock pulse sequences (C7/POST C7) will be elucidated. Influence of their DQ dipolar average Hamiltonians (see section 2.5.1) on the spin system coupled via dipolar coupling will be studied. We will concentrate on the calculation of the intensities of the DQ coherence which can be used for determining dipolar couplings. Experimental confirmation of the spinning sideband pattern for DRAMA/BABA and C7 will be also presented. Two-dimensional MQ experiment is going to be considered only in this section (see also section 2.5.2).

For deriving DQ intensities at the end of the reconversion period the general form of the zero-order average Hamiltonian for excitation and reconversion period will be used and

$$\hat{H}_{DQ}^{exc/rec} = \sum_{i<j} \omega_{ij}^{exc/rec} \hat{T}_{2,2}^{ij} + (\omega_{ij}^{exc/rec})^* \hat{T}_{2,-2}^{ij}. \quad (3.4)$$

$\omega_{ij}^{exc/rec}$ in above equation represents the amplitude and the phase of the excitation/reconversion average Hamiltonian (see equations (2.51),(2.52)). In general $\omega_{ij}^{exc/rec}$ is the complex term and it is useful to separate the phase $\Phi_{ij}^{exc/rec}$ and the amplitude $|\omega_{ij}^{exc/rec}|$ variables from it as

$$\omega_{ij}^{exc/rec} = |\omega_{ij}^{exc/rec}| e^{i\Phi_{ij}^{exc/rec}}. \quad (3.5)$$

Detailed calculation for the DQ signal intensity for a two spin- $\frac{1}{2}$ system at the end of the reconversion period was shown in Appendix C and has the form (see equation (C.20)):

$$S_I^{DQ} = \cos(\Phi_{ij}^{rec} - \Phi_{ij}^{exc}) \sin(|\omega_{ij}^{rec}| \tau) \sin(|\omega_{ij}^{exc}| \tau). \quad (3.6)$$

In addition $|\omega_{ij}^{exc/rec}|$ and $\Phi_{ij}^{exc/rec}$ can depend from Euler angles ϑ and ψ (e.g. see section 2.5.1.1). Presuming the same probability for all angles ϑ, ψ powder average over angles ϑ, ψ has to be performed to get the resulting signal intensity of the DQ coherence S_I^{DQ} in equation (3.6). τ represents an equivalence of the duration of the excitation and reconversion period.

For the moment the phase factor in equation (3.6) inside of the \cos function will be not regarded because it has no influence to the amplitude of the DQ signal for pulse sequence like DRAMA/BABA as well as for C7 (see sections 3.2.1,3.2.2). In addition let us assume

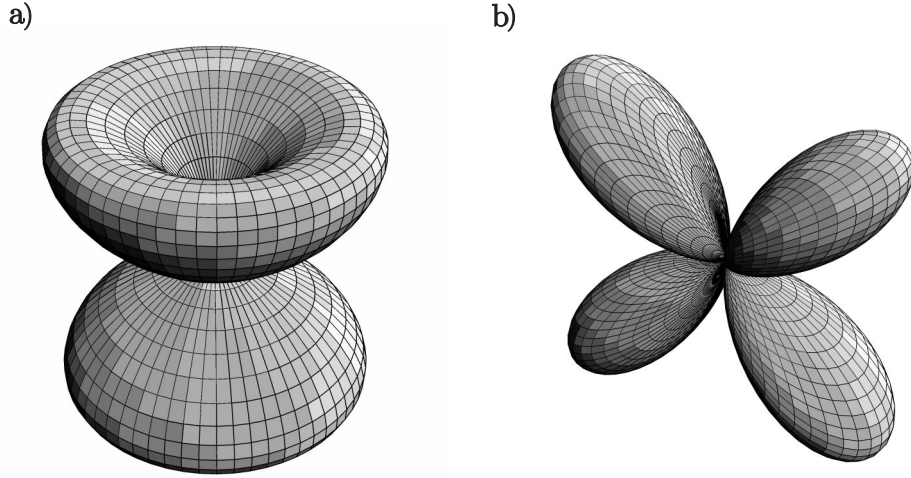


Figure 3.2: Orientation dependence of DQ intensities from angles ϑ, ψ presented in spherical coordinates for: a) C7/POST C7 pulse sequences, b) DRAMA/BABA pulse sequences.

for simplicity $|\omega_{ij}^{rec}| = |\omega_{ij}^{exc}| = |\omega_{ij}(\vartheta, \psi)|$ the DQ intensity gets the form

$$S_I^{DQ} = \langle \sin^2(|\omega_{ij}(\vartheta, \psi)|\tau) \rangle_{\vartheta, \psi}. \quad (3.7)$$

In the limit of small excitation/reconversion times $\tau \ll |\omega_{ij}(\vartheta, \psi)|^{-1}$ the *sin* function in equation (3.7) can be spread to the Taylor series, where higher orders can be neglected. Separating for convenience $|\omega_{ij}(\vartheta, \psi)|$ to the orientation independent norm $\omega_{ij, norm}$ and angle dependent function $g(\vartheta, \psi)$ where $|g(\vartheta, \psi)| < 1$ the DQ intensity for short time limits is derived and it holds that

$$S_I^{DQ} \simeq \langle |g(\vartheta, \psi)|^2 \rangle_{\vartheta, \psi} \omega_{ij, norm}^2 \tau^2. \quad (3.8)$$

The angle dependent functions $|g(\vartheta, \psi)|^2$ for C7 and DRAMA/BABA pulse sequences are shown in Figure 3.2. Equation (3.8) shows us that each pulse sequence is characterized by the average factor \bar{g} which can be derived for DRAMA/BABA pulse sequences (see also section 3.2.1) from¹

$$\bar{g}_{DRAMA/BABA}^2 = \frac{1}{4\pi} \int_0^\pi d\vartheta \sin(\vartheta) \int_0^{2\pi} d\psi \sin^2(2\vartheta) \cos^2(\psi) = \frac{4}{15} \quad (3.9)$$

and for C7 pulse sequence (see also section 3.2.2) from

$$\bar{g}_{C7}^2 = \frac{1}{2} \int_0^\pi d\vartheta \sin(\vartheta) \sin^2(2\vartheta) = \frac{8}{15}. \quad (3.10)$$

¹Powder averaging over angles ϑ, ψ is considered.

Multiplying the average factor \bar{g} with the orientation independent norm $\omega_{ij,norm}$ for particular pulse sequence (see equation (3.8)) effectiveness of the recoupling pulse sequences can be calculated. More details about DRAMA/BABA and C7 will be presented in the next sections.

3.2.1 DRAMA/BABA

It was shown in sections 2.5.1.1 and 2.5.1.2 that DRAMA and BABA pulse sequences can be described by the same zero-order average Hamiltonian. Improved version of BABA pulse sequence acting on the two rotor periods (see Figure 2.17b) has better compensation properties with respect to resonance offsets and small CSA ($\|\hat{\mathbf{H}}_{CSA}\| \ll \|\hat{\mathbf{H}}_D\|$). The signal intensity just after the detecting pulse in two-dimensional MQ experiment (section 2.5.2) can be assumed as the signal stored in the longitudinal magnetization just after the reconversion period (see also discussion in Appendix C). If in addition so-called total spin coherence ([Wei83, Mun87]) is excited during excitation period all coupled spins are active in MQ coherences and therefore no evolution occurs under the influence of dipolar Hamiltonian (equation (1.59)). Under this conditions signal intensity at the beginning of the detection period ($t_2 = 0$) can be calculated for two spin- $1/2$ system (see equation (3.6) and equation (C.14))

$$S_I(t_1) = \langle \cos(|\omega_{ij}^{rec}(t_1)|\tau) \cos(|\omega_{ij}^{exc}|\tau) \rangle + \cos(2\Delta\omega_\phi t_1) \langle \sin(|\omega_{ij}^{rec}(t_1)|\tau) \sin(|\omega_{ij}^{exc}|\tau) \rangle, \quad (3.11)$$

where

$$\omega_{ij}^{exc} = -\frac{3}{\pi\sqrt{2}} d_{ij}^{II} \sin(2\vartheta_{ij}) \cos(\psi_{ij}) e^{-i2\Delta\omega_\phi t_1} \quad (3.12)$$

$$\omega_{ij}^{rec}(t_1) = -\frac{3}{\pi\sqrt{2}} d_{ij}^{II} \sin(2\vartheta_{ij}) \cos(\psi_{ij} + \omega_r t_1). \quad (3.13)$$

The symbol $\langle \dots \rangle$ represents the powder average over the angles ϑ, ψ in equation (3.11). Time dependence of the ω_{ij}^{exc} in equation (3.12) is omitted because it appears only in the complex term $e^{-i2\Delta\omega_\phi t_1}$ and thus is not relevant in its absolute value used in equation (3.11). Nevertheless it influences the phase of the resulting signal described in the \cos term. τ corresponds to the duration of the excitation/reconversion period and can be only incremented in steps of the rotor period τ_r ($\tau = N \cdot \tau_r$, or $\tau = N \cdot 2\tau_r$ ²).

²For improved version of BABA pulse sequence acting on the two rotor periods (see section 2.5.1.2).

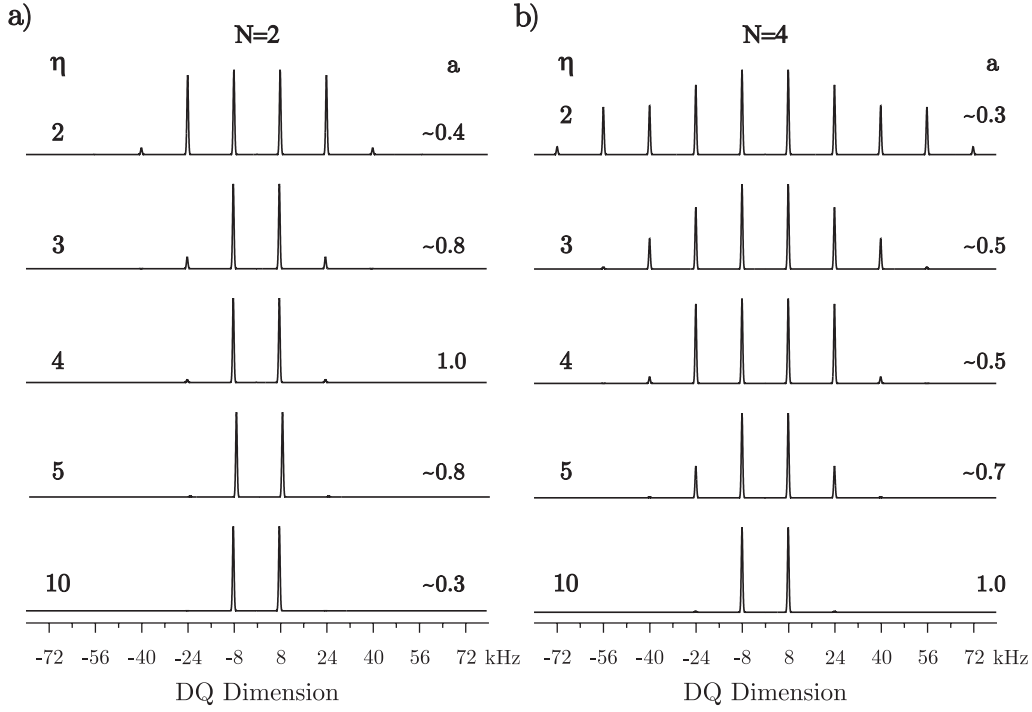


Figure 3.3: Simulated DQ spinning sideband pattern for DRAMA/BABA pulse sequence for different number of rotor cycles: a) $N = 2$, b) $N = 4$. The dependence on the parameter $\eta = \frac{\omega_r}{d_{ij}}$ for different coupling strength d_{ij} is shown. The relative amplitude of the first DQ sideband is represented by symbol **a**.

The first term in equation (3.11) describes the rotor-modulated longitudinal magnetization and is usually filtered out from the spectrum (see also section 4.3). The second term is the TPPI-labeled DQ coherence where TPPI-labeling is represented by the phase factor $\Phi_{exc} = 2 \Delta\omega_\phi t_1$. Using Fourier-Bessel series this term can be evaluated ([Got96])

$$S_I^{DQ}(t_1) = \sum_{k=-\infty}^{\infty} \frac{1}{2} \left\{ 1 - (-1)^k \right\} \left\langle J_k^2 \left(\frac{3}{\pi\sqrt{2}} d_{ij}^H \sin(2\vartheta_{ij}) \tau \right) \right\rangle \cos \left((2\Delta\omega_\phi + k\omega_r) t_1 \right), \quad (3.14)$$

where J_k are the integer-order Bessel functions. The presence of the *cos* factor in equation (3.14) shows that negative and positive frequencies can not be distinguished corresponding to single-channel detection. The argument of the *cos* function describes the separation of the DQ coherence by TPPI procedure. The DQ spectrum is then shifted to the frequency $(2 \Delta\omega_\phi)/2\pi$ with symmetrically distributed sidebands left from this point at $k \cdot \omega_r$ ($\omega_r = 2\pi f_r$). Hence, a symmetric spinning sideband pattern is generated in indirect t_1 dimension (DQ dimension) with no central line. Only odd-order spinning sidebands at the frequencies $\pm(2k + 1)f_r$, ($k \in \mathbf{N}$) are present with an intensity modulated by Bessel functions. The relative intensities of the sidebands are determined by the orientation

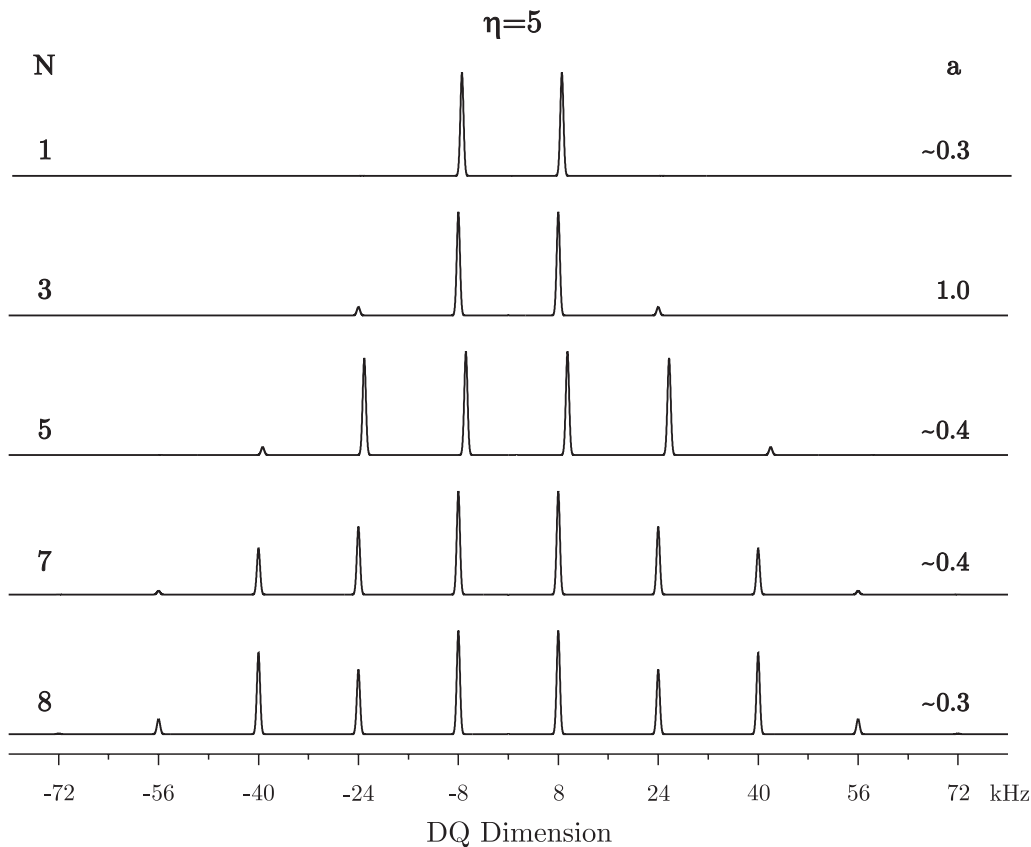


Figure 3.4: Simulated DQ spinning sideband pattern for different excitation times $\tau = N \cdot \tau_r$. Dipolar coupling strength is chosen 5 times smaller than rotational frequency f_r which corresponds to the dipolar coupling strength $d_{ij} = 2\pi 1.6$ kHz for $f_r = 8$ kHz. More details see description under Figure 3.3.

and the strength of the dipolar coupling and by duration of the excitation/reconversion period τ .

Simulated spectra of DQ spinning sideband pattern for DRAMA/BABA pulse sequence are shown in Figure 3.3. Isolated spin- $1/2$ pairs in a powder have been only considered. Simulations of equation (3.11) (DQ part only) and equation (3.14) showed the conformity for powders as it was expected. The patterns for different excitation time $\tau = N \cdot \frac{1}{f_r}$ of DRAMA and the basic version of BABA pulse sequence are shown in Figure 3.3 as a function of the ratio $\frac{\omega_r}{d_{ij}} = \eta$ (see equation (3.14)) for $N = 2$ and $N = 4$. The powder average is performed numerically. Rotational frequency is chosen $f_r = 8$ kHz. As can be seen from Figures 3.3a and 3.3b number of sidebands are decreasing with increasing η (decreasing the coupling strength d_{ij}) in both cases. For very weak dipolar couplings (or very high spinning speeds) only the first order sidebands govern the spectrum. In

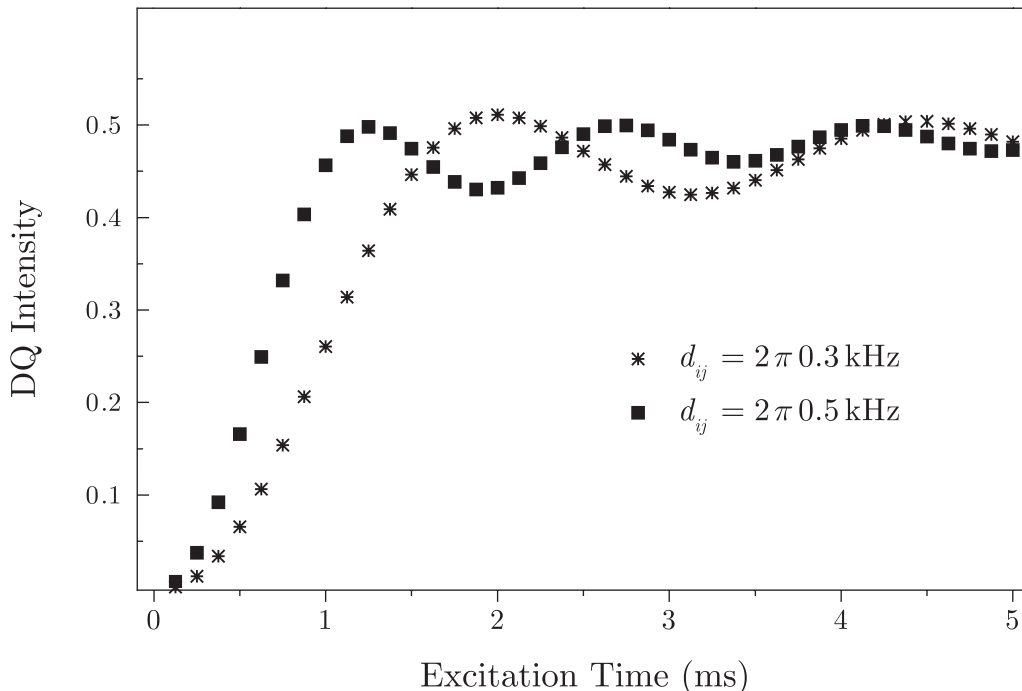


Figure 3.5: Simulated DQ build-up curves for spin- $1/2$ pairs with different dipolar couplings $d_{ij} = 2\pi 0.3$ kHz (asterisks) and $d_{ij} = 2\pi 0.5$ kHz (squares) for DRAMA/BABA pulse sequence. Rotor frequency was chosen $f_r = 8$ kHz. The points represent integral intensities of DQ coherence calculated at full rotor periods.

this regime, the strength of the dipolar coupling is solely reflected in the intensity of this lines and no additional information can be obtained from other spinning sidebands. With increasing number of cycles $N = 4$ (Figure 3.3b) number of sidebands is increasing, thus for very high excitation times one has to expect many sidebands where the probability of overlapping with sidebands from other coherence orders is very high. Growing of the sidebands with increasing excitation/reconciliation time is shown in Figure 3.4. Dipolar coupling was chosen five times smaller than the spinning frequency ($d_{ij} = 2\pi 1.6$ kHz).

Summing the intensities of the odd-order DQ sidebands up to the sufficient order³ (equation (3.14)) for different excitation times τ ($\tau = N \cdot \tau_r$) so-called build-up curves can be generated. The simulated DQ build-up curves for spin- $1/2$ pairs in a powder are presented in Figure 3.5. Comparison of different dipolar coupling strengths for DRAMA/BABA pulse sequence in the regime of fast MAS ($\omega_r \gg d_{ij}$) is presented. The strong dependence on the coupling strength is evident from the figure even for small changes of the coupling. The initial part of the build-up curves can be used for evaluating dipolar coupling strength.

³Where the influence of higher orders is negligible.

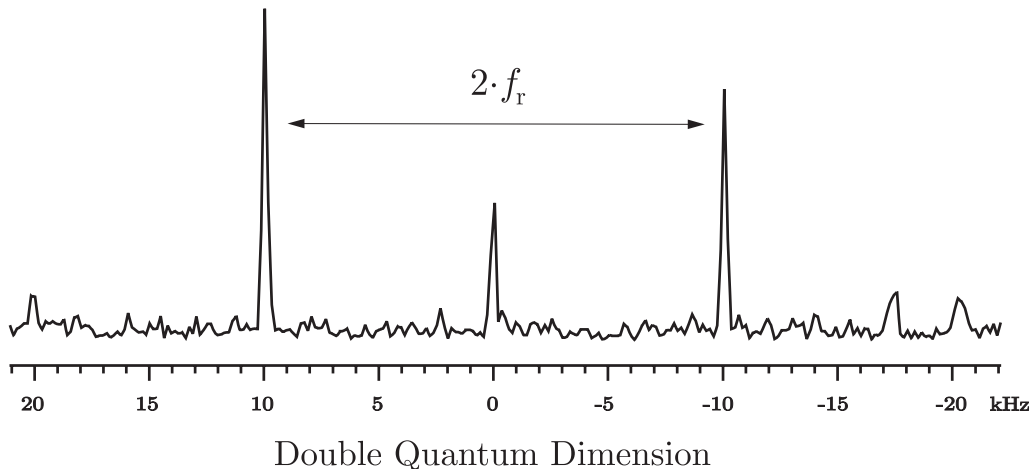


Figure 3.6: ^1H 400 MHz DQ spectrum of polybutadiene melt measured with DRAMA pulse sequence at room temperature. Only the trace which corresponds to the CH_2 group from 2D experiment (more details see section 3.3) was chosen to visualize the appearance of the DQ sidebands. TPPI is performed to separate DQ coherence ($\Delta\omega_\phi = \pi/(4\Delta t_1)$; $\Delta t_1 = 12.5 \mu\text{s}$). In addition 32 step DQ filter (see section 4.3) was used to filter out higher order coherences and pulse imperfections. Rotational frequency was chosen $f_r = 10 \text{ kHz}$ and excitation time $\tau = 300 \mu\text{s}$. The length of the $\frac{\pi}{2}$ r.f. pulses was $3 \mu\text{s}$. 20 ms delay after the reconversion period was chosen to allow unwanted transients to decay (see Figure 2.20; $n_0 = 200$).

Its slope versus the square of the excitation/reconversion time $(N\tau_r)^2$ is proportional to the square of the dipolar coupling d_{ij}^2 (see also equation (3.8)). As can be seen from Figure 3.5 the maximum integral intensity of the DQ coherence can reach about 52% of the initial Zeeman order for a spin- $\frac{1}{2}$ pair in a powder. Increasing excitation/reconversion time τ further the DQ coherence exhibits oscillatory behaviour. Experimental results shows (see section 3.3) that this behaviour can not be used for evaluating dipolar couplings. Increasing number of rotor synchronized cycles both the intensity of DQ spectra and the sideband pattern might be influenced by the molecular dynamics and pulse imperfections. Therefore, oscillatory regime will be in most of the cases strongly influenced in real system.

Experimental confirmation of the spinning sidebands pattern is shown in Figure 3.6 for DRAMA pulse sequence. Investigated sample was polybutadiene melt $\{-\text{CH}_2 - \text{CH} = \text{CH} - \text{CH}_2-\}$ (more details see section 3.3 and Figure 3.10). Experimental results shows that in the fast spinning regime $f_r = 10 \text{ kHz}$ the first order spinning sidebands dominate the spectrum for protons (^1H) in CH_2 group. In fact this is

only illustrative result that spinning sidebands appear and can not be used for further investigation. Due to the bad compensation property of DRAMA pulse sequence (see section 2.5.1.1) resonance offsets influence the spectrum. Influence of CSA can be neglected for this high spinning regime for this sample. Even after the DQ filtration (see section 4.3) performed in this experiment the rotor modulated magnetization behaving like a zero-quantum coherence (first term in equation (3.11)) is observed in the middle of the spectrum (see Figure 3.6). Influence of the neighbored protons from CH group on the protons in CH_2 group was completely not visible for DRAMA pulse sequence. More details see section 3.3.

Experimental results performed on the same sample with C7 pulse sequence will be presented in the following part.

3.2.2 C7/POST C7

C7 pulse sequence is much more efficient with the comparison to DRAMA and BABA pulse sequences for powders. Improved version called POST C7 is even much less sensitive to the resonance offsets as the original one (more details see section 2.5.1.3). To calculate the signal intensity just after the detecting pulse (see section 2.5.2) zero-order average Hamiltonians for excitation and reconversion period have to be derived, respectively. According to equations (3.4), (2.51) and (2.52) the complex factors $\omega_{ij}^{exc/rec}$ can be estimated for both periods

$$\omega_{ij}^{exc} = \omega_{C7}^{ij} e^{-i(2\Delta\omega_\phi t_1 + \psi_{ij})} \quad \text{and} \quad \omega_{ij}^{rec} = \omega_{C7}^{ij} e^{i(\omega_r t_1 - \psi_{ij})}, \quad (3.15)$$

where

$$\omega_{C7}^{ij} = \frac{343(i + e^{i\pi/14})}{520\pi\sqrt{2}} d_{ij}^{II} \sin(2\vartheta_{ij}). \quad (3.16)$$

As can be seen from above relations both ω_{ij}^{exc} and ω_{ij}^{rec} are time t_1 independent in their absolute values which is not the case for DRAMA/BABA pulse sequence (see equations (3.12), (3.13)). Separating the phase and the amplitude variables from equation (3.15) the intensity of the signal ($t_2 = 0$) for system consisting of two coupled spins- $1/2$ can be calculated (see equation (3.6) and equation (C.14)) as

$$S_I(t_1) = \left\langle \cos^2(|\omega_{C7}^{ij}|\tau) \right\rangle + \cos\left((2\Delta\omega_\phi + \omega_r)t_1\right) \left\langle \sin^2(|\omega_{C7}^{ij}|\tau) \right\rangle, \quad (3.17)$$

where

$$|\omega_{C7}^{ij}| = \frac{343}{520\pi} d_{ij}^{II} \sin(2\vartheta_{ij}) \sqrt{1 + \sin\frac{\pi}{14}}. \quad (3.18)$$

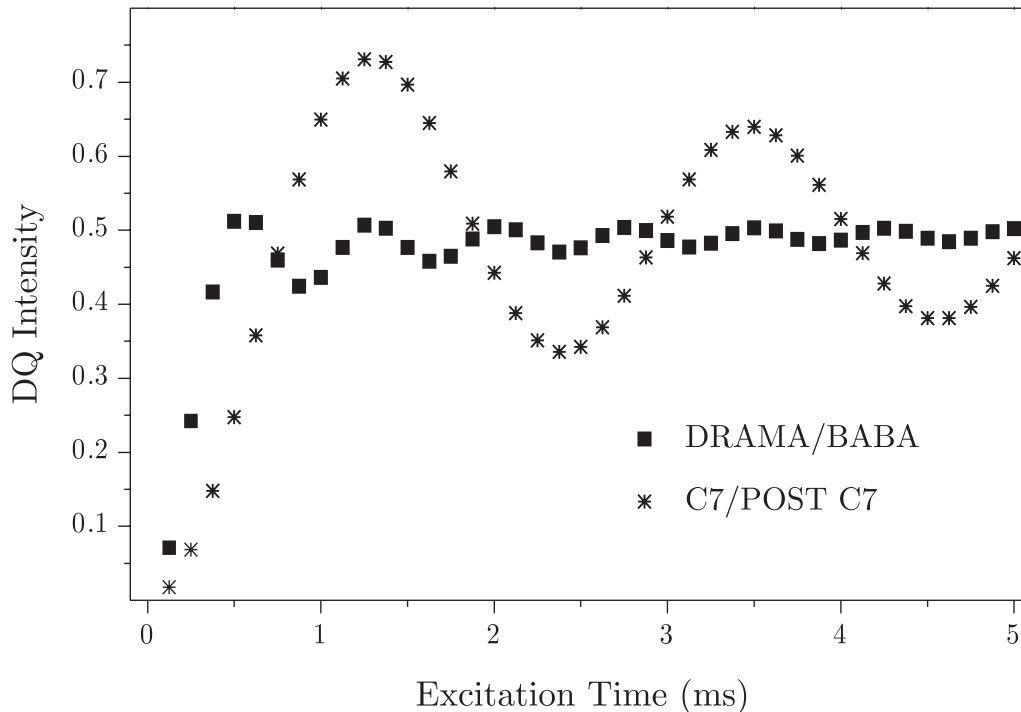


Figure 3.7: Comparison of the effectiveness of C7/POST C7 (asterisks) and DRAMA/BABA (squares) pulse sequence. DQ build-up curves were simulated for dipolar coupling strength $d_{ij} = 2\pi 1.0$ kHz and for rotational frequency $f_r = 8$ kHz. The points represent integral intensities of the DQ coherence calculated at full rotor periods.

Averaging over all possible orientations is described by the symbol $\langle \dots \rangle$ in equation (3.17). Unlike DRAMA and BABA pulse sequences the magnitude of the factor $|\omega_{C7}^{ij}|$ for C7 pulse sequence does not depend on the Euler angle ψ_{ij} (see equation (3.18)), leading to a high overall efficiency for orientationally disordered samples such as powders.

The first term in equation (3.17) describes the remaining part of the initial Zeeman order and has to be filtered out from the resulting spectrum. Despite of DRAMA/BABA pulse sequence (see first term in equation (3.11)) it is not rotor modulated. The second term in equation (3.17) is the most important DQ coherence, modulated by the rotor frequency. Modulation can be seen from the argument of the *cos* function. Orientation dependent norm $|\omega_{C7}^{ij}|$ of the C7 pulse sequence (equation (3.18)) does not depend on the evolution time t_1 hence no spinning sidebands will be seen unlike DRAMA/BABA pulse sequence. Desired DQ signal will be found at the frequency $(2\Delta\omega_\phi + \omega_r)/2\pi$ in indirect dimension (ω_1 dimension), where $\Delta\omega_\phi$ represent the phase shifting of the pulses during excitation period by TPPI procedure (see section 2.5.2). The relative intensity of the DQ

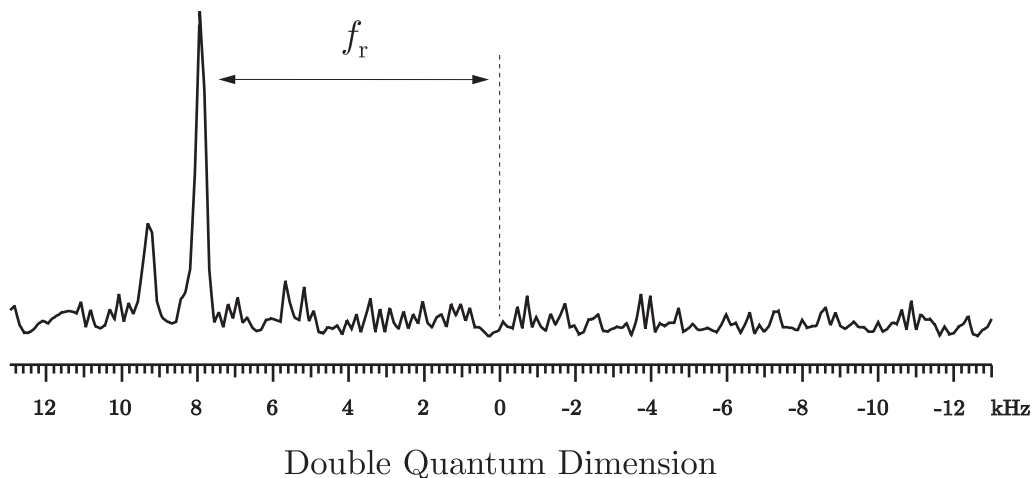


Figure 3.8: ^1H 400 MHz DQ spectrum of polybutadiene melt measured with POST C7 pulse sequence at room temperature. Similar like in Figure 3.6 only the trace corresponding to the frequency of the CH_2 group in ω_2 (direct) dimension is shown. Separation of DQ coherence was made by TPPI so: $\Delta\omega_\phi = \pi/(4\Delta t_1)$, $\Delta t_1 = 15.625 \mu\text{s}$. 32 step DQ filter (see section 4.3) was chosen to filter out all unwanted coherences and pulse imperfections. Excitation time τ was set to 500 μs . Strength of the r.f. pulses was $\omega_{B_1} = 7\omega_r$ ($\omega_{B_1} \simeq 56 \text{ kHz}$). To allow unwanted transients to decay 15 μs delay was inserted between reconversion and detection pulse (see Figure 2.20; $n_0 = 120$).

signal is determined by the orientation and the strength of the dipolar coupling and by the duration of the excitation/reconversion period (see argument in the *sin* function in equation (3.17)).

Assuming spin- $1/2$ pairs in a powder simulation of the DQ build-up curves was performed to compare the effectiveness of C7/POST C7 and DRAMA/BABA pulse sequences. It is shown in Figure 3.7. The maximum DQ integral intensity for C7 pulse sequence is about 73% of the initial Zeeman order, unlike DRAMA where it is only about 52%. For higher excitation times C7 exhibit oscillatory behaviour similar like DRAMA. To evaluate dipolar coupling strength it is enough to regard the initial part of the build-up curve. The slope of this part versus τ^2 is proportional to the square of the dipolar coupling d_{ij}^2 (see equation (3.8)).

DQ spectrum of the polybutadiene melt $\{-\text{CH}_2 - \text{CH} = \text{CH} - \text{CH}_2-\}$ with POST C7 pulse sequence is shown in Figure 3.8 similar like for DRAMA pulse sequence (see page 74). Fast spinning regime was chosen with the frequency $f_r = 8 \text{ kHz}$. The highest peak in the figure corresponds to the strong connectivity between the protons in the CH_2 group. Zero frequency position in Figure 3.8 was set to the frequency related to the TPPI

phase shifting procedure which results for DQ coherence as $2\Delta\omega_\phi/2\pi$. No additional peaks appear in the negative frequency region in the DQ spectrum as was expected. Remaining peak left from the CH_2 group is related to the dipolar coupling between protons in the CH and CH_2 group in polybutadiene which was not observable in the case of DRAMA pulse sequence (see Figure 3.6). Experimental results from POST C7 show much highest effectiveness than from DRAMA pulse sequence. Positive and negative frequencies were clearly distinguished in DQ spectrum which was not the case for DRAMA as well as for BABA pulse sequence. More details will be presented in the next section.

3.3 DQ spectroscopy under MAS

In this section 2D MQ spectroscopy will be explained. As was already mentioned in sections 2.5.2 and 3.2 MQ coherences are detectable in indirect ω_1 dimension. Thus two-dimensional experiment is necessary to perform. The coherences are excited during excitation period (see e.g. Figure 2.20) followed by the evolution period t_1 . If so-called total spin coherence is excited MQ coherences does not evolve under the influence of the dipolar Hamiltonian (see equation (2.11)). Nevertheless evolution under the influence of chemical shift interaction is present⁴. In real system pure on-resonance excitation is usually impossible, thus resonance offsets caused by linear interactions like e.g. isotropic chemical shifts or CSA will appear p -times shifted from resonance frequency in ω_1 dimension for each p -quantum coherence (see equation (2.35)). Broadening caused by CSA will be than p -times higher in ω_1 dimension compared to ω_2 dimension. For DQ coherence these frequency shifts (caused by linear interactions) will be twice larger in ω_1 dimension (double quantum dimension) than in ω_2 dimension (single quantum dimension).

In Figure 3.9 the model system of two *functional groups* representing with two chemical shifts ω_A and ω_B is shown. It serves as the intuitive model for understanding DQ coherence. In Figure 3.9a system with two isolated spins is shown. The dipolar coupling between them is very weak and can be neglected. Only DQ coherence between spins within the same group (intragroup coupling) is excited during the excitation period of the pulse sequence and it appears at the frequency positions $2\omega_A$ and $2\omega_B$ in the DQ dimension, respectively. In the single quantum (SQ) dimension frequencies for different groups remains unchanged at positions ω_A and ω_B . In Figure 3.9b a model system is shown for

⁴Other interactions like e.g. J -coupling will be not assumed because they are negligible for our samples.

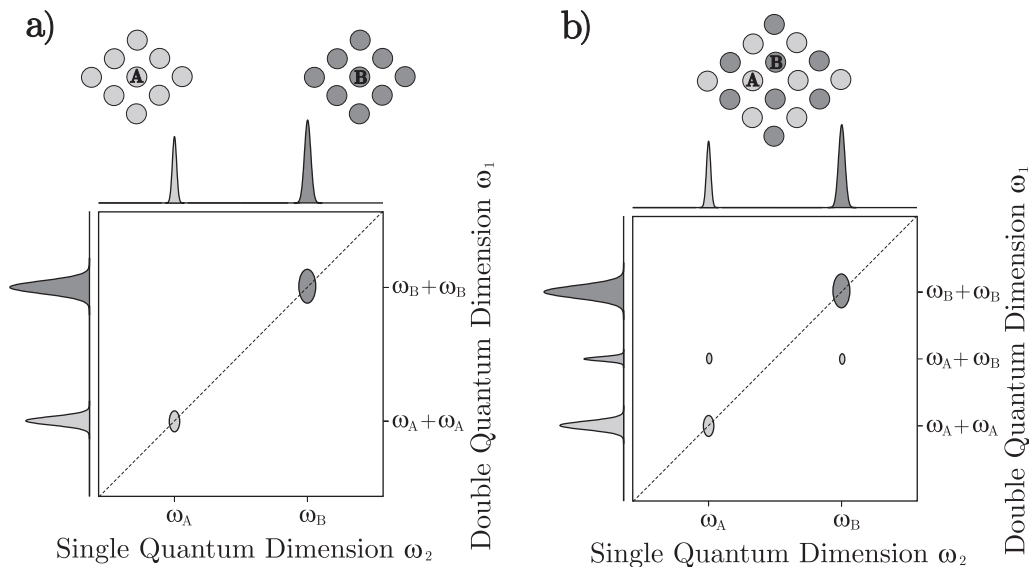


Figure 3.9: Structure of DQ spectrum for two model systems consisting of two functional groups.

spins where dipolar coupling between different functional groups is already present (inter-group coupling). This coupling evolves during evolution time with sum of the chemical shifts for both groups and thus appear at the frequency $\omega_A + \omega_B$ in DQ dimension. After reconversion period spins from the different groups carries the original frequency at which they appear in the SQ dimension during detection period. Drawing diagonal line between the coherences appeared from spins originated from the same functional groups, DQ coherences representing the connectivities between this groups appear equally distributed around this line as can be seen from Figure 3.9b.

For demonstrating connectivities between different functional groups the sample of polybutadiene melt was chosen. From the viewpoint of NMR polybutadiene exhibit both liquid-like and solid-like features. At temperatures well about the glass transition temperature dipolar couplings are averaged out by fast molecular motion. However, the presence of topological constrains and permanent crosslinks prevent the chain motion to be free. Thus, dipolar interaction is not completely averaged out and the *residual dipolar coupling* is possible to measure. Our measurements were performed at room temperature which was well above the glass transition temperature ($T_g = 175\text{K}$ for our sample). At this temperature residual dipolar coupling is scaled in order of 1 kHz which allows us to measure connectivities between groups like e.g. CH and CH_2 in the regime of fast MAS ($\omega_r \gg \omega_D$). Influence of the CSA for our investigated polybutadiene melt will be neglected ($\|\hat{H}_{CSA}\| \ll \|\hat{H}_D\|$).

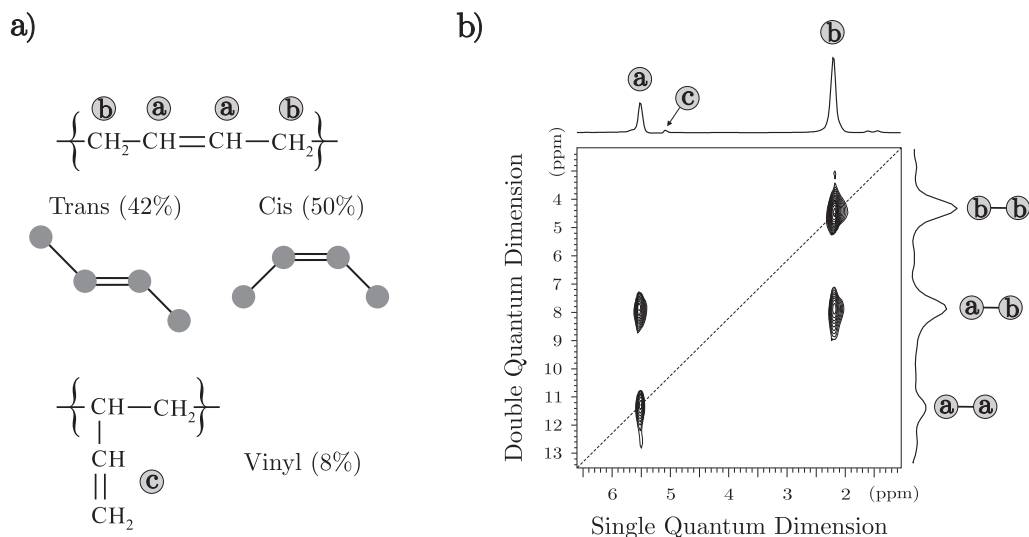


Figure 3.10: 1H 400 MHz DQ MAS spectrum of polybutadiene melt at room temperature. POST C7 was used at rotor frequency 8 kHz. To separate DQ coherence TPPI phase shifting scheme is performed as in Figure 3.8. Excitation time τ was 1.5 ms to see the maximal DQ signal intensity. A delay 15 ms was included after reconversion period to allow unwanted transients to decay.

Chemical structure of the polybutadiene melt is shown in Figure 3.10a ($M_w=129\,000$ g/mol, $M_n=125\,000$ g/mol). *Cis* and *Trans* conformations of polybutadiene were not possible to distinguish from our measurements. The spinning speed $f_r = 8$ kHz was not high enough to separate them at the proton frequency $\omega_{0,^1H}/2\pi = 400$ MHz. The percentage of the vinyl butadiene (labeled (c) in Figure 3.10a) was found to be 8% and thus, it was not visible in DQ spectrum (see Figure 3.10b). The SQ projection is found at the top of the DQ spectrum. Experiment qualitatively agree with that made by R. Graf ([Gra97a]). Existence of the peaks in DQ spectrum shows that DQ coherences were established between spins which are relatively close neighbours in space. Only such spins which are close together can contribute to the intensity of the peaks. Dipolar connectivities were found between both groups CH and CH_2 . Due to the low intensity of the signal originated from protons (labelled c) in vinyl group connectivities between other groups were not observed. When comparing intensities of different groups one should keep in mind that also the (relative) number of protons of the corresponding group influence them as well as the molecular dynamics. The strongest DQ signal is found between protons inside of CH_2 group (labelled $b-b$) in polybutadiene. Dipolar connectivities between protons from the double bond group ($a-a$) are also visible. Cross-peaks equally distributed from diagonal

line (labelled $a - b$) shows that dipolar coupling between different groups CH and CH_2 is not completely averaged out by fast molecular motion. The cross-peaks indicates that DQ spectroscopy is an unique technique for measuring dipolar connectivities between different groups in polybutadiene melt and thus residual dipolar couplings can be estimated (see section 3.3.1).

For measuring residual dipolar couplings between different and within the same functional groups single DQ experiment presented in Figure 3.10 is still not sufficient. Necessity of more 2D experiment for different excitation/reconversion times is required. Build-up curves has to be generated as will be shown in the next part.

3.3.1 DQ build-up curves

Intensities of DQ coherences were already expressed in sections 3.2.1 and 3.2.2 for DRAMA/BABA and C7/POST C7 pulse sequences, respectively (see DQ part of equations (3.11) and (3.17)). For short excitation times τ this relations, valid for two spin- $\frac{1}{2}$ system, can be approximated by parabolic time τ dependence (equation (3.8)). It was shown ([Gra97a]) by computer simulations that this approximative solution can be used even for systems where more spins interact together. In these cases amplitude of the build-up curve is strongly modulated as well as its oscillatory behaviour (see e.g. Figure 3.7). Thus for longer excitation times two spin approximation can not be used. Nevertheless the short excitation time part of the build-up curve can be used for evaluating the dipolar coupling strength. It was simulated ([Gra97a]) that for excitation time $\tau < 0.5 \frac{2\pi}{d_{ij}}$ for C7/POST C7 pulse sequence ($\tau < 0.25 \frac{2\pi}{d_{ij}}$ for DRAMA/BABA pulse sequence) the error assuming isolated pairs of spins is less than 10% comparing results from a system where more spins were coupled together. This allow us to use two spin system model in the limit of short excitation and reconversion times. In real experiment equation (3.8) for intensity of the DQ coherence can be in this cases rewritten in the more useful way⁵

$$I_{DQ} \approx A \bar{g}^2 \mathcal{K}_{norm}^2 (d_{ij}^{II})^2 \tau^2, \quad (3.19)$$

where A represents the instrumental parameter and can not be avoided from an experiment. \bar{g} is the average geometrical factor and together with the norm \mathcal{K}_{norm} of the particular pulse sequence describes their excitation strength. Pulse sequence parameters

⁵ \mathcal{K}_{norm} is the dipolar coupling independent norm of the particular pulse sequence, $\mathcal{K}_{norm} = \frac{\omega_{ij, norm}}{d_{ij}^{II}}$ (see equation (3.8)).

Pulse Sequence	$ g(\vartheta, \psi) $	\mathcal{K}_{norm}	$\bar{g} \cdot \mathcal{K}_{norm}$
DRAMA/BABA	$\sin(2\vartheta) \cos(\psi)$	$\frac{3}{\pi\sqrt{2}}$	0.348
C7/POST C7	$\sin(2\vartheta)$	$\frac{343}{520\pi} \sqrt{1 + \sin \frac{\pi}{14}}$	0.169

Table 3.1: Excitation strength of the pulse sequences. In the last column powder average is used for calculating average geometrical factor \bar{g} .

\bar{g} and \mathcal{K}_{norm} are listed in Table 3.1. Excitation/reconversion time τ in equation (3.19) can be incremented only in steps of $2\tau_r$ for C7/POST C7 and BABA⁶. In real systems relaxation of spins during excitation as well as during reconversion period has to be taken into account. It can be described approximately through effective relaxation rate T_{eff} and equation (3.19) can be extended as

$$I_{DQ} \approx A \bar{g}^2 \mathcal{K}_{norm}^2 (d_{ij}^{II})^2 \tau^2 e^{-\frac{\tau}{T_{eff}}}. \quad (3.20)$$

Experimental factor A plays a crucial role and can not be removed from above equation. As a consequence only relative intensities are possible to measure with the help of build-up curves.

DQ build-up curves measured on the polybutadiene melt which has been already presented in Figure 3.10a are shown in Figure 3.11. Different intensities correspond to the different functional groups as it is indicated. Experimental results show that the strongest coupling comes from the protons in CH_2 group as was expected. Fitting the experimental DQ build-up curves for different functional groups using equation (3.20) the relative values of the residual couplings for different groups can be estimated by⁷

$$(D_{CH_2}^{res}) : (D_{CH_2-CH}^{res}) : (D_{CH=CH}^{res}) = 1.0 : 0.63 : 0.51. \quad (3.21)$$

The relative values are scaled to the value of $D_{CH_2}^{res}$. D^{res} represent the scaled dipolar coupling due to the fast molecular motion. Error during the fitting process was 2%, 4% and 6% for each group respectively. It has to be noted that the fitting curves already represent quite big error because we were out of the limit for small excitation times. Thus this fitting errors are not so relevant and they might be even higher for our sample. At

⁶Extended version of BABA is only assumed (see Figure 2.17b). DRAMA and basic version of BABA will be not used because of their bad compensation effects.

⁷We will use the symbol D^{res} instead of d^{II} for residual dipolar coupling.

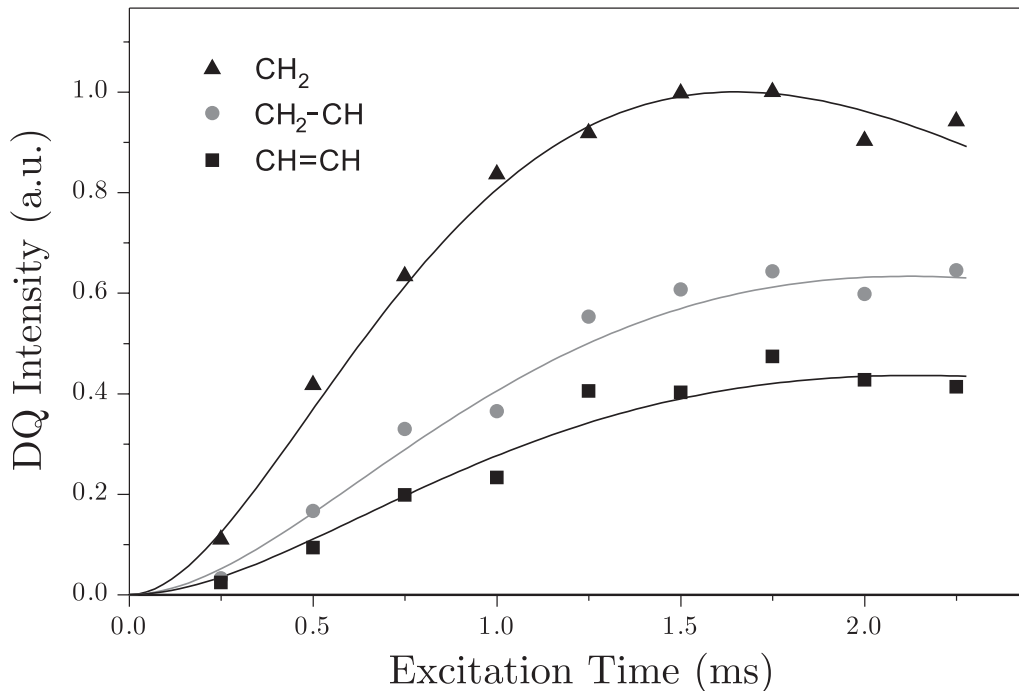


Figure 3.11: Proton DQ build-up curves for polybutadiene melt measured at room temperature. POST C7 pulse sequence was used to record build-up curves (more details see description under the Figure 3.10). Excitation time was varied in steps of $2\tau_r$ ($\tau_r = 125 \mu\text{s}$) to achieve full compensation in POST C7 (see section 2.5.1.3). Solid lines represent fitting results from equation (3.20) with fitting parameters d_{ij}^{II} and T_{eff} .

this rotor frequency $f_r = 8 \text{ kHz}$ we were not able to distinguish between *Cis* and *Trans* conformations in polybutadiene thus, all values $D_{CH_2}^{res}$, $D_{CH_2-CH}^{res}$ and $D_{CH=CH}^{res}$ represent effective residual dipolar couplings coming from both conformations. To resolve *Cis* from *Trans* conformations from DQ spectra higher rotational frequencies or stronger \vec{B}_0 fields are required.

3.3.2 Residual dipolar couplings in natural rubber.

In this section residual dipolar couplings between different functional groups in natural rubber will be measured with the help of ^1H DQ spectroscopy. Results from different pulse sequences namely BABA, C7 and POST C7 will be qualitatively compared.

Natural rubber (NR) belongs to the category of elastomers. In elastomers at temperatures well above the glass transition temperature dipolar couplings are much reduced due to the fast molecular motions. However, presence of topological constraints and permanent crosslinks prevent the chain motion to be free so dipolar interactions are not fully

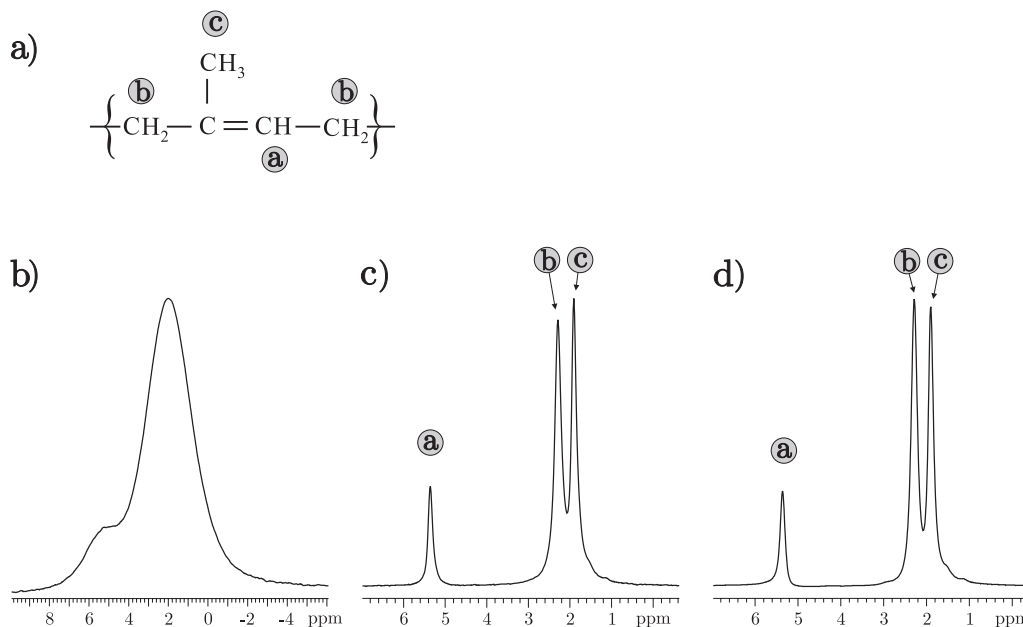


Figure 3.12: 400 MHz ^1H spectra of Natural Rubber with its structure schematically shown in figure a) measured at different rotational frequencies namely: b) $f_r = 0$ Hz; c) $f_r = 4$ kHz; d) $f_r = 8$ kHz.

averaged out. Depending on the degree of motional restrictions, these residual dipolar interactions may be quite small. In NR residual dipolar couplings are scaled on the order of few kHz. This gives rise to measure dipolar connectivities between different functional groups with DQ spectroscopy under the condition of fast MAS.

NR investigated in this section was crosslinked with sulfur (S) in the traditional way where a certain amount of sulfur was added together with an accelerator into the rubber material, before the vulcanization at temperature 150 °C was done. The sulfur and accelerator content was 3.0 phr (*parts-per-hundred rubber*) and 0.54 phr, respectively. The glass transition temperature has been estimated by DSC (*differential scanning calorimetry*) to be $T_g = 208\text{K}$. Thus NR was at room temperature (298K) well above the glass transition temperature. From GPC (*gel-permeation chromatography*) molecular mass of the precursor chains was established as $M_w = 850\,000$ g/mol. Averaged molecular mass of inter-crosslink chains M_c was estimated using uniaxial stress-strain measurements and swelling measurements ([Men99]) as $M_c = 3700$ g/mol.

Measured NR is schematically shown in Figure 3.12a. Three different groups were found with ^1H NMR spectroscopy namely CH , CH_2 and CH_3 . Spectra at different rotational frequencies are shown in Figure 3.12b–d. Without MAS the three different groups

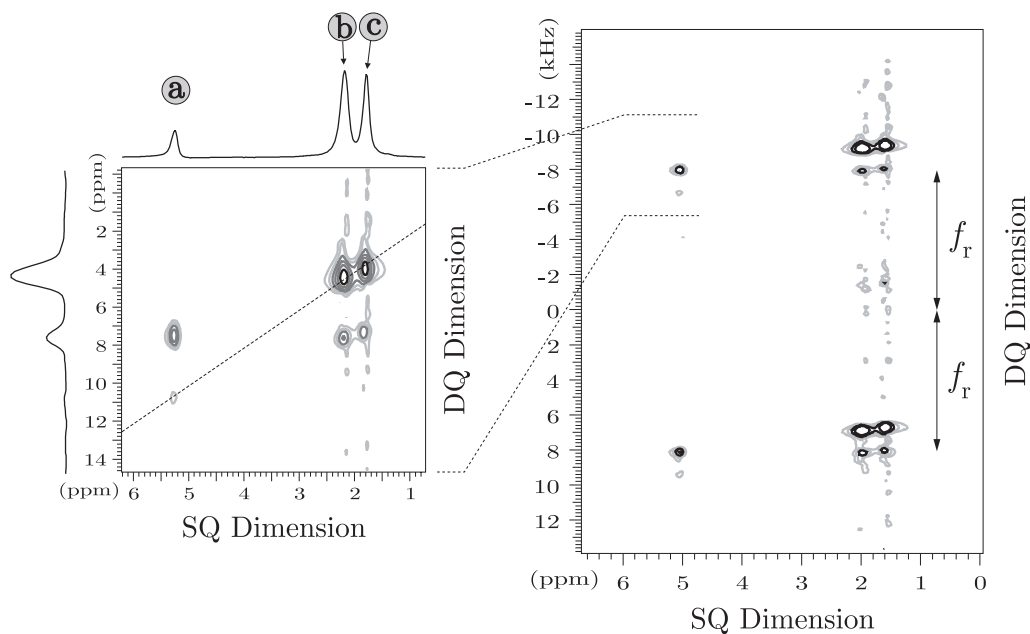


Figure 3.13: ^1H DQ spectrum of Natural Rubber (Figure 3.12a) acquired with BABA pulse sequence (see Figure 2.17b) at rotor frequency $f_r = 8$ kHz. R.f. pulse width was chosen comparable to C7 pulse sequence (see Figure 3.14) as $t_p = 4.3$ μs . DQ coherences were excited during excitation period with duration $\tau = 500$ μs .

were not resolved (see Figure 3.12b). Spinning the sample about the rotor axes tilted by 54.7° from the \vec{B}_0 field direction additional averaging is introduced. Thus, for high rotational frequencies dipole-dipole coupling as well as CSA⁸ are averaged out and only isotropic chemical shift survives (more details see section 1.6). At frequencies 4 kHz and 8 kHz (Figure 3.12c and d) the different groups were almost fully resolved. Comparing figures c) and d) it can be seen that the ratio between CH_2 (labeled (b)) and CH_3 (labeled (c)) group is changed with increasing rotational frequency. This interesting behaviour is most probably caused by better averaging during MAS for protons in CH_2 group than in CH_3 group. CH_2 group is "fixed" to the chain therefore is much less mobile than CH_3 group which is relatively free, hence MAS acting like complementary averaging has stronger influence to the CH_2 group so the line becomes higher and narrower. In addition also intergroup dipolar coupling (b) – (b) (see Figure 3.12a) is averaged out by MAS and can cause similar effects of narrowing of the line corresponding to the CH_2 group.

DQ spectrum of NR is shown in Figure 3.13. BABA pulse sequence was chosen (see Figure 2.17b) to excite DQ coherences at rotational frequency $f_r = 8$ kHz. Clear evidence

⁸Asymmetry part of the chemical shift interaction is not considered (see equation (1.23)).

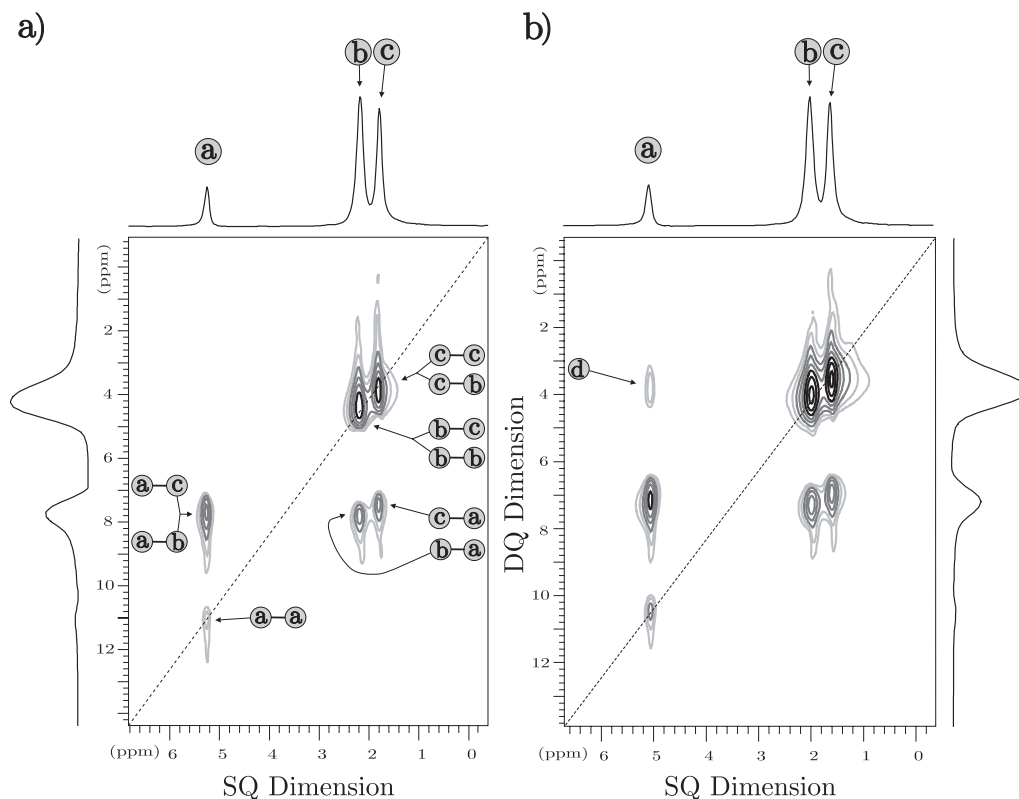


Figure 3.14: Comparison of effectiveness of C7 a) and POST C7 b) pulse sequences. Proton DQ spectra are presented for NR similar like in Figure 3.13 at spinner frequency $f_r = 8$ kHz and excitation/reconversion time $\tau = 1.25$ ms. Peaks marked (a), (b), (c) corresponds to the various functional groups in NR (see Figure 3.12a). Dipolar connectivities between different groups are assigned in DQ dimension as it is indicated. Peak (d) represents unwanted magnetization exchange which was established during time $\tau_0 = 15$ ms, needed after reconversion period for dephasing unwanted transients.

of rotational sidebands in DQ dimension can be seen from the right spectrum in Figure 3.13 as was already explained in section 3.2.1. Dipolar connectivities between different functional groups can be seen from the left spectrum in the figure. BABA pulse sequence was not so efficient for exciting DQ coherences. Quite a lot of noise in DQ dimension can be seen in the spectrum. Intensity of the inter-molecular dipolar coupling $CH \leftrightarrow CH$ was hardly resolved from noise. Detailed description of dipolar connectivities between different functional groups can be seen from Figure 3.14a where C7 was used for recording the signal. C7 as well as POST C7 (Figure 3.14b) were much more effective than BABA pulse sequence. It can be directly seen comparing Figures 3.14 and 3.13 that signal to noise in DQ dimension was increased and all possible dipolar couplings were seen as it is indicated

in Figure 3.14a. On the top of the two-dimensional spectra the SQ projections are shown.

Some conclusions can be made from qualitative analysis of the DQ spectra. First of all it has to be noted that we were not able to separate intergroup dipolar coupling $CH_2 \leftrightarrow CH_3$ (labeled as $(c) - (b)$, $(b) - (c)$ in Figure 3.14a) from intragroup couplings between protons of CH_2 ($(b) - (b)$) and CH_3 ($(c) - (c)$) groups. Hence, effective residual dipolar couplings can be only discussed for this groups. Nevertheless dipolar connectivities through space between $CH_2 \leftrightarrow CH$ ($(b) - (a)$) and $CH_3 \leftrightarrow CH$ ($(c) - (a)$) were clearly distinguished in DQ dimension. However, when comparing intensities of the different functional groups, one should keep in mind that (relative) number of protons of the corresponding group has to be also taken into account as well as the molecular dynamics. Assuming only structural parameters DQ signal from CH_3 group is expected to be higher comparing to CH_2 group. However, CH_3 group is relatively free in motion while CH_2 group is "fixed" in the chain which limits its mobility. This results in reduction of the residual dipolar coupling for CH_3 group. Results from POST C7 (see Figure 3.14b) pulse sequence are qualitatively the same as from C7 pulse sequence. In addition peak labeled as (d) appeared which was not the case of C7 pulse sequence. This indicates that the delay between reconversion period and detecting pulse $t_0 = n_0\tau_r$ (see Figure 2.20) for POST C7 during which unwanted transients are supposed to decay was a little bit longer as was necessary. Thus unwanted magnetization exchange between protons of CH_2 and CH as well as CH_3 and CH could be established. Another experiments with shorter τ_0 showed vanishing of this peak which is the confirmation that magnetization exchange took place.

The experimental proton DQ build-up curves for the NR are presented in Figure 3.15. Different categories of functional groups are assigned with symbols A, B, \dots, E as it is indicated in the left part of the figure. Series of two-dimensional experiments at different excitation times with POST C7 pulse sequence were performed to record the signal. As was already mentioned we were not able to resolve all couplings from the experiment thus, symbols A and B corresponds to the overall residual couplings as it is indicated in the figure. Due to the fast axial rotation of the CH_3 group around three fold axis the proton dipolar coupling is reduced by the factor of $\frac{1}{2}$ compared to the rigid case ([Sch99]). This is the main reason why residual dipolar coupling of the CH_3 group is reduced such that it is a little bit lower than residual dipolar coupling of the CH_2 group (compare intensities B and A in Figure 3.15). As a consequence of existence of crosslinks between chains, intermolecular dipolar coupling between protons of $CH \leftrightarrow CH$ (labeled as E) of neighbored

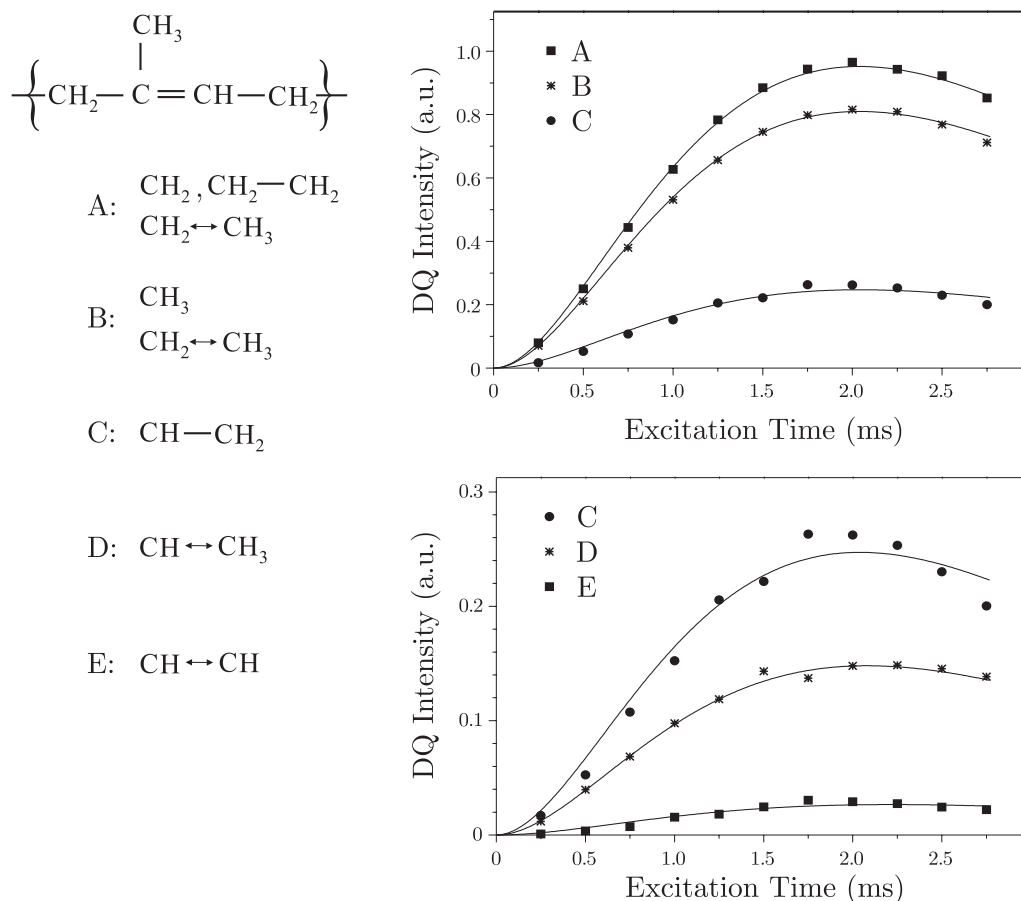


Figure 3.15: ^1H DQ build-up curves of NR recorded with POST C7 pulse sequence (Figure 2.19b). Symbols A, ..., E corresponds to the dipolar connectivities between different groups as it is indicated in the left part of the figure. Solid lines represent fitting curves (more details see text).

chains⁹ is not fully averaged out. As expected this residual dipolar coupling was found to be smallest. Equation (3.20) was used to fit experimental DQ build-up curves for different groups. Due to the unknown experimental factor A of that equation only relative values of residual couplings D^{res} could be calculated. Fitting results

$$(D_A^{res}) : (D_B^{res}) : (D_C^{res}) : (D_D^{res}) : (D_E^{res}) = 1.0 : 0.92 : 0.51 : 0.38 : 0.15 \quad (3.22)$$

are normalized to the maximal value of the residual coupling D_A^{res} found in the spectrum. Fitting errors were calculated for A, ..., E respectively as 1%, 1%, 2%, 4%, 8%. Similar like in section 3.3.1 these error values are not so relevant and can be even higher for our sample.

⁹Also coupling between protons from the same chain might contribute to the resulting intensity of the DQ signal labeled as E.

Absolute values of residual dipolar coupling which may be estimated from the first order spinning sidebands in SQ MAS experiment (see section 3.1) were not possible to be measured due to the non-symmetrical spinning sidebands. This asymmetry might be caused by spectrometer problems or by presence of CSA. Therefore more detailed analysis of NR were not made. Nevertheless it was shown that ^1H DQ spectroscopy permits site-selective measurements of residual dipolar couplings between protons belonging to the same or to the different functional groups even for more complicated structures like NR. To resolve all dipolar connectivities higher rotational speeds or stronger \vec{B}_0 fields are required which was not available.

3.4 Spin counting under MAS

Experimental results from spin counting experiment will be shown in this section. Theoretical bases can be found in section 2.5.3. Adamantane was used as a test sample to excite higher order coherences under MAS. As was already explained in section 2.5.3 no evolution of the spin system in spin counting experiment take place on contrary to the DQ spectroscopy (see section 3.3) thus, no spinning sidebands are expected in second dimension. POST C7 will be used to excite multiple quantum (MQ) coherences. Only even quantum coherences will be expected because POST C7 is described by 'pure' DQ Hamiltonian for two spin- $\frac{1}{2}$ system ([War80]).

Experimental results from MQ spin counting experiment made on Adamantane are shown in Figure 3.16. Adamantane represents a relatively strong coupled spin system (more details see page 45) where higher order coherences can be expected. Experiment was carried out at MAS frequency $f_r = 8$ kHz. Two different excitation times τ were chosen to demonstrate the effect of dynamics of the MQ coherences. Increasing excitation time higher order coherences were excited with POST C7 pulse sequence as was expected (compare Figure 3.16a and b). MQ coherences are modulated by $\cos(p\Delta\phi \cdot m)$ (see [Shy88] and section 2.5.3) therefore Fourier transformation with respect to m (representing second dimension) give rise to a series of δ -function spikes corresponding to the MQ coherence order p . Separation of different quantum orders is accomplished by $\Delta\phi$. Up to the 14-th order of coherences were clearly visible in Adamantane with excitation time $\tau = 1$ ms (Figure 3.16b) recording the signal with this phase incremented method.

Effective size of the dipole-dipole coupled spin clusters $N(\tau)$ for given

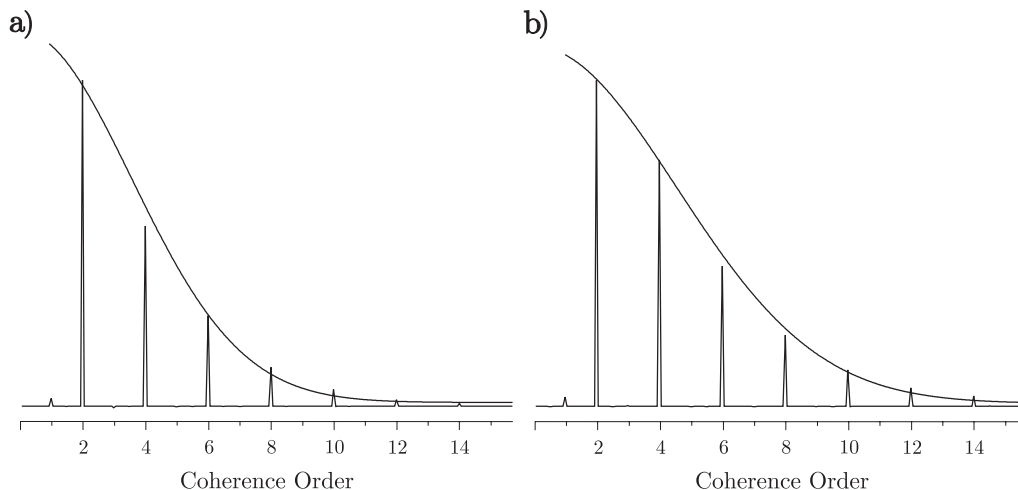


Figure 3.16: ^1H MAS spin counting MQ experiment for Adamantane at rotational frequency $f_r = 8$ kHz. POST C7 was chosen to excite MQ coherences. Two different excitation times a) $\tau = 750$ μs and b) $\tau = 1$ ms corresponding to complete multiples of rotor period were used to visualize growing of higher order coherences. DQ coherence is normalized to the same amplitude for both experiments. Solid lines represent the fitting curve for evaluating sizes of the spin clusters $N(\tau)$ by equation (3.23). $\Delta\phi$ was chosen 11.25° to see up to the 16-th order ($p_{max} = 16$) of coherence. Only 32 phase increments were recorded which correspond to the full 2π cycle. 1 ms delay (τ_0) was included after reconversion period to allow unwanted transients to decay.

excitation/reconversion time τ can be extracted from spin counting experiment by assuming that the intensity of p -quantum coherence is related to the number of different transitions of order p in a system of $N(\tau)$ spins. These can be calculated directly from combinatorial arguments which can then be approximated by a Gaussian distribution ([Bau85]) for large clusters $N(\tau) \geq 6$. Hence, MQ intensities can be fitted by Gaussian distribution of the form ([Bau86, Shy88])

$$I_{MQ}(p, \tau) = A \exp\left(\frac{-p^2}{N(\tau)}\right) \quad (3.23)$$

with variance $\sigma^2 = N(\tau)/2$, where A is normalization constant and $N(\tau)$ is the cluster size which develops over the time τ . Solid lines plotted over the intensities of MQ coherences in Figure 3.16 represent fitting curves by equation (3.23). Fitting results $N(750\mu\text{s}) = 24.7 \pm 2.0$ and $N(1 \text{ ms}) = 41.2 \pm 1.7$ shows increasing amount of correlated spins as was expected. Results are in a good agreement with R. Graf measurements ([Gra97a]), where C7 pulse sequence was used.

It is important to note that in spin counting experiment the linewidth information from the second dimension is eliminated which is not always desired. However, when

MQ intensities are required, rather than lineshape information, spin counting experiment provides a sensitive and much less time consuming experiment than conventional two-dimensional MQ experiment where t_1 is incremented in the sense of TPPI as was presented in section 2.5.2. In the case of Adamantane where resonance offsets are negligible also incomplete cycles ([Gee99]) can be used for exciting higher order coherences with C7 pulse sequence. Care has to be taken when more isotropic lines can be resolved by MAS. Full compensation of resonance offsets and r.f. field inhomogeneities is accomplished only after complete 7-fold cycles (multiples of twice rotor period) in C7 as well as in POST C7 pulse sequence ([Lee95, Hoh98]) so incomplete cycles are not desired in these cases when on resonance excitation is impossible.

3.5 MQ coherences for static solids

In this section a quantitative comparison of eight pulse sequence (see section 2.4.1.2) and thirty-two pulse sequence (see sections 2.4.1.3) will be made. DQ build-up curves for static solids where dipolar couplings are relatively weak (in the order of few kHz) will be presented for both pulse sequences. Comparison with high resolution MAS (see section 3.3.1) will be also discussed. In the second part of this section MQ spin counting experiment with thirty-two pulses sequence will be described. Up to the 6-th order of coherences were observed in polybutadiene rubber. Two samples were chosen to accomplish experiments.

The first one was polybutadiene melt (PBM) (see Figure 3.17a,b) already described in section 3.3 (see page 79 and Figure 3.10). MAS spectrum recorded at rotational frequency $f_r = 3$ kHz is shown in Figure 3.17b. At this spinning frequency both groups CH and CH_2 were clearly resolved. The vinyl group (Figure 3.17b labelled as c) was much smaller than another isotropic lines so its influence to the resulting integral in static experiment in Figure 3.17a is less than 10% so it will be neglected. PBM will be used in section 3.5.1.

The second sample was polybutadiene rubber (PBR) with a high crosslink density. It is based on a commercial *cis*-1,4 polybutadiene (BUNA *cis* 132) with $M_n = 120\,000$ g/mol and $M_w = 450\,000$ g/mol. Crosslinking has been done with dicumyl peroxide (DCP) in the traditional way where DCP was mixed with the rubber material, before the vulcanization process at temperature 145 °C during 1 h with pressure 10 MPa was performed. The resulting mean molecular mass between two crosslinks, $M_c = 6500$ g/mol ([Eka00]), was determined as the average value from stress-strain measurements [Mat92], swelling

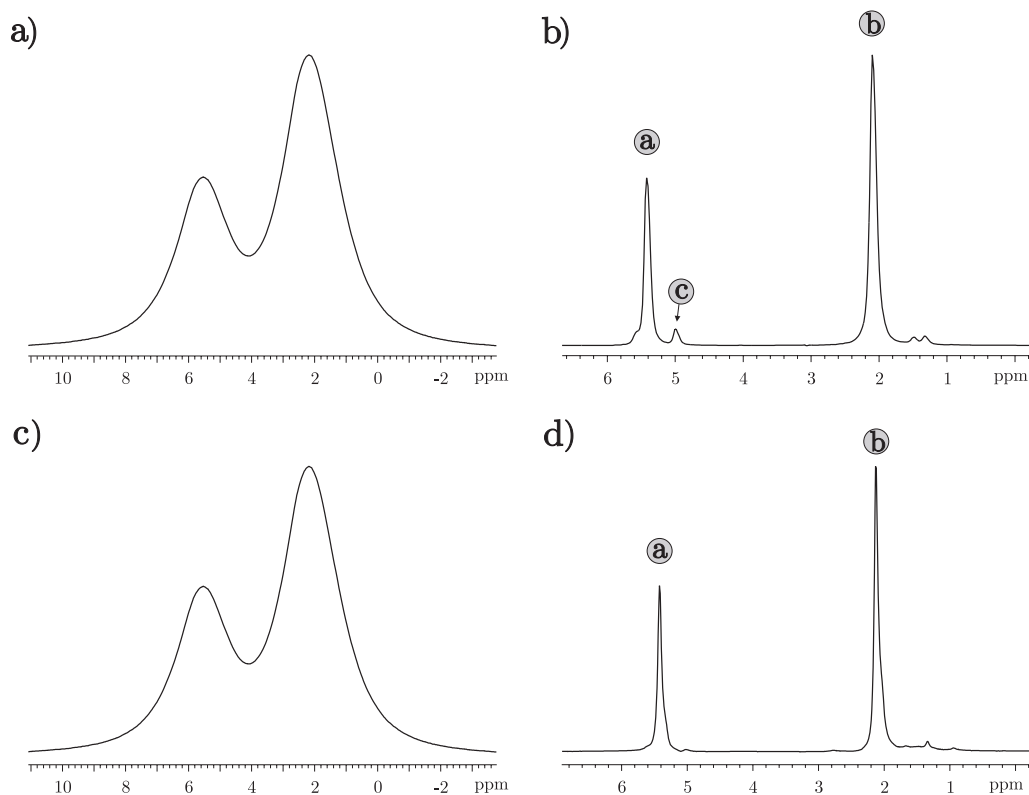


Figure 3.17: Proton ^1H spectra measured at rotational frequencies $f_r = 0$ Hz for a), c) and $f_r = 3$ kHz for b), d). Two different samples were measured: a), b) polybutadiene melt (PBM); c), d) polybutadiene rubber (PBR). Labels a,b,c correspond to the different groups resolved by MAS (see Figure 3.10a).

measurements ([Lec93]) and NMR relaxation measurements ([Sim92]). Free chains of polybutadiene melt with $M_n = 1800$ g/mol were incorporated into the rubber network with weight amount of 20% (wt.%) ([Eka00]). Originally two effects due to this incorporation were expected. The first one is like swelling and should give rise for small swelling degrees to a better mobility. For large swelling degrees the mobility can decrease again ([Men99, Sch89]). The second effect could result in additional topological hindrances due to the comparable incorporated free chain length with the size of the entanglement chain length. This should increase the residual coupling (decrease mobility). But after this incorporation procedure rubber network appears extremely rigid. The mechanical properties were extremely worse (it breaks immediately), which was not expected. The most possible cause for this behaviour is additional crosslinking of the short free chains inside the original sample, which result in extremely high crosslinked piece of the sample. As a check measurement the resulting mean molecular mass between two crosslinks after

incorporation was measured again with 1H Hahn-Echo experiment ([Men99, Sim92]) as $M_c = 700$ g/mol. This high crosslinking density can increase the probability to observe higher order coherences in PBR. Glass temperature of PBR was estimated from DSC (*differential scanning calorimetry*) to be $T_g = 168K$. Proton NMR spectra of PBR at $f_r = 0$ kHz and $f_r = 3$ kHz are shown in Figure 3.17c and 3.17d, respectively. Comparing Figure 3.17a with Figure 3.17b not so much differences can be seen. PBR will be used as a test sample in section 3.5.2 to observe higher order coherences.

3.5.1 DQ build-up curves of polybutadiene melt

Similar formalism like for C7 and DRAMA/BABA pulse sequences (see sections 3.2.1 and 3.2.2) can be used for calculating intensities of the signal arising from dipolar coupled two spins $1/2$ for eight pulse sequence as well as for thirty-two pulse sequence (more details see Appendix C and e.g. section 3.2.1 or section 3.2.2). To derive DQ average Hamiltonians during excitation and reconversion periods equations (2.51) and (2.52) (or equations (2.53) and (2.54)) can be used, respectively. With the help of equation (2.34) which represents zero-order average Hamiltonian for both pulse sequences for a system of spins- $1/2$ coupled via dipole-dipole interaction, factors $\omega_{ij}^{exc/rec}$ (see section 3.2) can be estimated for excitation as well as for reconversion period¹⁰:

$$\omega_{ij}^{exc} = D_{ij} e^{-2\phi} \quad \text{and} \quad \omega_{ij}^{rec} = D_{ij}, \quad (3.24)$$

where

$$D_{ij} = d_{ij}^{II} \frac{1}{2} (3 \cos^2 \vartheta_{ij} - 1). \quad (3.25)$$

ϕ corresponds to the phase shifting of the pulses during excitation period and can be $\phi = \Delta\omega_\phi t_1$ for TPPI MQ experiment (see section 2.4.3) or $\phi = m \cdot \Delta\phi$ for spin counting MQ experiment (see section 2.4.4).

The phase and the amplitude can be separated from equation (3.24) and for dipolar coupled spin- $1/2$ pair the signal intensity arising from this coupling can be calculated for $t_2 = 0$ (see equation (C.20) and equation (C.14)) as

$$S_I(\phi) = \langle \cos^2(D_{ij} \tau) \rangle + \cos(2\phi) \langle \sin^2(D_{ij} \tau) \rangle. \quad (3.26)$$

Averaging over all possible orientations is described by the symbol $\langle \dots \rangle$. The first term in equation (3.26) similar like for C7 and DRAMA/BABA pulse sequences represents

¹⁰More details see section 2.5.2 or section 2.5.3.

Pulse Sequence	$ g(\vartheta, \psi) $	\mathcal{K}_{norm}	$\bar{g} \cdot \mathcal{K}_{norm}$
8p/32p	$\frac{1}{2} (3 \cos^2 \vartheta - 1)$	1	0.447
DRAMA/BABA	$\sin(2\vartheta) \cos(\psi)$	$\frac{3}{\pi\sqrt{2}}$	0.348

Table 3.2: Comparison of excitation strengths of eight (8p) and thirty-two (32p) pulse sequence with DRAMA/BABA pulse sequence. In the last column powder average is used for calculating average geometrical factor \bar{g} (see e.g. equation (3.9)).

remaining part from the initial magnetization. It can be filtered out from the spectrum by conventional double quantum (DQ) filter (see section 4.3). DQ part of the signal is described by the second term in equation (C.14). The first term of the DQ signal ($\cos(2\phi)$) carries information about the phase and only the second *sin* term represents the intensity of the DQ signal.

In the limit of short excitation and reconversion times τ the intensity of DQ signal (see *sin* part of equation (3.26)) can be approximated by quadratic dependence on τ (more details see section 3.3.1). Assuming relaxation of the spin system during excitation/reconversion period described through T_{eff} the DQ intensity can be written in the form

$$I_{DQ} \simeq A \bar{g}^2 \mathcal{K}_{norm}^2 (d_{ij}^{II})^2 \tau^2 e^{-\frac{\tau}{T_{eff}}}. \quad (3.27)$$

Average geometrical parameter \bar{g} and orientation independent norm \mathcal{K}_{norm} for eight pulse sequence as well as for thirty-two pulse sequence are listed in Table 3.2. Comparison with DRAMA/BABA pulse sequence (Table 3.1) is also shown. Simulation of the DQ intensities from equation (3.26) shows (performed numerically with home made program) that maximum DQ intensity for powders is about 61% of the initial Zeeman order which is even higher than for DRAMA/BABA pulse sequence where it was about 52% (see section 3.2.1). Disadvantage of eight and thirty-two pulse sequences are their low resolution capabilities in comparison to pulse sequences working under MAS. Nevertheless if high resolution is not required static MQ pulse sequences can be sometimes preferred. Their excitation/reconversion time τ is not rotor synchronized in spite of C7 as well as BABA/BRAMA pulse sequences, which is an advantage in some cases when high speed MAS is not available and beginning part of the build-up curve has to be recorder with higher accuracy.

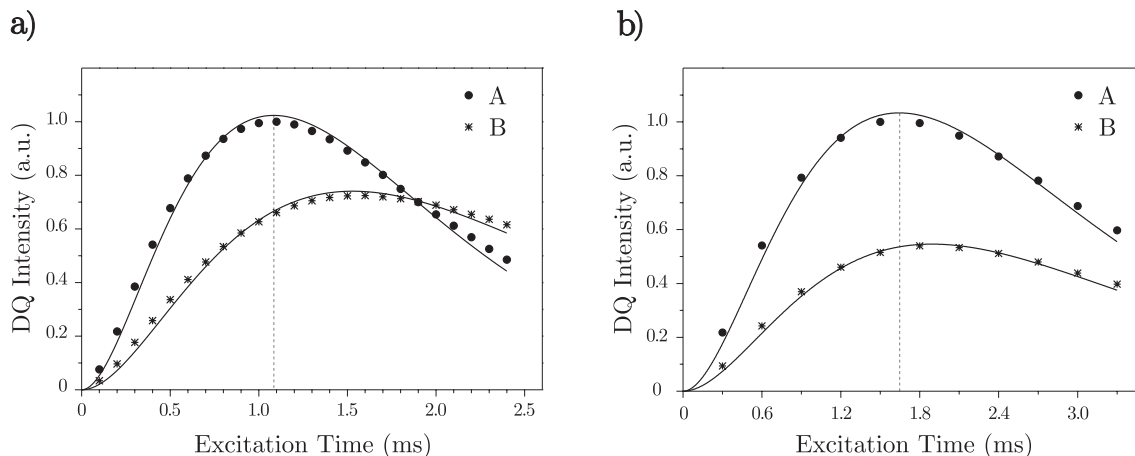


Figure 3.18: Comparison of 1D DQ build-up curves between eight pulse sequence a) and thirty two pulse sequence b) for polybutadiene melt (PBM). Experiment was carried out at 400 MHz Larmor frequency for protons 1H . Solid lines represent fitting curves by equation (3.27). The vertical dashed lines mark the excitation times for maximum signal for the protons of group A, which differs for each pulse sequence. The group A symbolized DQ signal corresponding to the $-CH_2-$ and $CH_2 - CH$ couplings and the group B to $CH_2 - CH$ and $CH = CH$ couplings. The cycle time τ_c was 100 μs ($t_p = 3.4 \mu s$, $\Delta = 4.9 \mu s$ and $\Delta' = 13.2 \mu s$) for a) and 300 μs ($t_p = 3.4 \mu s$, $\Delta = 21.6 \mu s$ and $\Delta' = 46.6 \mu s$) for b), respectively (see sections 2.4.1.2 and 2.4.1.3). A delay of $\tau_0 = 4$ ms was included after reconversion period to allow unwanted transients to decay away from the spectrum.

DQ build-up curves for eight pulse sequence (see Figure 2.10b) and for thirty-two pulse sequence (see Figure 2.11) are shown in Figure 3.18. As was already mentioned polybutadiene melt (PBM) was chosen (see Figure 3.17a). Performing double quantum filtration (DQF) in equation (3.26) (see section 4.3) the first term can be filtered out from the spectrum and only DQ term survives¹¹. For PBM higher order coherences are low probable due to its high mobility. Thus, DQF is sufficient to filter out all unwanted coherences. This kind of experiment was performed in Figure 3.18 while time t_1 between excitation and reconversion period was zero ($t_1 = 0$) and only excitation/reconversion time τ was incremented. This experiment will be called one dimensional (1D) DQ experiment. The main drawback of 1D DQ is that it is no able to resolve dipolar couplings between different groups (intergroup coupling). Hence, we were not able to resolve the dipolar coupling $CH - CH_2$. In comparison with two-dimensional (2D) DQ experiment (see

¹¹This assumption can be made only in the limit of relatively short excitation and reconversion times τ , where higher order coherences (6, 10, ...-orders) are not expected.

Figure 3.11) 1D DQ experiment provides less information. Nevertheless 1D DQ experiment is much less time consuming, hence full build-up curves can be obtained in couple of hours which is not the case of 2D MQ experiment.

Comparing Figures 3.18a and 3.18b the different relaxation rates of the spin system during excitation/reconversion period can be directly seen (compare e.g. excitation times belonging to the vertical dashed lines in the figure). For eight pulse sequence (Figure 3.18a) even the relaxation rates for different groups (labeled *A* and *B* in the figure) are seen. The origin of this behaviour might be in insufficient compensation of isotropic chemical shifts for eight pulse sequence (see also section 2.4.1.2). Higher order terms in average Hamiltonian in Magnus expansion (section 1.3) can influence the spectrum, thus, with increasing excitation time τ the error is rising for eight pulse sequence. Thirty-two pulse sequence on the other hand provides better compensation of resonance offsets so this spurious effects are not seen (see Figure 3.18). Nevertheless the initial part of the build-up curves can be used for fitting to obtain residual dipolar couplings for different groups *A* and *B* also for eight pulse sequence. Equation (3.27) was used for fitting 1D DQ build-up curves for both pulse sequences (solid lines in Figure 3.18) with the result

$$(D_{8p,A}^{res}) : (D_{8p,B}^{res}) = 1.0 : 0.60 \quad \text{and} \quad (D_{24p,A}^{res}) : (D_{24p,B}^{res}) = 1.0 : 0.63, \quad (3.28)$$

where $D_{8p,A}^{res}$ and $D_{8p,B}^{res}$ represents residual dipolar coupling for eight pulse sequence for groups *A* and *B*, respectively, and $D_{32p,A}^{res}$, $D_{32p,B}^{res}$ for thirty-two pulse sequence. Fitting errors were for both cases up to 2%. It has to be noted that PBM only hardly corresponds to the isolated two spin system so using the initial part of the build-up curve for fitting an error of about 10% ([Gra97a]) in real experiment is introduced. In addition group labeled as *A* in Figure 3.18 carries an information about overall residual dipolar coupling arising from $CH = CH$ and $CH - CH_2$ groups and group *B* from $CH - CH_2$ and CH_2 (intragroup) groups as can be seen from 2D DQ experiment (see Figure 3.10b). Hence, intergroup and intragroup couplings can not be distinguished from 1D DQ experiment. In spite of that neglecting chemical shift anisotropy comparison with two-dimensional DQ MAS experiment can be made where C7 pulse sequence was used (see section 3.3.1). Simple quadratic dependence of the dipolar coupling strength to the integrated intensity can be used (see equation 3.27) and assuming results (3.21) the ratio between residual

couplings from the group A and the group B can be calculated as¹²

$$(D_A^{res}) : (D_B^{res}) = 1.0 : 0.61. \quad (3.29)$$

Assuming an experimental error of around 10% for estimating of each residual coupling constant from results (3.21) the overall standard deviation error for estimating the ratio (3.29) can be up to 14% for each group, respectively. In spite of this relatively big error we find a good agreement with the results from thirty-two pulse sequence as well as from eight pulse sequence (ratios (3.28)).

3.5.2 Spin counting in polybutadiene rubber

Recently thirty-two pulse sequence proposed by Antzugin and Tycko has been used for exciting higher order coherences in singly-¹³C-labeled organic solids (see section 2.4.1.3 and [Ant99]). In this section demonstration of excitation and detection of higher order coherences among ¹H nuclei in elastomers using this pulse sequence will be presented. Higher order MQ NMR spectroscopy has not been previously reported on elastomers. In strongly dipole-dipole coupled spin- $\frac{1}{2}$ systems in solids high-order MQ coherences were demonstrated over 16 years ago by Yen and Pines ([Yen83] and Figure 2.13) with the help of eight pulse sequence (see section 2.4.1.2 and Figure 2.13). In elastomers well above the glass temperature fast molecular motion reduce the dipolar coupling to few kHz. We found eight pulse sequence to be not enough effective to excite higher order coherences in high crosslinked polybutadiene rubber (PBR) presented in Figure 3.17c,d. Nevertheless thirty-two pulse sequence was more effective.

Up to the 6-th order of coherences were clearly visible in the proton spectrum of PBR with thirty-two pulse sequence. The experimental results are shown in Figure 3.19. MQ coherences are modulated by $\cos(p \Delta\phi \cdot m)$ function similar like in spin counting MQ experiment under MAS (see section 3.4). Hence, performing Fourier transformation with respect to m which represents second dimension, give rise to a series of δ -functions corresponding to the MQ coherence order p . Different orders of coherence are separated by $\Delta\phi = \frac{\pi}{p_{max}}$, where $p_{max} = 16$ to observe up to the 16-th order of coherent transitions. Single quantum (SQ) dimension (see Figure 3.19a) corresponds to the Fourier transformed signal which evolves in the direct ω_2 dimension during detection period (see Figure 2.14). In Figure 3.19b traces representing different groups CH and CH_2 are shown, respectively.

¹²Complementary normalization to the D_A^{res} was used.

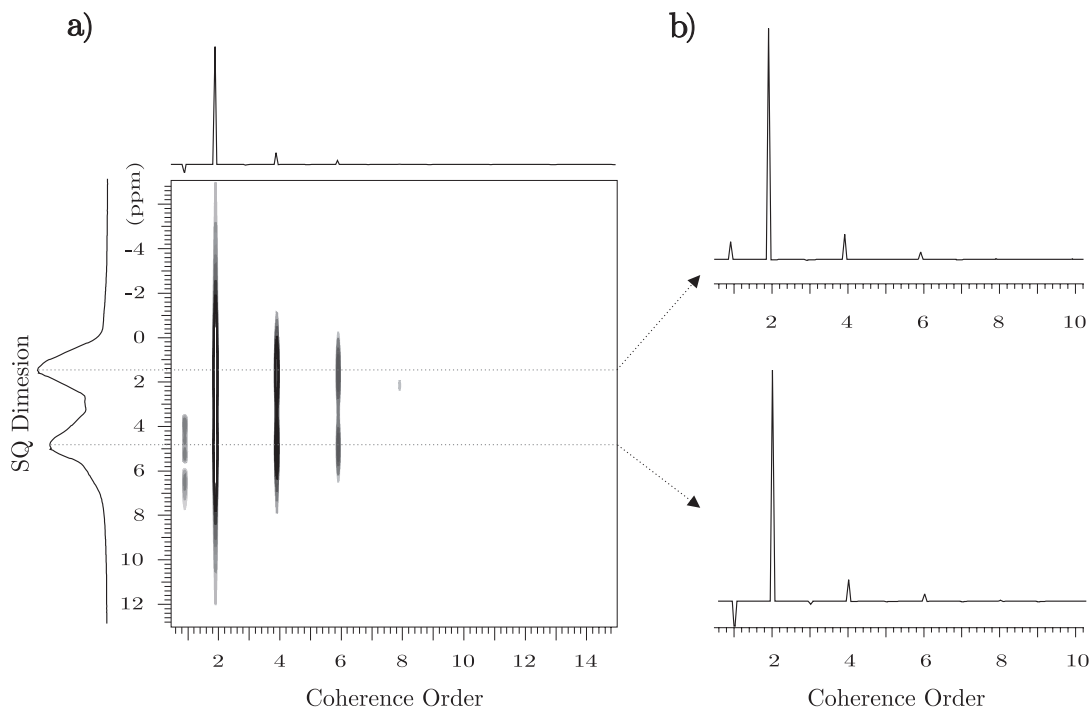


Figure 3.19: ^1H spin counting MQ experiment for PBR (see page 91). MQ coherences were excited with thirty-two pulse sequence with excitation and reconversion time $\tau = 8$ ms. At the top and at the side of the figure a) projections of MQ coherences and single quantum (SQ) spectrum (ω_2 dimension) are shown, respectively (More details about SQ dimension see Figure 3.17c,d). Figure b) represents the traces corresponding to the different functional groups as it is indicated. To separate different orders of coherences $\Delta\phi$ was chosen 11.25° to resolve up to the 16-th order ($p_{max} = 16$) of coherence (more details see section 2.4.4). Only 32 phase increments were recorded corresponding to the full 2π cycle. The cycle time τ_c was 2 ms ($t_p = 3.2 \mu\text{s}$, $\Delta = 163.4 \mu\text{s}$ and $\Delta' = 330 \mu\text{s}$). A delay of $\tau_0 = 1$ ms was included after reconversion period to allow unwanted transients to decay.

Pulse imperfections and higher order correction terms in Magnus expansion (see equations (1.55) and (1.56)) leads to the odd-order signals in Figure 3.19b for both groups.

It has to be noted that it was quite difficult to observe higher order coherences in PBR. Most probably it is due to the fast relaxation of the spin system during excitation period. Relatively low dipole-dipole coupling strength caused by fast molecular motion force to choose long excitation/reconversion times τ to excite higher order coherences which interfere with relaxation of the spin system during this time τ . Solution of this problem might be to choose even high crosslinked samples or to decrease the temperature. It has to be stressed that decreasing the temperature leads to lowering the molecular

motion which increase the line-width, so static MQ spin counting experiment might be not able to resolve different functional groups. To overcome this difficulty high resolution MAS pulse sequences like C7 or POST C7 can be used in spin counting experiment (see section 3.4) to excite higher order coherences.

Chapter 4

Realization of MQ Experiment

In this section some practical hints will be elucidated for realization of MQ experiment. It will be shown that TPPI in two-dimensional experiment (see sections 2.4.3 and 2.5.2) can be sometimes replaced by hypercomplex ([Ern87, SR94]) method for recoding the data. Also experimental methods like DQ filtering and phase cycling for removing spectrometer errors will be presented, respectively.

4.1 Spectrometer

To perform MQ experiment fast electronic which allows quick switching between r.f. pulses has to be available. To achieve high resolution of MQ spectra also high B_0 fields are preferred. In this work Varian Unity Plus and later Unity INOVA has been used to perform experiments with $B_0 = 9.4$ T corresponding to 400 MHz for protons 1H . Short switching delays are especially important for C7, POST C7 as well as for BABA pulse sequences. In our case the minimal time between r.f. pulses until the phase is settled has been $0.2 \mu s$ for phases differing in 90° . In addition NMR spectrometer has to be equipped to perform r.f. pulses with phases which differ in phase smaller than 90° called *small angle phase switching*. Also strong B_1 r.f. fields allowing short r.f. pulses (of order of $3 \mu s$) for proton experiments are an advantage especially for pulse sequences working with δ -like pulses (DRAMA, BABA, eight and thirty-two pulse sequences).

4.1.1 Requirements for MAS

To realize MAS experiment, probes which allows high spinning speeds are required. Measured sample has to be filled into the cylindrical rotor closed by the cap which rotate

about the axes tilted from the \vec{B}_0 field by *magic angle* 54.7° . Nowadays the rotors are made by ceramic materials like Zirconia-oxid (ZrO_2) or Silicon Nitride (Si_3N_4), which have proper mechanical features under high spinning speeds in the presence of magnetic field. They should not be made from materials, which consists of the same nuclei as an investigated sample to prevent overlapping of the signals. Due to the high rotational frequencies ($f_r \geq 10$ kHz) the centrifugal force acting on the outer wall of the rotor is very high which has to be also taken into account for the design of the rotor. The high spinning caps (schematically shown in Figure 1.3a) usually made from Torlon has a special design to allow high rotations realized by driven-air. To get the stable rotation the rotor is surrounded by the bearing-air flow which can be regulated independently to the driven-air. The resulting rotational frequency f_r can be regulated by the increasing or decreasing of the driving-air pressure. For all MAS experiments in this work rotors with an average of the cylinder of 5 mm are used. They allow to rotate up to $f_r = 13$ kHz. To get better B_1 field homogeneity the sample should not exceed the size of the r.f. coil which can be achieved by the filling of the rotor by the Teflon cylindrical fillers inserted from both sides of the sample.

4.2 Hypercomplex versus TPPI acquisition

In two-dimensional (2D) DQ spectroscopy it is sometimes preferred to record the DQ signal in the sense of *hypercomplex* data sets ([Ern87, SR94]) instead of TPPI (see e.g. section 2.4.3) data sets. When it is useful will be discussed in this section.

Intensity of the DQ signal can be written according to equations (3.14), (3.17) and (3.26) in general in the form

$$S_I^{DQ}(t_1, t_2 = 0) = \cos\left(2 \Delta\omega_\phi t_1 + \Omega(t_1)\right) I_{DQ}, \quad (4.1)$$

where I_{DQ} represents the amplitude of DQ signal. The *cos* term in equation (4.1) determines the phase of the DQ signal. For pulse sequences acting under MAS like DRAMA, BABA, C7 or POST C7 factor $\Omega(t_1)$ represents rotor modulation of the DQ signal. It can be $\Omega(t_1) = \omega_r t_1$ for C7/POST C7 pulse sequence or $\Omega(t_1) = k \cdot \omega_r t_1$ ($k = \pm 1, \pm 3, \pm 5, \dots$)¹ for DRAMA/BABA pulse sequence. For eight pulse sequence and thirty-two pulse sequence $\Omega(t_1) = 0$, so there is no rotor modulation (see equation (3.26)).

¹More details about DQ signal for DRAMA/BABA pulse sequence see equation (3.14).

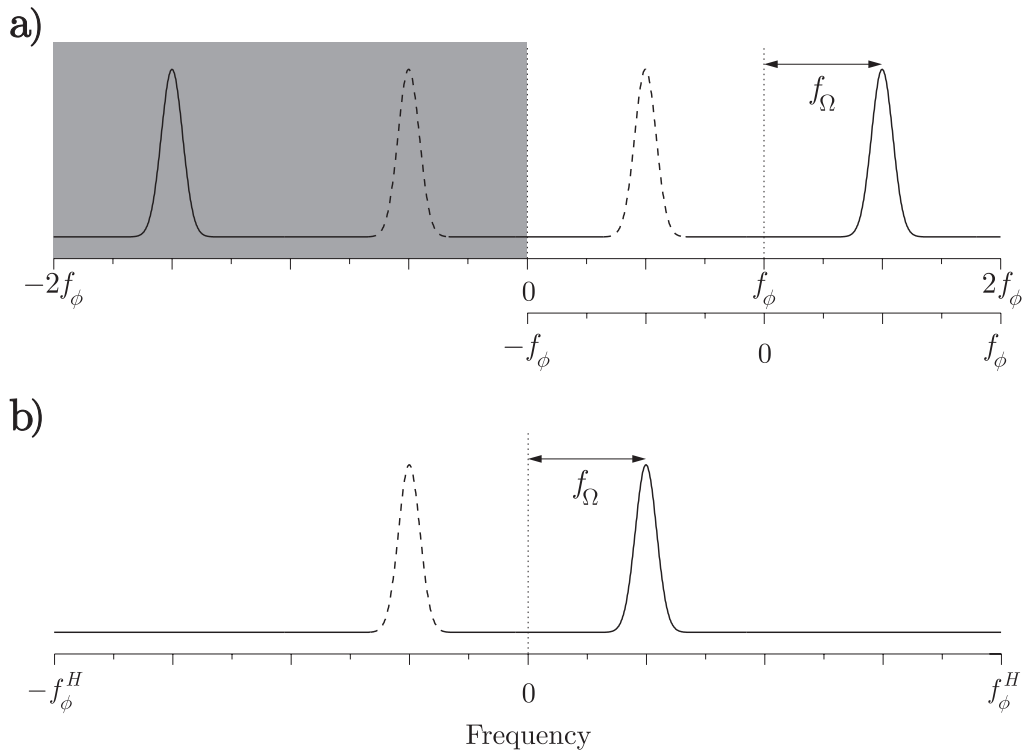


Figure 4.1: Comparison of TPPI a) and hypercomplex b) sampling of the data in DQ spectroscopy. Shaded area in figure a) corresponds to the mirroring of the right part of the spectrum due to the cosine Fourier transformation. Frequency f_Ω describes the rotor modulation of the DQ signal. It is $f_\Omega = f_r$ for C7/POST C7 pulse sequence and $f_\Omega = k \cdot f_r$ for DRAMA/BABA pulse sequence, respectively. Dashed peaks represent symbolically negative first-order spinning sideband ($k = -1$) for DRAMA/BABA pulse sequence (see section 3.2.1).

If we choose in TPPI experiment $2\Delta\omega_\phi t_1 = \frac{\pi}{2}m$ in equation (4.1), where $m = 0, 1, 2, \dots$ represents time proportional incrementing of the phase of the r.f. pulses during excitation period ($t_1 = \Delta t_1 \cdot m$) the DQ signal will follow the scheme

$$\cos(\Omega(0))I_{DQ}, \sin(\Omega(\Delta t_1))I_{DQ}, -\cos(\Omega(2\Delta t_1))I_{DQ}, -\sin(\Omega(3\Delta t_1))I_{DQ}, \dots \quad (4.2)$$

This directly corresponds to the sampling of the data in the sense of Redfield ([Red75]). Hence, this acquisition technique allows to distinguish between positive and negative frequencies even when no imaginary part of the signal in ω_1 dimension is available. Cosine Fourier transformation of the DQ signal recorded in the sense of scheme (4.2) leads to the spectrum shown in Figure 4.1a. Only the right part of the full spectrum in Figure 4.1a represent the correct spectrum. To display it in the proper way the scale has to be changed as it is indicated. Thus, in TPPI experiment recorded by this technique only frequencies

inside of the 'Nyquist zone' ([SR94]) between positive and negative Nyquist frequencies $\pm f_\phi = \pm(4\Delta t_1)^{-1}$ can be seen. To prevent aliasing of the signal from outside of the Nyquist zone, f_ϕ has to be chosen in 2D DQ experiment as

$$f_\phi \geq f_r \quad \text{and} \quad f_\phi \geq |k| \cdot f_r \quad (k = \pm 1, \pm 3, \dots) \quad (4.3)$$

for C7/POST C7 and for DRAMA/BABA² pulse sequences, respectively.

Instead of TPPI it follows from equation (4.1) that DQ signal can be recorded in the sense of *hypercomplex* data sampling if $2\Delta\omega_\phi t_1 = \frac{\pi}{2}m$ and $m = 0, 1$ without incrementing the time t_1 . Hence DQ signal will follow the scheme³

$$\begin{aligned} & \cos(\Omega(0)) I_{DQ}, \cos(\Omega(\Delta t_1)) I_{DQ}, \dots \\ & \sin(\Omega(0)) I_{DQ}, \sin(\Omega(\Delta t_1)) I_{DQ}, \dots \end{aligned} \quad (4.4)$$

Fourier transformation of this signal leads directly to the spectrum shown in Figure 4.1b where positive and negative frequencies are clearly distinguished. Nyquist zone is in this case defined by the Nyquist frequency $\pm f_\phi^H = \pm(2\Delta t_1)^{-1}$.

Comparing TPPI and *hypercomplex* acquisition with connection to the DQ spectroscopy one might think that hypercomplex method of sampling of the data is preferred due to its twice higher Nyquist frequency $f_\phi^H = 2f_\phi$. In fact the cost of this is recording twice number of data points in ω_1 dimension, thus, measuring time is doubled. It has to be noted that the same conditions can be achieved by TPPI choosing the sampling period half of the original one presented by acquisition scheme (4.2), $\Delta t_1 \rightarrow \Delta t_1/2$, and increasing twice number of measuring points. Hence, TPPI and hypercomplex acquisition in DQ spectroscopy will become equivalent.

In fact *hypercomplex* acquisition may be preferred for C7 as well as for POST C7 pulse sequences in DQ spectroscopy. Cumbersome mirroring (see shaded area in Figure 4.1a) caused by recording the data in the sense of Redfield ([Red75]) is overcome by hypercomplex data sampling. In addition if for some reasons (caused by e.g. r.f. pulse imperfections) double quantum filtration (see section 4.3) will not work properly, the remaining part of the initial Zeeman order described by the first term in equation (3.17) (see section 3.2.2) appear in the spectrum. It is important to note that it will appear in the middle of the spectrum in Figure 4.1b, thus, it will not disturb DQ signal if rotational frequency f_r is

² k represents the highest DQ spinning sideband order in the ω_1 dimension (see section 3.2.1).

³Second two data sets rising from ω_2 dimension are for simplicity omitted (more details see e.g. [SR94]).

high enough. On the other hand hypercomplex acquisition is not preferred for DRAMA as well as for BABA pulse sequences. The first term in equation (3.11) despite of C7 pulse sequence is rotor modulated and in the case of hypercomplex acquisition will merge with DQ signal. Hence, TPPI method where this problem is overcome by shifting of the DQ signal to the frequency $f_\phi + k \cdot f_r$ ($k = \pm 1, \pm 3, \dots$) is preferred for DRAMA and BABA pulse sequences. To prevent overlapping of DQ signal in TPPI method with mentioned remaining part of the initial Zeeman order enough small sampling interval Δt_1 has to be chosen to fit all expected DQ sidebands to the spectrum without overlapping and aliasing.

4.3 Double quantum filtering

Multiple quantum (MQ) filtration techniques are often used to select desired order of coherence and suppress other coherent transitions. Characteristic response to a phase shift ϕ of the r.f. pulses used during excitation period to a p -quantum coherence can be written as ([Mun87, Wei83])

$$\hat{\rho}^p(\phi) = \hat{\rho}^p(0) e^{-i p \phi}, \quad (4.5)$$

where $\hat{\rho}^p(\phi)$ describes coherence order p according to the phase ϕ . This behaviour can be used to select coherences of order p .

If phase between excitation and reconversion period (see e.g. Figure 2.12) is incremented in steps of $\Delta\phi = \frac{\pi}{p}$ after each experiment and, in addition, experiments are step by step added and subtracted, all coherences p' up to the certain order⁴ which differ from p , $|p'| \neq |p|$, will be filtered out from the spectrum. To realize this selection of p -quantum coherence one need $2p$ sets of data. To proof this p -quantum filter the intensity of p' -quantum coherence $I_{MQ,p'}$ can be calculated as ([Bod81, Gra97a])

$$I_{MQ,p'} = \sum_{k=0}^{2p-1} (-1)^k e^{-i \frac{\pi}{p} p' \cdot k} = \sum_{k=0}^{2p-1} e^{-i \frac{\pi}{p} (p-p') \cdot k}. \quad (4.6)$$

In the last summation the relation $(-1)^k = e^{i\pi k}$ is used. It can be directly seen from equation (4.6) that for $p' = \pm p$ the exponent is 0 or 2π , thus, the full intensity of coherence order p equal to $2p$ will be seen. To calculate intensities of orders $|p'| \neq |p|$ summation in equation (4.6) can be expressed as a geometrical series as

$$I_{MQ,p'} = \frac{e^{i 2\pi(p-p')} - 1}{e^{i \frac{\pi}{p}(p-p')} - 1}. \quad (4.7)$$

⁴See later discussion.

ϕ_{exc}	ϕ_{ref}
0°	0°
90°	180°
180°	0°
270°	180°

Table 4.1: Phase cycling to select DQ coherence ($p = 2$).

Analysing equation (4.7) it can be seen that nearly all coherences $p' \in \mathbf{N}$ are filtered out. Only coherences where also denominator is zero i.e. $p' = p(2k + 1)$, where $k \in \mathbf{N}$ can not be filtered out from the spectrum by this p -quantum filter.

To realize double quantum (DQ) filter ($p = 2$), it follows from above discussion, it is sufficient to add and subtract four different coherences. The phase of the r.f. pulses acting during excitation period is then advanced in increments of $\frac{\pi}{2}$ (90°) which cause the DQ signal to alternate in sign. The phases of excitation period ϕ_{exc} and reference frequency (receiver phase) ϕ_{ref} are shown for DQ filter in Table 4.1. It has to be noted that coherences of order 6, 10, 14, \dots will be not filtered out from the spectrum. Hence, this filter is $4k + 2$ ($k \in \mathbf{N}$) quantum selective. To realize even higher selectivity more sophisticated approach proposed by Wokaun and Ernst ([Wok77]) can be used. Disadvantage of this method is that it requires $2p_{max}$ different two-dimensional experiments which are stored separately, where p_{max} is the maximum desired order of coherence to be filtered out. Hence, to distinguish 6-quantum coherence from DQ coherence it would be necessary to record separately 12 two-dimensional experiments. This would increase measuring time three times with comparison to the DQ filter presented in Table 4.1. Nevertheless, if higher order coherences are expected to see in the MQ experiment this price has to be payed for selecting DQ coherence, if good results are required.

4.4 MQ phase cycling techniques

In MQ spectroscopy only rarely multiple-pulse sequences generate pure MQ coherences according to the theoretical predictions. It is often necessary to use sophisticated phase cycling techniques to remove spurious signals coming from r.f. pulse imperfections as well as from background signals. In this work mainly two different phase cycling techniques were

ϕ_{exc}	ϕ_{rec}	ϕ_{det}	ϕ_{ref}	$\phi_{rec}^{32+\dots}$	$\phi_{det}^{32+\dots}$	$\phi_{ref}^{32+\dots}$
$0^\circ + \phi$	90°	0°	0°	0°	0°	180°
$90^\circ + \phi$	90°	0°	180°	0°	0°	0°
$180^\circ + \phi$	90°	0°	0°	0°	0°	180°
$270^\circ + \phi$	90°	0°	180°	0°	0°	0°
$0^\circ + \phi$	90°	180°	180°	0°	180°	0°
$90^\circ + \phi$	90°	180°	0°	0°	180°	180°
$180^\circ + \phi$	90°	180°	180°	0°	180°	0°
$270^\circ + \phi$	90°	180°	0°	0°	180°	180°
$0^\circ + \phi$	90°	90°	90°	0°	90°	270°
$90^\circ + \phi$	90°	90°	270°	0°	90°	90°
$180^\circ + \phi$	90°	90°	90°	0°	90°	270°
$270^\circ + \phi$	90°	90°	270°	0°	90°	90°
$0^\circ + \phi$	90°	270°	270°	0°	270°	90°
$90^\circ + \phi$	90°	270°	90°	0°	270°	270°
$180^\circ + \phi$	90°	270°	270°	0°	270°	90°
$270^\circ + \phi$	90°	270°	90°	0°	270°	270°
$0^\circ + \phi$	270°	0°	0°	180°	0°	180°
$90^\circ + \phi$	270°	0°	180°	180°	0°	0°
\vdots	\vdots	\vdots	\vdots	\vdots	\vdots	\vdots

Table 4.2: Phase cycling for DQ filtered experiment. It can be performed in steps of 4, 8, 16, 32 or 64 increments. Phase ϕ corresponds to the TPPI or hypercomplex acquisition (see section 4.2). In TPPI DQ experiment it is varied in steps of $\Delta\phi = 45^\circ$ as $\phi = \{0, 45^\circ, 90^\circ, 135^\circ, 180^\circ, 225^\circ, 270^\circ, 315^\circ\}$ with respect to evolution time t_1 .

used. The first one in the connection to the DQ spectroscopy presented in sections 3.3 and 3.5.1 where DQ filtering (see section 4.3) was used to select DQ coherence. This phase cycling of excitation ϕ_{exc} and reconversion ϕ_{rec} period, detecting pulse ϕ_{det} , and reference frequency (receiver phase) ϕ_{ref} is shown in Table 4.2, respectively. It was adopted from Gottwald ([Got96]) and extended to the full compensation 64 phase cycle to remove even more artifacts. The second phase cycling technique has been used in spin counting experiments in section 3.4 for MAS experiments as well as in section 3.5.2 for experiments

ϕ_{exc}	ϕ_{rec}	$\phi_{det} = \phi_{ref}$
$0^\circ + \phi$	90°	0°
$0^\circ + \phi$	90°	90°
$0^\circ + \phi$	90°	180°
$0^\circ + \phi$	90°	270°
$180^\circ + \phi$	270°	0°
$180^\circ + \phi$	270°	90°
$180^\circ + \phi$	270°	180°
$180^\circ + \phi$	270°	270°
$90^\circ + \phi$	180°	0°
$90^\circ + \phi$	180°	90°
$90^\circ + \phi$	180°	180°
$90^\circ + \phi$	180°	270°
$270^\circ + \phi$	0°	0°
$270^\circ + \phi$	0°	90°
$270^\circ + \phi$	0°	180°
$270^\circ + \phi$	0°	270°

Table 4.3: Phase cycling for spin counting MQ experiment. Phase of a detecting pulse ϕ_{det} and a reference (receiver) phase ϕ_{ref} has to be cycled synchronically. Phases 0° , 90° , 180° and 270° correspond to the phases of r.f. pulses marked in this work as x , y , \bar{x} , and \bar{y} , respectively.

without MAS. The phase cycle is shown in Table 4.3. It is in principle modified CYCLOPS (cyclically ordered pulse sequence, [Ste74a, Ste74b]) for MQ excitation. To perform full compensation 16-step phase cycle is sufficient to remove all possible artifacts coming from r.f. pulse imperfections. The phase of the reconversion period can not be set arbitrary. It has to follow excitation period to achieve proper time reversal (see section 2.3.1).

Conclusions

Multiple quantum (MQ) NMR spectroscopy has been used to investigate the dipole-dipole couplings in amorphous polymers. Various high resolution MQ and double quantum (DQ) NMR techniques under fast *magic angle spinning* (MAS) and low resolution static MQ techniques were compared with respect to application to polymers.

The theory for exciting MQ coherences under fast MAS and under static conditions has been unified for multiple-pulse sequences which are characterized by DQ Hamiltonian. It is shown that intensity of DQ coherence, which is used for estimating dipolar couplings, has the same form for MAS as well as for static experiments in the limit of two spin approximation. Initial part of the DQ build-up curve was used to evaluate dipolar couplings. In addition numerical simulations of intensities of DQ build-up curves confirm the theoretical predictions that POST C7 and C7 r.f. pulse sequences are more efficient than DRAMA and BABA r.f. pulse sequences.

The theoretical calculations show that the influence of finite switching times between r.f. pulses to the zero-order average Hamiltonian for BABA r.f. pulse sequence is small if the delays between these pulses are smaller than $0.5 \mu\text{s}$, which is nowadays in commercial spectrometers good fulfilled. Care has to be taken for proper design of the multiple-pulse sequences especially under fast MAS. The timing of the pulses has to be symmetric with respect to the rotor period.

Proton experimental results on elastomers confirm the theoretical predictions that POST C7 as well as C7 r.f. pulse sequences are more efficient in comparison to BABA r.f. pulse sequence. DRAMA r.f. pulse sequence was not applicable on elastomers. It does not remove resonance offsets and chemical shift anisotropies (CSA) during excitation/reconversion period, which has dramatic influence to the DQ zero-order average Hamiltonian produced by this pulse sequence. It was also shown that ^1H DQ spectroscopy permits site-selective measurements of residual dipolar couplings between protons belonging

to the same or to the different functional groups even for more complicated samples like natural rubber.

Measurements of the residual dipolar couplings in polybutadiene melt (PBM) under fast MAS conditions and without sample spinning show in the frame of experimental error the same results. In PBM the effect of rotation to the residual coupling is expected to be small because of no crosslinks present. It has to be noted that with such a comparison one has to be very careful especially for samples with higher crosslinking density. High spinning frequencies induce high centrifugal forces, which press the sample to the wall inside of the rotor. Due to this high pressure sample can be deformed and mobility of the crosslinks can be influenced. Hence, residual dipolar couplings for different functional groups can be different when comparing fast MAS and static experiment.

It is shown that high resolution MAS MQ experiment can be used for determining growing of the spin clusters. Number of correlated spins is increased with increasing excitation time. It was experimentally confirmed that also POST C7 can measure sizes of the spin clusters in Adamantane. Results are in the good agreements with the literature ([Gra97a, Gee99]) where C7 was used.

A thirty-two r.f. pulse sequence successfully excite up to the 6-th order of coherences in high crosslinked polybutadiene rubber (PBR) under static conditions. Gaussian distribution ([Bau85]) was not appropriate to measure sizes of the dipolar spin clusters in PBR. Its use is limited for large clusters bigger than: 6. Our attempt to fit higher order coherences using Gaussian distribution model shows the size of the clusters: 4, hence this is the confirmation that Gaussian model can not be used for PBR. Nevertheless, this experiment showed that both groups CH and CH_2 exhibit the same amount of correlated spins.

Problems of TPPI and 'hypercomplex' Fourier transformation are discussed in connection to DQ spectroscopy for various multiple-pulse sequences. It is shown that 'hypercomplex' acquisition may be preferred for C7 based r.f. pulse sequences but on the other hand for BABA and DRAMA r.f. pulse sequences TPPI acquisition is preferred.

Proton DQ NMR spectroscopy permits site-selective measurements of residual dipolar couplings belonging to the same or to the different functional groups. Another possibility to measure directly such couplings has been recently reported by Malveau et al. ([Mal97]). It exploits the indirect observation of protons through ^{13}C resonances in two-dimensional (2D) WISE experiment ([SR94, Eul00]). The advantage of site-selective DQ experiment

with comparison to this conceptually relatively simple technique is that the acquisition of the signal from low abundant nuclei is avoided. Dipolar connectivities between different functional groups can be investigated also by 2D magnetization exchange spectroscopy in the short mixing-time regime ([Gas99]). However, for evaluating the data, a model of the spin topology is required. In comparison to DQ spectroscopy this is a disadvantage. DQ high resolution MAS as well as static DQ spectroscopy allows a model-free access to the ratio of the site-selective couplings when a spin- $\frac{1}{2}$ pair approximation is valid.

MQ as well as DQ spectroscopy are well established in modern NMR. They are not restricted to use only for ^1H systems. They can be extended also to other spin- $\frac{1}{2}$ nuclei. Recently published experiment based on C7 r.f. pulse sequence shows that modified C7 ([Hon99]) can be used to achieve even higher selectivity in INADEQUATE ([Ern87]) experiment. This with the connection to DQ techniques presented in this work might be used to measure connectivities between functional groups, which can not be distinguished with classical DQ spectroscopy.

Appendix

A. Irreducible tensors

Basic relations:

$$\begin{aligned}
 \hat{\mathbf{I}}_{\pm}^i &= \hat{\mathbf{I}}_x^i \pm i\hat{\mathbf{I}}_y^i \\
 \hat{\mathbf{I}}_x^i &= \frac{1}{2} \left(\hat{\mathbf{I}}_+^i + \hat{\mathbf{I}}_-^i \right) \\
 \hat{\mathbf{I}}_y^i &= \frac{i}{2} \left(\hat{\mathbf{I}}_-^i - \hat{\mathbf{I}}_+^i \right).
 \end{aligned} \tag{A.1}$$

Single spin irreducible operators:

$$\begin{aligned}
 \hat{\mathbf{T}}_{1,0}^i &= \hat{\mathbf{I}}_z^i \\
 \hat{\mathbf{T}}_{1,\pm 1}^i &= \mp \frac{1}{\sqrt{2}} \left(\hat{\mathbf{I}}_x^i \pm i\hat{\mathbf{I}}_y^i \right).
 \end{aligned} \tag{A.2}$$

Irreducible tensors for two spin system coupled via dipolar coupling:

$$\begin{aligned}
 \hat{\mathbf{T}}_{2,0}^{ij} &= \frac{1}{\sqrt{6}} \left(3\hat{\mathbf{I}}_z^i \hat{\mathbf{I}}_z^j - \vec{\mathbf{I}}^i \cdot \vec{\mathbf{I}}^j \right) \\
 \hat{\mathbf{T}}_{2,\pm 1}^{ij} &= \mp \frac{1}{2} \left(\hat{\mathbf{I}}_z^i \hat{\mathbf{I}}_{\pm}^j + \hat{\mathbf{I}}_{\pm}^i \hat{\mathbf{I}}_z^j \right) \\
 \hat{\mathbf{T}}_{2,\pm 2}^{ij} &= \frac{1}{2} \hat{\mathbf{I}}_{\pm}^i \hat{\mathbf{I}}_{\pm}^j.
 \end{aligned} \tag{A.3}$$

We can drop indexes in equation (A.3) and for two spins I^i and I^j we will write ($\alpha = x, y, z$ and $k = 0, 1, 2$):

$$\begin{aligned}
 \hat{\mathbf{I}}_{\alpha} &= \hat{\mathbf{I}}_{\alpha}^i + \hat{\mathbf{I}}_{\alpha}^j \\
 \hat{\mathbf{T}}_{2,k} &= 2\hat{\mathbf{T}}_{2,k}^{ij}.
 \end{aligned} \tag{A.4}$$

With the help of these definitions the relations in Tables A.1 and A.2 can be derived.

Table A.1: *Effect of dipolar Hamiltonian $\hat{H}_D = -\sqrt{\frac{2}{3}}\omega_D \hat{T}_{2,0}$ on spherical tensor operators.*

$\hat{\rho}$	$e^{i\sqrt{\frac{2}{3}}\hat{T}_{2,0}\omega_D t} \hat{\rho} e^{-i\sqrt{\frac{2}{3}}\hat{T}_{2,0}\omega_D t}$	
\hat{I}_z	\hat{I}_z	(invariant)
$\hat{T}_{2,0}$	$\hat{T}_{2,0}$	(invariant)
$(\hat{T}_{2,2} \pm \hat{T}_{2,-2})$	$(\hat{T}_{2,2} \pm \hat{T}_{2,-2})$	(invariant)
\hat{I}_x	$\hat{I}_x \cos(\omega_D t) - i(\hat{T}_{2,1} + \hat{T}_{2,-1}) \sin(\omega_D t)$	
\hat{I}_y	$\hat{I}_y \cos(\omega_D t) - (\hat{T}_{2,1} - \hat{T}_{2,-1}) \sin(\omega_D t)$	
$(\hat{T}_{2,1} + \hat{T}_{2,-1})$	$(\hat{T}_{2,1} + \hat{T}_{2,-1}) \cos \omega_D t - i\hat{I}_x \sin(\omega_D t)$	
$(\hat{T}_{2,1} - \hat{T}_{2,-1})$	$(\hat{T}_{2,1} - \hat{T}_{2,-1}) \cos \omega_D t + \hat{I}_y \sin(\omega_D t)$	

Table A.2: *Effect of 90⁰ r.f. pulses x,y on spherical tensor operators, respectively.*

$\hat{\rho}$	$e^{\mp i\frac{\pi}{2}\hat{I}_x} \hat{\rho} e^{\pm i\frac{\pi}{2}\hat{I}_x}$	$e^{\mp i\frac{\pi}{2}\hat{I}_y} \hat{\rho} e^{\pm i\frac{\pi}{2}\hat{I}_y}$
\hat{I}_z	$\mp \hat{I}_y$	$\pm \hat{I}_x$
\hat{I}_x	\hat{I}_x (invariant)	$\mp \hat{I}_z$
\hat{I}_y	$\pm \hat{I}_z$	\hat{I}_y (invariant)
$\hat{T}_{2,0}$	$-\frac{1}{2}\hat{T}_{2,0} - \sqrt{\frac{3}{8}}(\hat{T}_{2,2} + \hat{T}_{2,-2})$	$-\frac{1}{2}\hat{T}_{2,0} + \sqrt{\frac{3}{8}}(\hat{T}_{2,2} + \hat{T}_{2,-2})$
$(\hat{T}_{2,1} + \hat{T}_{2,-1})$	$-(\hat{T}_{2,1} + \hat{T}_{2,-1})$	$\mp(\hat{T}_{2,2} - \hat{T}_{2,-2})$
$(\hat{T}_{2,1} - \hat{T}_{2,-1})$	$\mp i(\hat{T}_{2,2} - \hat{T}_{2,-2})$	$-(\hat{T}_{2,1} - \hat{T}_{2,-1})$
$(\hat{T}_{2,2} + \hat{T}_{2,-2})$	$-\sqrt{\frac{3}{2}}\hat{T}_{2,0} + \frac{1}{2}(\hat{T}_{2,2} + \hat{T}_{2,-2})$	$\sqrt{\frac{3}{2}}\hat{T}_{2,0} + \frac{1}{2}(\hat{T}_{2,2} + \hat{T}_{2,-2})$
$(\hat{T}_{2,2} - \hat{T}_{2,-2})$	$\mp i(\hat{T}_{2,1} - \hat{T}_{2,-1})$	$\pm(\hat{T}_{2,1} + \hat{T}_{2,-1})$

B. Wigner rotation matrices

The coordinate transformation with Euler angles $(\varphi, \vartheta, \psi)$ is described by the Wigner rotation matrices $\mathcal{D}_{k,q}^{(L)}$ given by ([SR94, Hae76])

$$\mathcal{D}_{k,q}^{(L)}(\varphi, \vartheta, \psi) = e^{-ik\varphi} d_{k,q}^{(L)}(\vartheta) e^{-iq\psi}, \quad (\text{B.1})$$

where factors $d_{k,q}^{(2)}(\vartheta)$ relevant for this work are defined in Table B.1.

A useful relation of the Wigner matrices is their 'addition theorem'. It relates the Wigner matrices of two successive rotations A→B and B→C to the Wigner matrices of overall rotation A→C:

$$\mathcal{D}_{q,q'}^{(L)}(\Omega_{AC}) = \sum_{m=-L}^L \mathcal{D}_{q,m}^{(L)}(\Omega_{AB}) \mathcal{D}_{m,q'}^{(L)}(\Omega_{BC}). \quad (\text{B.2})$$

Euler angle $\Omega_{AC} = (\varphi_{AC}, \vartheta_{AC}, \psi_{AC})$ represents overall rotation A→C, etc.

Table B.1: ϑ dependent factors $d_{k,q}^{(2)}(\vartheta)$ of the Wigner functions $\mathcal{D}_{k,q}^{(L)}(\varphi, \vartheta, \psi)$.

$d_{k,q}^{(2)}(\vartheta)$	$q = 2$	$q = 1$	$q = 0$
$k = 2$	$\frac{1}{4}(1 + \cos \vartheta)^2$	$-\frac{1}{2}(1 + \cos \vartheta) \sin \vartheta$	$\sqrt{\frac{3}{8}} \sin^2 \vartheta$
$k = 1$	$\frac{1}{2}(1 + \cos \vartheta) \sin \vartheta$	$\frac{1}{2}(\cos \vartheta - 1) + \cos^2 \vartheta$	$-\sqrt{\frac{3}{8}} \sin 2\vartheta$
$k = 0$	$\sqrt{\frac{3}{8}} \sin^2 \vartheta$	$\sqrt{\frac{3}{8}} \sin 2\vartheta$	$\frac{1}{2}(3 \cos^2 \vartheta - 1)$
$k = -1$	$\frac{1}{2}(1 - \cos \vartheta) \sin \vartheta$	$\frac{1}{2}(1 + \cos \vartheta) - \cos^2 \vartheta$	$\sqrt{\frac{3}{8}} \sin 2\vartheta$
$k = -2$	$\frac{1}{4}(1 - \cos \vartheta)^2$	$\frac{1}{2}(1 - \cos \vartheta) \sin \vartheta$	$\sqrt{\frac{3}{8}} \sin^2 \vartheta$
$d_{k,q}^{(2)}(\vartheta)$	$q = -1$	$q = -2$	
$k = 2$	$-\frac{1}{2}(1 - \cos \vartheta) \sin \vartheta$	$\frac{1}{4}(1 - \cos \vartheta)^2$	
$k = 1$	$\frac{1}{2}(1 + \cos \vartheta) - \cos^2 \vartheta$	$-\frac{1}{2}(1 - \cos \vartheta) \sin \vartheta$	
$k = 0$	$-\sqrt{\frac{3}{8}} \sin 2\vartheta$	$\sqrt{\frac{3}{8}} \sin^2 \vartheta$	
$k = -1$	$\frac{1}{2}(\cos \vartheta - 1) + \cos^2 \vartheta$	$-\frac{1}{2}(1 + \cos \vartheta) \sin \vartheta$	
$k = -2$	$\frac{1}{2}(1 + \cos \vartheta) \sin \vartheta$	$\frac{1}{4}(1 + \cos \vartheta)^2$	

C. Intensity of the DQ coherence for two spins- $\frac{1}{2}$ coupled via dipolar coupling

Intensity of the signal S_I just after the reconversion period in MQ experiment is going to be calculated. System of two spins- $\frac{1}{2}$ coupled via dipolar coupling isolated from the surrounding will be only considered. It will be shown that DQ signal just after the reconversion period is stored in the longitudinal magnetization. Considering this assumption no evolution during purging period between reconversion and detection pulse (see e.g. Figure 2.20) take place because of the vanishing commutator relation $[\hat{T}_{2,0}, \hat{I}_z] = 0$ valid for dipolar coupled spins (see also equation (1.59)). Under this circumstance DQ signal just after the reconversion period is assumed to be the signal detected just after the detecting pulse.

In addition if so-called total spin coherence ([Wei83, Mun87]) is excited during excitation period all coupled spins are active in MQ coherences, therefore, no evolution (during evolution period) under total dipolar Hamiltonian (equation (1.59)) take place. Assuming this condition signal intensity just after the reconversion period can be written as

$$S_I = \frac{\text{Tr} \left\{ \hat{I}_z \hat{U}_{rec} \hat{U}_{exc} c \hat{I}_z \hat{U}_{exc}^+ \hat{U}_{rec}^+ \right\}}{\text{Tr} \left\{ \hat{I}_z c \hat{I}_z \right\}}. \quad (\text{C.1})$$

\hat{U}_{exc} and \hat{U}_{rec} are propagators for excitation and reconversion period, respectively. Initial state of the system is $\hat{\rho}(0) = c \hat{I}_z$. Invariance of the trace from the cyclic change of the operators can be used for equation (C.1) and we will get ($\text{Tr} \{ \hat{I}_z^2 \} = 2$ for two spin- $\frac{1}{2}$ system)

$$S_I = \frac{1}{2} \text{Tr} \left\{ \hat{U}_{rec}^+ \hat{I}_z \hat{U}_{rec} \hat{U}_{exc} \hat{I}_z \hat{U}_{exc}^+ \right\}. \quad (\text{C.2})$$

We will for the moment assume that $\hat{U}_{rec} = \hat{U}_{exc}^+ = e^{i\hat{H}_{DQ}t}$. This is good valid for static solids. In general it is also valid for rotating solids with an exception that reconversion Hamiltonian is in addition rotor modulated (see e.g. equations (2.52) and (2.48)). To calculate equation (C.2) it is enough to concentrate to the evaluation of the term

$$f(t) \stackrel{\text{def}}{=} \hat{U} \hat{I}_z \hat{U}^+, \quad (\text{C.3})$$

where \hat{U} will be expressed in the form $\hat{U} = e^{-i\hat{H}_{DQ}t}$. At this point it is good to define DQ Hamiltonian in the general form $\hat{H}_{DQ} = \sum_{i<j} \omega_{ij} \hat{T}_{2,2}^{ij} + \omega_{ij}^* \hat{T}_{2,-2}^{ij}$ which represents time independent average Hamiltonian during excitation period as well as during reconversion

period for particular pulse sequence (see e.g sections 2.5.1.1 - 2.5.1.3 or section 2.4.1.2). Propagator of the time independent average Hamiltonian is than given as

$$\hat{U} = e^{-i \sum_{i < j} (\omega_{ij} \hat{T}_{2,2}^{ij} + \omega_{ij}^* \hat{T}_{2,-2}^{ij}) t}. \quad (\text{C.4})$$

In general operators in exponent do not commute and thus we will now assume only two spin approximation. Hence, in the limit of two spin system interaction summation from equation (C.4) can be removed. Substituting propagator \hat{U} in equation (C.3) with above equation we will get

$$f(t) = e^{-i(\omega \hat{T}_{2,2}^{ij} + \omega^* \hat{T}_{2,-2}^{ij}) t} \hat{I}_z e^{i(\omega \hat{T}_{2,2}^{ij} + \omega^* \hat{T}_{2,-2}^{ij}) t}. \quad (\text{C.5})$$

Differentiating of this equation by time up to the second order and using commutator relation valid for two spin- $\frac{1}{2}$ system

$$[\hat{T}_{2,\pm 2}^{ij}, \hat{I}_z] = \mp 2 \hat{T}_{2,\pm 2}^{ij}, \quad (\text{C.6})$$

we will get

$$\begin{aligned} \dot{f}(t) &= -i e^{-i(\omega \hat{T}_{2,2}^{ij} + \omega^* \hat{T}_{2,-2}^{ij}) t} [\omega \hat{T}_{2,2}^{ij} + \omega^* \hat{T}_{2,-2}^{ij}, \hat{I}_z] e^{i(\omega \hat{T}_{2,2}^{ij} + \omega^* \hat{T}_{2,-2}^{ij}) t} \\ &= 2i e^{-i(\omega \hat{T}_{2,2}^{ij} + \omega^* \hat{T}_{2,-2}^{ij}) t} (\omega \hat{T}_{2,2}^{ij} - \omega^* \hat{T}_{2,-2}^{ij}) e^{i(\omega \hat{T}_{2,2}^{ij} + \omega^* \hat{T}_{2,-2}^{ij}) t} \end{aligned} \quad (\text{C.7})$$

$$\begin{aligned} \ddot{f}(t) &= 2 e^{-i(\omega \hat{T}_{2,2}^{ij} + \omega^* \hat{T}_{2,-2}^{ij}) t} [\omega \hat{T}_{2,2}^{ij} + \omega^* \hat{T}_{2,-2}^{ij}, \omega \hat{T}_{2,2}^{ij} - \omega^* \hat{T}_{2,-2}^{ij}] e^{i(\omega \hat{T}_{2,2}^{ij} + \omega^* \hat{T}_{2,-2}^{ij}) t} \\ &= -4 (\omega \cdot \omega^*) e^{-i(\omega \hat{T}_{2,2}^{ij} + \omega^* \hat{T}_{2,-2}^{ij}) t} [\hat{T}_{2,2}^{ij}, \hat{T}_{2,-2}^{ij}] e^{i(\omega \hat{T}_{2,2}^{ij} + \omega^* \hat{T}_{2,-2}^{ij}) t}. \end{aligned} \quad (\text{C.8})$$

In the limit of two spin interaction we can write commutator in equation (C.8) as

$$[\hat{T}_{2,2}^{ij}, \hat{T}_{2,-2}^{ij}] = \frac{1}{4} (\hat{I}_z^i + \hat{I}_z^j) = \frac{1}{4} \hat{I}_z, \quad (\text{C.9})$$

so second derivation of the $f(t)$ can be now directly evaluated

$$\ddot{f}(t) = -|\omega|^2 e^{-i(\omega \hat{T}_{2,2}^{ij} + \omega^* \hat{T}_{2,-2}^{ij}) t} \hat{I}_z e^{i(\omega \hat{T}_{2,2}^{ij} + \omega^* \hat{T}_{2,-2}^{ij}) t} = -|\omega|^2 f(t). \quad (\text{C.10})$$

This represents differential equation with the formal solution

$$f(t) = A \cos(|\omega|t) + B \sin(|\omega|t). \quad (\text{C.11})$$

Arguments A and B can be simply derived comparing results from equations (C.5), (C.7) at $t = 0$ ($f(t = 0)$, $\dot{f}(t = 0)$). It can be found that

$$A = \hat{I}_z \quad \text{and} \quad B = 2i \left(\frac{\omega}{|\omega|} \hat{T}_{2,2}^{ij} - \frac{\omega^*}{|\omega|} \hat{T}_{2,-2}^{ij} \right). \quad (\text{C.12})$$

If $f(t)$ is already known intensity of the signal S_I at the end of the reconversion period can be calculated (see equation (C.2)). Under the assumption $\hat{U}_{rec} = \hat{U}_{exc}^+$ and relations valid for two spin- $\frac{1}{2}$ system

$$\hat{T}_{2,\pm 2}^{ij} \cdot \hat{T}_{2,\pm 2}^{ij} = 0 \quad \text{and} \quad \text{Tr} \left\{ \hat{T}_{2,\pm 2}^{ij} \cdot \hat{I}_z \right\} = 0 \quad (\text{C.13})$$

the signal intensity gets the form

$$S_I = \frac{1}{2} \text{Tr} \left\{ f(t)^2 \right\} = \frac{1}{2} \text{Tr} \left\{ \hat{I}_z^2 \cos^2(|\omega|t) \right\} + \text{Tr} \left\{ 2 \left(\hat{T}_{2,2}^{ij} \cdot \hat{T}_{2,-2}^{ij} + \hat{T}_{2,-2}^{ij} \cdot \hat{T}_{2,2}^{ij} \right) \sin^2(|\omega|t) \right\}. \quad (\text{C.14})$$

The second term in this equation correspond to the DQ signal and the first one represents the polarization of the spin system and has to be filtered out from the spectrum. The first term also can not be manipulated through e.g. TPPI (see section 2.4.3) and will appear at the different frequency position as DQ coherence. Using the condition valid for two spin- $\frac{1}{2}$ system

$$\text{Tr} \left\{ \hat{T}_{2,2}^{ij} \cdot \hat{T}_{2,-2}^{ij} + \hat{T}_{2,-2}^{ij} \cdot \hat{T}_{2,2}^{ij} \right\} = \text{Tr} \left\{ \frac{1}{8} \hat{\mathbf{1}} \right\} = \frac{1}{2} \quad (\text{C.15})$$

intensity of DQ coherence from equation (C.14) can be simply evaluated

$$S_I^{DQ} = \sin^2(|\omega|t). \quad (\text{C.16})$$

The rest magnetization of the spin system is than

$$M_z = \cos^2(|\omega|t). \quad (\text{C.17})$$

In the case when $\hat{U}_{rec} \neq \hat{U}_{exc}^+$ the result given in equation for DQ intensity is not more valid and equation (C.2) has to be solved in more details. One has to calculate separately differential equation for reconversion period and the result will end up with the following equation¹

$$S_I^{DQ} = \Phi_\omega \sin(|\omega_{rec}|t) \sin(|\omega_{exc}|t), \quad (\text{C.18})$$

where

$$\Phi_\omega = \frac{\omega_{rec} \omega_{exc}^* + \omega_{rec}^* \omega_{exc}}{2 |\omega_{rec}| |\omega_{exc}|}. \quad (\text{C.19})$$

Complex terms ω_{exc} and ω_{rec} represent amplitudes and phases of DQ excitation and reconversion Hamiltonian one by one. Φ_ω is the phase of the DQ signal. t is excitation/reconversion time usually marked in this work like τ . To write equations (C.18) and (C.19) in more convenient way it is useful to separate amplitude and the phase from ω so:

¹We will assume that duration of the excitation and the reconversion period is equal $t_{exc} = t_{rec} = t$.

$\omega_{rec} = |\omega_{rec}|e^{i\Phi_{rec}}$, $\omega_{exc} = |\omega_{exc}|e^{i\Phi_{exc}}$. Using this definitions equations (C.18) and (C.19) will become more transparent. It holds that

$$S_I^{DQ} = \cos(\Phi_{rec} - \Phi_{exc}) \sin(|\omega_{rec}|\tau) \sin(|\omega_{exc}|\tau). \quad (\text{C.20})$$

The phase modulation of the DQ signal is from above equation evident from cosine factor $\cos(\Phi_{rec} - \Phi_{exc})$. It has to be noted that this phase modulation has no influence to the signal originating from the polarization of the spin system described by equation (C.17).

Bibliography

- [Abr61] A. Abragam. *The Principles of Nuclear Magnetism*. Oxford University Press, London (1961).
- [Add93] J.-P. Cohen Addad. *Prog. NMR Spectrosc.* **25**, 1 (1993).
- [And58] E.R. Andrew, A. Bradbury, R.G. Eades. *Nature* **182**, 1659 (1958).
- [Ant99] O.N. Antzukin, R. Tycko. *J. Chem. Phys.* **110**, 2749 (1999).
- [Aue76] W.P. Aue, E. Bartholdi, R.R. Ernst. *J. Chem. Phys.* **64**, 2229 (1976).
- [Bau85] J. Baum, M. Munowitz, A.N. Garroway, A. Pines. *J. Chem. Phys.* **83**, 2015 (1985).
- [Bau86] J. Baum, K.K. Gleason, A. Pines, A.N. Garroway, J.A. Reimer. *Phys. Rev. Letters* **56**, 1377 (1986).
- [Blo46] F. Bloch, W.W. Hansen, M.E. Packard. *Phys. Rev.* **69**, 127 (1946).
- [Bod81] G. Bodenhausen. *Progr. NMR Spectrosc.* **14**, 137 (1981).
- [Dol97] W.A. Dollase, M. Feike, H. Förster, T. Schaller, I. Schnell, A. Sebald, S. Steuernagel. *J. Am. Chem. Soc.* **119**, 3807 (1997).
- [Eka00] P. Ekanayake. *Orientation and Dynamics of Unfilled and Filled Poly(Butadiene) Networks Studied by Deuterium NMR*. Promotion: Martin-Luther-Universität Halle-Wittenberg in Halle (2000).
- [Ern87] R.R. Ernst, G. Bodenhausen, A. Wokaun. *Principles of Nuclear Magnetic Resonance in One and Two Dimensions*. Oxford University Press Inc., Oxford (1987).

- [Eul00] V. Eulry, P. Tekely, F. Humbert, D. Canet, J. Marcilloux. *Polymer* **41**, 3405 (2000).
- [Fei96a] M. Feike, D.E. Demco, R. Graf, J. Gottwald, S. Hafner, H.W. Spiess. *J. Magn. Reson. A* **122**, 214 (1996).
- [Fei96b] M. Feike, R. Graf, I. Schnell, C. Jäger, H.W. Spiess. *J. Am. Chem. Soc.* **118**, 9631 (1996).
- [Fei98] M. Feike, C. Jäger, H.W. Spiess. *J. Non-Cryst. Solids* **223**, 200 (1998).
- [Fil97] C. Filip, X. Filip, D.E. Demco, S. Hafner. *Mol. Phys.* **92**, 757 (1997).
- [Fre97] R. Freeman. *A Handbook of Nuclear Magnetic Resonance*. Addison Wesley Longman, Harlow (Essex) (1997).
- [Gas99] L. Gasper, D.E. Demco, B. Blümich. *Solid State NMR* **14**, 105 (1999).
- [Gee94] H. Geen, J.J. Titman, J. Gottwald, H.W. Spiess. *Chem. Phys. Letters* **227**, 79 (1994).
- [Gee95] H. Geen, J.J. Titman, J. Gottwald, H.W. Spiess. *J. Magn. Reson. A* **114**, 264 (1995).
- [Gee97] H. Geen, J. Gottwald, R. Graf, I. Schnell, H.W. Spiess, J.J. Titman. *J. Magn. Reson.* **125**, 224 (1997).
- [Gee99] H. Geen, R. Graf, A.S.D Heindrichs, B.S. Hickman, I. Schnell, H.W. Spiess, J.J. Titman. *J. Magn. Reson. A* **138**, 167 (1999).
- [Got95] J. Gottwald, D.E. Demco, R. Graf, H.W. Spiess. *Chem. Phys. Letters* **243**, 314 (1995).
- [Got96] J. Gottwald. *Hochaufgelöste Multiquanten-NMR-Spektroskopie von Festkörpern*. Promotion: Johannes Gutenberg-Universität in Mainz (1996).
- [Gra97a] R. Graf. *Hochauflösende Doppelquanten-NMR-Spektroskopie am Amorphen Polymeren*. Promotion: Johannes Gutenberg-Universität in Mainz (1997).
- [Gra97b] R. Graf, D.E. Demco, J. Gottwald, S. Hafner, H.W. Spiess. *J. Chem. Phys.* **106**, 885 (1997).

- [Gra98a] R. Graf, D.E. Demco, S. Hafner, H.W. Spiess. *Solid State NMR* **12**, 139 (1998).
- [Gra98b] R. Graf, A. Heuer, H.W. Spiess. *Phys. Rev. Lett.* **80**, 5738 (1998).
- [Hae76] U. Haeberlen. *Advan. Magn. Reson. Supplement 1: High Resolution NMR in Solids, Selective Averaging*. Academic Press, New York (1976).
- [Haf98] S. Hafner, H.W. Spiess. *Concepts Magn. Reson.* **10**, 99 (1998).
- [Hoh98] M. Hohwy, H.J. Jakobsen, M. Edén, M.H. Levitt, N.C. Nielsen. *J. Chem. Phys.* **108**, 2686 (1998).
- [Hon99] M. Hong. *J. Magn. Reson.* **136**, 86 (1999).
- [Lec93] M.D. Lechner, K. Gehrke, E.H. Nordmeier. *Makromolekulare Chemie*. Birkhäuser Verlag, Basel (1993).
- [Lee95] Y.K. Lee, N.D. Kurur, M. Helmle, O.G. Johannessen, N.C. Nielsen, M.H. Levitt. *Chem. Phys. Letters* **242**, 304 (1995).
- [Low58] I.J. Lowe. *Phys. Rev. Letters* **2**, 285 (1958).
- [Mal97] C. Malveau, P. Tekely, D. Canet. *Solid State NMR* **7**, 271 (1997).
- [Mat92] D. Matzen, E. Straube, E. Colloid. *Colloid & Polym. Sci.* **270**, 1 (1992).
- [Meh83] M. Mehring. *High Resolution NMR in Solids*. Springer, Berlin (1983).
- [Mei86] B.H. Meier, W.L. Earl. *J. Chem. Phys.* **85**, 4905 (1986).
- [Mei87] B.H. Meier, W.L. Earl. *J. Am. Chem. Soc.* **109**, 7937 (1987).
- [Men99] H. Menge, S. Hotopf, S. Pönitzsch, S. Richter, K.-F. Arndt, H. Schneider, U. Heuert. *Polymer* **40**, 5303 (1999).
- [Mun87] M. Munowitz, A. Pines. *Advan. Chem. Phys. (Vol. 66, p. 1-152), Principles and Applications of Multiple-Quantum NMR*. Wiley-Interscience, New York (1987).
- [Nie94] N.C. Nielsen, H. Bildsøe, H.J. Jakobsen, M.H. Levitt. *J. Chem. Phys.* **101**, 1805 (1994).
- [Now45] W. Nowacki. *Helv. Chim. Acta* **28**, 1233 (1945).

- [Pin88] A. Pines. In *Proc. 100th Fermi School*. North Holland, Amsterdam (1988). Lectures on Pulsed NMR.
- [Pur46] E.M. Purcell, H.C. Torrey, R.V. Pound. *Phys. Rev.* **69**, 37 (1946).
- [Rah86] A.-ur-Rahman. *Nuclear Magnetic Resonance, Basic Principles*. Springer, New York (1986).
- [Red75] A.G. Redfield, S.D. Kunz. *J. Magn. Reson.* **19**, 250 (1975).
- [Rhi73] W.-K. Rhim, D.D. Elleman, R.W. Vaughan. *J. Chem. Phys.* **59**, 3740 (1973).
- [Rie98] C.M. Rienstra, M.E. Hatcher, L.J. Mueller, B. Sun, S.W. Fesik, R.G. Griffin. *J. Am. Chem. Soc.* **120**, 10602 (1998).
- [Sch89] C. Schmit, J.-P. Cohen Addad. *Macromolecules* **22**, 142 (1989).
- [Sch99] M. Schneider, L. Gasper, D.E. Demco, B. Blümich. *J. Chem. Phys.* **111**, 402 (1999).
- [Shy88] D. N. Shykind, J. Baum, S.B. Liu, A. Pines, A. N. Garroway. *J. Magn. Reson.* **76**, 149 (1988).
- [Sim92] G. Simon, K. Baumann, W. Gronski. *Macromolecules* **25**, 3624 (1992).
- [Sli92] C.P. Slichter. *Principles of Magnetic Resonance*. 3rd edn, Springer, Berlin (1992).
- [Som95] W. Sommer, J. Gottwald, D.E. Demco, H.W. Spiess. *J. Magn. Reson. A* **113**, 131 (1995).
- [Spi78] H.W. Spiess. *NMR-Basic Principles and Progress, vol 15: Rotation of Molecules and Nuclear Spin Relaxation*. Springer Verlag, Heidelberg (1978).
- [Spi97] H.W. Spiess. *Annu. Rep. NMR Spectrosc.* **34**, 1 (1997).
- [SR94] K. Schmidt-Rohr, H.W. Spiess. *Multidimensional Solid-State NMR and Polymers*. Academic Press, New York (1994).
- [Ste74a] E.O. Stejskal, J. Schaefer. *J. Magn. Reson.* **13**, 249 (1974).
- [Ste74b] E.O. Stejskal, J. Schaefer. *J. Magn. Reson.* **14**, 160 (1974).

- [Sun94] B.-Q. Sun, P.R. Costa, D. Kocisko, P.T. Lansbury Jr., R.G. Griffin. *J. Chem. Phys.* **102**, 702 (1994).
- [Tyc90] R. Tycko, G. Dabbagh. *Chem. Phys. Letters* **173**, 461 (1990).
- [Tyc91] R. Tycko, G. Dabbagh. *J. Am. Chem. Soc.* **113**, 9444 (1991).
- [Tyc93] R. Tycko, S.O. Smith. *J. Chem. Phys.* **98**, 932 (1993).
- [War79] W.S. Warren, S. Sinton, D.P. Weitekamp, A. Pines. *Phys. Rev. Letters* **43**, 1791 (1979).
- [War80] W.S. Warren, D.P. Weitekamp, A. Pines. *J. Chem. Phys.* **73**, 2084 (1980).
- [War81] W.S. Warren, A. Pines. *J. Chem. Phys.* **74**, 2808 (1981).
- [Wei83] D.P. Weitekamp. *Advan. Magn. Reson.* (Vol. 11, p. 111-274), *Time-Domain Multiple-Quantum NMR*. Academic Press. Inc., New York (1983).
- [Wok77] A. Wokaun, R.R. Ernst. *Chem. Phys. Letters* **52**, 407 (1977).
- [Yen83] Y.S. Yen, A. Pines. *J. Chem. Phys.* **78**, 3579 (1983).

Acknowledgements

At this point I would like to thank all who contribute to this work. My special thank is intended to:

- Prof. Dr. Horst Schneider for his sustained advice and inspiration throughout this work and also for his invaluable supervision and unfailing encouragement, only with which this work is succeeded. I would like to thank him also for important proposals concerning the structure and the contents of this thesis.
- Dr. Günter Hempel for his great help in all aspects of my study, theoretical support, wealthy suggestions in order to succeed this work and critical reading of the manuscript with a lot of suggestions and corrections.
- Dr. Heike Menge I wish to thank for a good collaboration especially at the end of this work, for answering me a lot of questions concerning elastomers, reading of the manuscript of this work and correcting mistakes, and giving me samples. At this point I would like to thank also Dr. Piyasiri Ekanayake who supported me also with samples. I would like to thank him for many interesting discussions about more or less scientific topics.
- Dr. Detlef Reichert who gave me a lot of advices concerning programming of our spectrometer and also for many stimulated discussions. My thank is extended also to Dr. Gerald Simon (Varian GmbH Darmstadt) for support concerning programming multiple-pulse sequences on which basis I was able to make C7 based r.f. pulse sequences workable.
- Dr. Manfred Knörger for amicable working atmosphere in our group, and Mrs. Karin Nowak for all her help throughout the study and for her great attempt to make a nice working environment.

- Dr. S. Hafner and Dr. R. Graf from MPI Mainz for stimulating discussions on multiple quantum NMR and the gentle accommodation in Mainz. In addition my thank is intended to Dr. Ulli Friedrich and Dr. Tilo Fritzhanns for taking care about my social life during my stay in Mainz.
- Prof. Dr. D.E. Demco for stimulated discussions concerning elastomers.
- Deutsche Forschungsgemeinschaft (DFG) (Graduiertenkolleg Polymerwissenschaften "Heterogene Polymere") for financial support.
- All my colleagues who are and were also graduate students. I wish to thank them individually, but there are many to be listed.
- My parents who encouraged me and supported me during my study. My special thank is intended to my father for checking main grammar and stylistic mistakes of the manuscript. Last and the most important thanks has to go to my wife, who patiently endured my absence from home, taking care about our son and supported me during my stay in Halle.

CURRICULUM VITAE

Name : Juraj **Pivarč**
Born : 4 October, 1971 in Bratislava, Slovak Republic
Sex : male
Nationality : Slovakia
Marital Status : married, one child (boy)

PROFESSIONAL BACKGROUND:

Ground and Secondary education:

1978-80: Ground school, Ladislava Novomeského 32, Bratislava (Slovakia)

1980-86: Ground school with specialization to English language, ZŠ Fraňa Kráľa Bratislava

1986-90: Gymnasium Jura Hronca Bratislava

Higher education:

1990-95: Student

University: Comenius University, Bratislava (Slovakia)

Faculty: Faculty of Mathematics and Physics

Graduated: 1995 at Department of Solid State Physics

Area of specialization: High-Temperature superconductors

Degree: **Mgr. (Magister in Physics)**

1995: Ph.D. Student

University: Comenius University, Bratislava (Slovakia)

Faculty: Faculty of Mathematics and Physics

Department: Solid State Physics

Area of specializaion: High-Temperature superconductors

1.10.1995 – 31.3.1996: **Guest student**, Friedrich-Schiller University in Jena (Germany)

Project Title: Numerical simulations of Josephson junction networks

Fellowship: DAAD

Since November 1996: Ph.D. Student/Scientific Collaborator

University: Martin-Luther University Halle-Wittenberg, Halle/Saale (Germany)

Department: Department of Physics

Area of specialization: Nuclear Magnetic Resonance

Fellowship: Deutsche Forschungs Gemaintschaft

Date 6. 07. 2000

Erklärung

Ich erkläre hiermit, dass die Dissertation selbständig verfasst wurde und nur die angegebenen Hilfsmittel benutzt wurden. Die Dissertation wurde noch an keiner anderen Universität oder Hochschule eingereicht.

Halle, den 6. 07. 2000

.....
(Juraj Pivarč)